GaN Micro-LED Integration with Thin-Film Transistors for Flexible Displays

by

Mohsen Asad

A thesis

presented to the University of Waterloo

in fulfillment of the

thesis requirement for the degree of

Doctor of Philosophy

in

Electrical and Computer Engineering

Waterloo, Ontario, Canada, 2020

Examining Committee

The following served on the Examining Committee for this thesis.

External Examiner	Kei May Lau
	Professor of Electrical and Computer Engineering
Supervisor	William S. Wong
	Professor of Electrical and Computer Engineering
Internal Examiner	Christopher J. Backhouse
	Professor of Electrical and Computer Engineering
Internal Examiner	Michael Reimer
	Professor of Electrical and Computer Engineering
Internal-External Examiner	John Yeow
	Professor of System Design Engineering

AUTHOR'S DECLARATION

I hereby declare that I am the sole author of this thesis. This is a true copy of the thesis, including any required final revisions, as accepted by my examiners.

I understand that my thesis may be made electronically available to the public.

Abstract

The research presented provides a systematic attempt to address the major challenges for the development of flexible micro-light-emitting diode (LED) displays. The feasibility of driving GaN-based micro-LEDs with a-Si:H-based thin-film transistors by using a thin-film bonding and transfer process was initially proposed. This approach was implemented to create an inverted pixel structure where the cathode of the LED is connected directly to the drain contact of the drive TFT resulting in a pixel circuit having more than 2× higher brightness compared to a standard pixel design. This "paste-and-cut" technique was further demonstrated for the development of flexible displays, enabling the study of the effect of mechanical strain and self-heating of the devices on plastic. Through a finite-element analysis, it was determined that the applied stress-induced strain near the quantum wells of the micro-LEDs are negligible for devices with diameters smaller than 20 microns. Thermal simulation of the LEDs on plastic revealed that a copper bond layer thicker than 600 nm can be used to alleviate self-heating effects of the micro-LEDs. Using these design parameters, micro-LED arrays with 20 micron diameter were integrated onto flexible substrates to validate the theoretical predictions. Further scaling of the LED size revealed substrate bending also tilts the direction of the LED structure, allowing further extraction of light. This effect was demonstrated using nanowire LEDs with a 250 nm diameter transferred onto plastic, where the light output could be enhanced by 2× through substrate bending. Finally, through the removal of bulk defect and surface states, fabrication of highly efficient micro-LEDs having > 400% increase in light output (compared to conventional diodes) was achieved. This outcome was accomplished through the removal of the defective buffer region adjacent to the active layers of the LED and minimization of the non-radiative recombination at the sidewalls. The former was accomplished through the removal of the buffer layer after separation of the LED from the process wafer while the latter is accomplished using a surround cathode gate electrode to deplete free carriers from the sidewall of the forward-biased LED. The resulting performance enhancements provided a basis for high-brightness flexible micro-LED displays developed in this dissertation.

Acknowledgements

I would like to express my special respect and thanks to my supervisor Professor William S. Wong for trusting me and providing the opportunity to work on a wonderful project. He not only taught me how to carry out the research and present it clearly, but he also showed me how to interact positively with other people and be a giver and not a taker. I could not have imagined having any grater supervisor than him. Thank you, Professor Wong.

I am extremely grateful to committee members, Professor Christopher Backhouse, Professor Michael Reimer, Professor John Yeow, and Professor Kei May Lau.

Finally, my sincerest gratitude to my wife Dr. Hadiseh Jamshidian for her love, support, and endless patience. I have to also appreciate you, Aiden Asad, for your understanding and make me happy even when I was so tired or frustrated. I also express my deepest respect to my mom, Soghra Fathi, for her prayers and innumerable support. Thank you for being always in my heart. I will be ever grateful to my superior and great dad, Abbas Asad. I'm deeply sad that he will not see me graduate.

I would like to express my deepest gratitude to Professor Manoj Sachdev for providing invaluable guidance and encouraging me to be a better person. My sincere thanks also go to Professor Bo Cui for everything he taught me and all the technical discussions. I would like to thank Qing Li for his constructive collaboration and all the technical and non-technical discussions. to Dr. Czang-Ho Lee for fabricating TFTs and training me on most of the G2N facilities. A special thanks go to Mr. Richard Barber for always being a great help in G2N for his friendship and a great sense of humor. I'm also truly grateful to my mentors in Quantum NanoFab who trained me and helped me to develop the GaN micro-LED fabrication smoothly. Thank you, Vito Logiudice, Nathan Nelson-Fitzpatrick, Lino Eugene, Greg Holloway, Sandra Gibson, Matt Scott, Rodello Salandanan, Paul Charles and Brian Goddard. I also appreciate Professor Siva Sivoththaman and Joe Street for access to their lab and equipment

I give the greatest thanks to my fellow friends at Advanced Flexible Electronic Technology group, Alireza Tari, Bright Iheanacho, Mohammad Noori, Leon Mintz, Melissa Chow, Lina Voloshin, Won-Tae Park, Hyunwoo Choi, Naeun Kim, Kendal Davis, Minoli Pathirane, Matan Winstok, Phillip Pearson, and Pranav Gavirneni. I would like to thank my friend who provided joyful time experience in Waterloo: Sorosuh Rasty, Dr. Navid Jahed, Mohammad Soltani, Celal Con, Ariel Petruk, Mozhgan Sadeghi, Ehsan Fathi, Bahareh Sadeghi, Ferhat Aydinoglu, Hoseyin Ekinci, Mohammad Komijani, and Amir Ameli.

I would like to acknowledge the support of the Canada Micro System (CMC) and Waterloo Institute of Nanotechnology (WIN) for assisting me in the further development of my research.

Dedication

This thesis is dedicated from the bottom of my heart to my love of life,

***Hadis**,*

and my lovely son,

***Aiden**.*

Table of Contents

AUTHOR'S DECLARATION iii

Abstract iv

Acknowledgements v

Dedication vi

List of Figures x

Chapter 1 Introduction 1

1.1 Miro-LED displays technology advantages and requirements 1

1.2 Background review 3

1.3 Thesis Structure 6

Chapter 2 Direct-transfer of GaN micro-LED from sapphire substrate onto flexible TFT 8

2.1 Introduction 8

2.2 Experimental Details 9

2.2.1 Integration process development 9

2.2.2 a-Si:H TFT fabrication on PEN substrates 11

2.2.3 GaN micro-LED fabrication 11

2.2.4 Micro-LED integration onto flexible TFTs 13

2.3 Optoelectrical Characteristics of the Flexible Pixel 14

2.4 Summary 19

Chapter 3 Demonstrating a low-power and high-brightness flexible micro-LED display with GaN micro-LED integration using a “double-transfer” approach 20

3.1 Introduction 20
3.1 Experimental details 22
3.2 Results 25
3.3 Summary 29
Chapter 4 Thermal and Optical Properties of High-density GaN Micro-LED Arrays on Flexible Substrates 30
4.1 Introduction 30
4.2 Mechanical bending simulation and analysis. 31
4.3 Thermal simulation and analysis. 32
4.4 Experiments Details 35
4.5 Results 37
4.6 Summary 43
Chapter 5 Optically invariant InGaN nanowire light-emitting diodes on flexible substrates under mechanical manipulation 44
5.1 Introduction 44
5.2 Mechanical bending simulation and analysis. 46
5.3 Experiment 47
5.4 Results 49
5.5 Summary 57
Chapter 6 Demonstration of highly efficient surface-emitting vertical GaN LED by optimizing the epitaxial layer thickness, and self-aligned sidewall gating 59

6.1 Introduction 59
6.2 Theoretical Simulation 60
6.3 Experiments 63
6.4 Results and Characterization 65
6.5 Summary 75
Chapter 7 Conclusion and Future Works 76
7.1 Conclusion 76
7.2 Future work 79
7.3 Published articles and conference papers 80
Bibliography 83
Appendix A Details of materials and methods from Chapter 3 89
Appendix B Details of materials and methods from Chapter 4 94
Appendix C Details of materials and methods from Chapter 5 99
Appendix D Details of materials and methods from Chapter 6 102

List of Figures

Figure 2.1 optical micrograph of the bonded micro-LEDs by (a) Au-Au (on silicon) (b) Au-In (on silicon) and (c) Au-In (on plastic) materials. The scale bars in (a), (b), and (c) are 90 μm, 90 μm, and 280 μm, respectively. 10

Figure 2.2 (a-h) Optical Figure: The process flow diagram of the integration of TFT and micro-LED on a flexible substrate (BM=Bonding Metal). 14

Figure 2.3 (a) The 2T pixel circuit before micro-LED transfer. (b) The 2T pixel circuit after transfer with micro-LED illuminating. (c) The I-V curves in positive voltage region (negative voltage region in the inset) and (d) the EL intensity of the micro-LED on the sapphire wafer with p-GaN facing up (Reference) and the transferred micro-LED on the flexible substrate with p-GaN facing down (Transferred).....16

Figure 2.4 (a) The micro-LED driven by T_0 only. (b) The micro-LED driven by a 2T pixel circuit. (c) The first 4ms of transient voltage waveforms of the input signals V_1 and V_{ada}=14V and the corresponding output current I_{LED}. (d) The output current I_{LED} vs. V_{data} and the EL intensity of the micro-LED from V_{data} = 9V to 15V for both circuits shown in [(a) and (b)]..18

Figure 2.5 (a) The EL intensity vs. wavelength of the 2T pixel circuit at various V_{data} voltages. (b) The 2T pixel circuit light output gradient under different V_{data}. (c) The pixel circuits on the flexible substrate. 19

Figure 3.1 Schematic diagram of different configurations for micro-LED and TFT integration where (a) micro-LED's anode is connected to the ground side of the TFT and (b) micro-

LED's cathode is connected to the source side. The dynamic ranges of the driving voltage of the micro-LED are shown inset of both figures. 22
Figure 3.2 Schematic of the "paste-and-cut" process for transferring micro-LEDs from the rigid sapphire substrate onto the flexible platform. (a) Bonding micro-LEDs onto the temporary carrier substrate using a wax layer. (b) LLO process and removing the sapphire substrate. (c) μμDry etching of the excess wax around the micro-LEDs. (d) Coating a Cr/Au bilayer on the backside of the devices. (e) Flip-chip bonding of the micro-LEDs onto the indium pads on the flexible substrate. (f) Removing the carrier substrate after immersing the structure in warm acetone. (g) SEM micrograph of the micro-LEDs on the carrier substrate after removing the sapphire. (h) Cross-section SEM micrograph of the micro-LEDs after etching the excess wax layer. (i) Optical micrograph of the flexible display after successful bonding of the micro-LEDs onto the drain electrodes. The scale bar in (g), (h), and (i) are 90 μm, 70 μm, and 1 cm, respectively. 24
Figure 3.3 (a) I-V characteristics of the micro-LED on sapphire substrate and after transfer onto PEN substrates. (b) I-V characteristics of the different micro-LEDs on flex chosen from the center and four corners of the array. (c) Electrical characteristics of the micro-LED under flat state and under mechanical bending. (d) Measured EL intensity of the micro-LEDs before and after the transfer process. (e) and (f) 3D-FDTD simulated optical power of the micro-LEDs with and without backside reflective metal layer, respectively.....27
Figure 3.4 (a) The fabricated flexible display taped on a curved aluminum sample holder for measuring the optoelectrical performance. (b) Measured EL intensity of the proposed pixel

circuit under different mechanical strain conditions. (c) Comparison between the optoelectrical performance of the proposed and conventional pixel circuit at different Vdata voltages.....29
Figure 4.1 The simulated strain gradient for different sizes micro-LED on PI/Cu substrate with concave-down (Tensile stress) and concave-up (Compressive stress) bending radius of 15 mm; (a) 50 µm, (b) 40 µm, (c) 30 µm, (d) 20 µm, (e) 10 µm, and (f) 5 µm. The place of the quantum wells (QWs) is shown by a dashed line.....32
Figure 4.2 Temperature gradient and depth profile of the generated heat by a 20 µm LED on (a) sapphire, (b) PI/Cu/SU8 (150/3/1 µm), (c) PI/Cu (150 µm/100 nm), and (c) PI/Cu (150/1 µm), respectively. 34
Figure 4.3 Schematic of the process flow for the selective mass-transfer of the GaN micro-LEDs from a sapphire substrate onto a flexible substrate; (a) bonding the micro-LEDs onto a carrier substrate through their p-side, (b) laser-liftoff and releasing the sapphire substrate, (c) dry-etching of the adhesive layer from the unwanted area in an oxygen plasma, (d) Coating of the micro-LEDs' backside with a Cr/Cu/Au (triple layer). The Au surface is shown by an arrow. (e) Flip-chip bonding of the micro-LEDs onto the desired places where Au/Sn pads are patterned, (f) releasing the carrier substrate.....37
Figure 4.4 Plan view scanning electron microscopy of the (a) 20 µm micro-LED arrays transferred onto the carrier substrate after removing the sapphire substrate by laser-liftoff, (b) selective-mass-transferred micro-LEDs on the large-scale flex by using Au/Sn-based eutectic bonding. The scale bars at (a) and (b) are 100 µm and 20 µm, respectively. 38

Figure 4.5 Electro-optical characterization of the 20 μm diameter micro-LEDs (a) The I-V characteristics of a micro-LED before transfer (on sapphire) and after transfer onto the flex. The series resistance (b) and threshold voltage (c) variation of the micro-LEDs after transfer onto the flex. The micro-LEDs are chosen from the center and four corners of the array. (d) I-V characteristics of the flexible micro-LED under flat and bending conditions. (e) EL before and after transfer. The inset presents the C.I.E 1931 color-space diagram of tested micro-LEDs (f) EL under different bending conditions. 41
Figure 4.6 (a) Electroluminescence characteristics of micro-LEDs on sapphire and flex substrate with different copper thicknesses driven continuously at 1000 A/cm2. (b) Measured emission peak wavelength and calculated device temperature for devices on different substrates.....43
Figure 5.1 The simulated strain gradient for the NW devices on PET with R = 38 mm. The device active region, near the tips of the nanowires, was found to be strain-free. A calculated bending moment of 0.02248 N·m for R = 38 mm was used in the simulation.....47
Figure 5.2 Process flow of the double-transfer process (a-d): (a) the NW LED device is bonded to a temporary receptor substrate, (b) the sapphire substrate is detached from the NW devices by illuminating a pulsed 266 nm Nd:YAG laser through the sapphire to decompose the GaN at the substrate interface, (c) a metallic Ag adhesive bonds the GaN NW devices/receptor substrate structure onto a 175 μm thick PET flexible substrate, and (d) the NW devices are transferred onto the PET by removing the epoxy bond using an acetone bath. (e) A schematic of the final transferred NW LED device on the PET substrate. (f) A cross-

sectional FE-SEM image of an array of GaN NW LED devices transferred onto the flexible substrate. The golden and blue colors represent the ITO top contact and GaN NWs, respectively. Scale bar = 1 μm. 49

Figure 5.3 (a) I-V characteristics of the NW LEDs on the sapphire substrate before and after integration onto PET substrates; the slight variation in the forward current is due to the Ag contact used to bond the LEDs onto the PET. The inset shows the blue light emission of the GaN NW LEDs operating at a 1 mA forward current and the PET substrate flexed to a 38 mm radius of curvature. (b) The I-V characteristics of the LEDs on PET with different concave up bending conditions. The results show similar I-V characteristics at different radii of curvature between 22 to 38 mm. (c-e) Planview SEM images of GaN nanowire array sample mounted on flat, 32 mm concave-up, and 32 mm concave-down curved substrate holder at an electron-beam operation voltage of 5 kV. 52

Figure 5.4 (a) The measured EL spectra of the blue NW LEDs on PET before and after the double-transfer process. The transferred devices show no emission shift with different concave up bending conditions while the EL intensity increases with decreasing radii of curvature. (b) The displacement of the flexible devices with 38 mm concave-up radius. The tilt angles of NWs were calculated based on displacement results using $\theta = \cos^{-1}\frac{\Delta x}{\sqrt{\Delta x^2 + \Delta y^2}}$, where θ is the angle between the nanowire structure during bending after shifting in the x and y-direction. 54

Figure 5.5 (a) 3D-FDTD simulated light-extraction efficiency for NW LEDs on different curved surfaces. The light intensity emitted from the topside of a (b) free-standing NW LED

device and (c) after bonding to the PET substrate using the reflective Ag adhesive. (d) The light intensity for NW LEDs on a flexible PET substrate having a 38 mm radius of curvature. 57

Figure 6.1 Light extraction efficiency of the blue GaN micro-LED in the range of 440-460 nm as a function of the epitaxial layer thickness when (a) only the device backside is covered with a reflective metal layer. (b) Time-averaged photon flow radiated from a TE mode dipole source mimicking the QWs. (c) The light extraction efficiency of the blue micro-LED structure as a function of the epitaxial layer thickness when both backside and sidewalls are covered with reflective aluminum. (d) Time-averaged photon emission of the device with both sidewalls and backside reflective layers. 63

Figure 6.2 Process flow for micro-LED epitaxial layer thickness engineering process: (a) Adhesive bonding the micro-LED onto a glass substrate, (b) Releasing the sapphire substrate after the LLO process, (c) Thinning the micro-LED backside by an ICP etching process, (d) Sidewalls and backside coating with a highly reflective aluminum layer (e) Flip-chip bonding of the micro-LEDs from the carrier substrate onto the final silicon substrate and releasing the carrier. (f) The SEM micrograph of a micro-LED pixel after bonding onto glass and releasing the sapphire substrate. (g) The SEM micrograph of the same micro-LED after backside thinning for 15 min and coating the sidewalls and backside with a 500 nm reflective aluminum layer. (h) The SEM micrograph of the 90 × 90 μm^2 micro-LED arrays after final transfer onto the silicon substrate. 65

Figure 6.3 (a) EL spectra of the REF GaN micro-LEDs and micro-LEDs with different epitaxial layer thicknesses. (b) The etch depth from the backside and the EL improvement versus the dry etch time. The sidewall of REF micro-LED is not covered with reflective metal. The schematic of the device structure with a total thickness of 6.5 μm is shown on the right side of the spectra. Optical micrographs of (c) REF micro-LED and (d) bonded onto a silicon substrate driven with continuous 10 A/cm^2. (e) The measured far-field radiation pattern of REF micro-LED and 5 min. 67
Figure 6.4 (a) Light-extraction efficiency calculated for 20 min thinned blue micro-LED. (b) Schematic of the light path in a thinned micro-LED and thick micro-LED. The QW is shown by a dashed line and the photon source is mimicked by a green point. 69
Figure 6.5 (a) Semi-logarithmic scale I-V characteristics of the REF micro-LED and micro-LEDs with different epitaxial layer thicknesses. The numbers in the picture show three main regions of the I-V characteristic. (b) The ideality factor of different devices extracted from I-V characteristics at region 2. (c) Simulated electric field distribution within the active region of REF-micro-LED and device with the gated sidewall. (d) Simulated SRH recombination profile in the QWs at the vicinity of the conventionally sidewall passivated and sidewall gated structure. (e) Linear scale I-V characteristics of the REF micro-LED and thinned devices. (f) Extracted series resistance versus dry etch time for thinning the backside. The etch depth in the epitaxial structure is schematically presented at the right side. (g) A numerically simulated electron density at the quantum wells in the vicinity of the passivation

layer. (h) Simulated electron current densities at the QWs interfaced with the dielectric. The structure with gated sidewall passes 10 times lower current density at the sidewall. 74

Chapter 1

Introduction

1.1 Miro-LED displays technology advantages and requirements

Introduced in 2001, GaN-based micron-size light-emitting diodes (micro-LEDs) have been used successfully in the fabrication of emissive micro-displays [1]. Every pixel was addressed separately and lights up without requiring a common backlight unit (BLU) which is commonly used in liquid crystal displays (LCDs). This new technology possesses the potential to decrease the total power consumption of flat-panel displays while providing enhanced contrast ratio by achieving true black when the pixel is off [2]. The higher luminescence of micro-LEDs is also promising for the development of brighter outdoor display screens that would be easier to read under direct sunlight. Micro-LEDs also consume less power, requiring smaller batteries and enhanced form factors for wearable displays [3].

Organic light-emitting diodes (OLEDs), the most widely used emissive display technology, still suffer from degradation by exposure to the environment, lower brightness, and optical instability compared to micro-LEDs [4]. As a result, the necessary encapsulation process increases the cost and complexity of the manufacturing of OLEDs [5] while compensation circuits may be used to alleviate optical instability. Furthermore, the nature of organic semiconductors makes them incompatible with conventional microfabrication processes. Specifically, the lithography and etching processes for patterning the OLED pixel suffer from the lack of the selectivity to produce high-resolution displays that require fine-sized pixel

structures [6]. Due to these limitations, the common patterning approach for OLED displays incorporate shadow-mask techniques to define and pattern the display media [7]. This approach also constrains the OLED display pixel circuit design due to the poor selectivity of the organic materials fabrication process. For example, indium-tin-oxide (ITO) is mainly used for the OLED anode, a high-temperature process is typically required to achieve a low resistance which may degrade the organic emitters. To prevent any degradation, the organic layers are typically coated after the ITO processing. However, this process requires the anode of the OLED to be deposited first onto the pixel circuit and only allows the pixel structure to have one configuration.

Contrary to OLED materials, GaN is normally grown on substrates such as silicon or sapphire, making mechanical flexibility difficult to achieve; flexible substrates made from low-melting-point materials cannot survive the typical thermal budget for GaN film growth or the harsh chemical processes required to fabricate LEDs. However, GaN micro-LEDs may be grown and processed on the growth substrate and can be transferred onto the final flexible platforms using an efficient transfer process. In addition, this approach provides more flexibility in how the pixel circuit may be assembled, providing a higher degree of freedom for pixel circuit design. Therefore, an efficient transfer process could enable the successful integration of micro-LEDs with flexible substrates without degrading its efficiency while also providing a means to scale their assembly and enhance their performance over large-area platforms.

1.2 Background review

In order to transfer micro-LEDs from a rigid growth substrate onto a flexible disparate substrate, several techniques have been developed. In this section, the recent progress and challenges in developing flexible micro-LED displays are presented.

The direct transfer of micro-LEDs onto flexible substrates was initially realized by bonding micro-LEDs using a thick layer of silver paste onto a plastic substrate followed by a laser-liftoff (LLO) process [8]. However, the interface between the micro-LEDs and plastic was not optimized and the thermal shock from the laser processing caused the degradation of the LED electroluminescence during the transfer. Additionally, the difficulty in patterning the silver-paste bonding layer limited the selective integration of the micro-LEDs. As a result, a selective low-temperature integration process needs to be developed to maintain the micro-LED performance during the transfer.

Earlier reports also demonstrated that mechanical bending degraded the optoelectrical characteristics of the GaN LEDs on flexible substrates [9, 10]. For flexible GaN micro-LEDs, the change in the piezoelectric field inside the quantum well can alter the induced interface charges within the heterostructure and consequently changes the quantum efficiency of the device. In addition, the LED peak emission shift under mechanical bending is another unwanted issue that needs to be addressed [11]. Different strategies have been suggested to mitigate the degradation under mechanical strain such as embedding the devices in the neutral plane of the flexible substrate [12]. However, further processing steps increases the complexity and the fabrication-cost. Thus, the development of a novel low-cost micro-LED geometry,

which is insensitive to external mechanical bending, is required and would benefit the development of flexible displays.

While most of the plastic substrates have very poor thermal conductivity, the thermal stability of the micro-LEDs due to the self-heating effect should be considered in developing flexible displays. In addition, for using the micro-LED for wearable or photo-stimulation applications the generated heat should be effectively extracted from the display [13]. Studies have also found that the LED self-heating degrades the optoelectrical characteristics of the LED leading to decreasing optical power and a red-shift of the emission spectrum due to the bandgap shrinkage [8, 14] -. A plastic substrate coated with a layer of graphene was proposed to improve the thermal characteristics [17]. However, the poor adhesion of the graphene thin-film limited the development of the post-integration process at low-temperatures [17]. As a result, an improved system design and integration approach is necessary for addressing the self-heating effect and maintaining the micro-LED performance on thermally insulating plastic substrates. Also, the necessity for integrating high-capacity and typically larger batteries for portable applications can be mitigated by reducing the power consumption through enhancing the brightness without increasing the applied operating voltage. To address this requirement the light extraction of the GaN micro-LED should be maximized and the non-radiative carrier recombination needs to be minimized. The light extraction of the GaN micro-LEDs is limited by the high refractive index of the material itself [1]. It was shown that the light extraction efficiency can be improved by employing thinner LED epitaxial layers [18]. The LED epitaxial structure typically consists of a several microns thick buffer layer grown on the sapphire

substrate to separate the active region of the LED from the defective interface. Earlier reports showed flip-chip bonding of the micro-LED onto another substrate and thinning the backside can reduce the series resistance and improve the optical performance [19, 20]. However, the choice of the reflective metals on the p-GaN surface are limited to a few metals such as Ni/Au and Ag which can make an ohmic contact to the p-GaN layer and are not optimized for a wide range of emission wavelengths. As a result, a new combined integration-fabrication approach compatible with a variety of reflective layers should be developed to eliminate the unwanted series resistance of the defective layer.

In addition, for developing a full-color micro-LED display, the intensity of the emitted photons from each individual LED should be uniformly irradiated through the top of the device. An earlier report showed that the blue and green GaN-based devices have a broader emission angle compared to red GaAs-based LEDs which causes an angular color mismatch in a full-color display [21]. To solve this issue, various groups have attempted filling the gap between the micro-LEDs with a black polymer to limit the amount of light emitting from the LED sidewall [21, 22]. Although this method may minimize the angular color mismatch, the display power consumption can be increased due to wasting a portion of the emitted photon that is absorbed by the black matrix material. Employing a reflective metal layer surrounding the micro-LED sidewall may improve the directional emission of the LEDs and decreasing the device power-consumption by recycling the side-emitted photons. It was also shown, for infrared photodetectors [23], a surrounding gate electrode on the passivated sidewalls can effectively minimize the surface leakage current and defect-assisted carrier recombination at the sidewalls.

While this approach has not been yet employed in micro-LED devices, the gated sidewall structure can deplete the carriers away from the surface states along the LED sidewalls when the diode is forward biased and consequently may decrease the non-radiative carrier recombination.

1.3 Thesis Structure

This Ph.D. dissertation is organized as follows: the first chapter provides an introduction to micro-LED displays and their advantages over LCDs and OLEDs. A brief review of the previously developed technologies for transferring LEDs from the growth substrate onto a disparate substrate and the challenges in realizing a low-power and optically stable wearable displays are also presented in Chapter 1. Chapter 2 covers the feasibility of driving GaN micro-LEDs with a-Si:H-based thin-film transistors (TFTs) by using a direct transfer integration approach. Chapter 3 presents a novel inverted pixel circuit demonstrated by using a "paste-and-cut" integration approach to improve the pixel circuit performance and decrease the power consumption. Other requirements for developing flexible displays such as mechanical characteristics and thermal properties of devices on plastic are investigated in Chapter 4. Through a finite-element analysis (FEA), it was determined that the applied stress-induced strain near the quantum wells of the micro-LEDs can be negligible for devices with diameters smaller than 20 microns. It was also found that using a copper pad thicker than 600 nm can alleviate the heart generated by the micro-LEDs. Using the developed paste-and-cut approach, micro-LEDs with 20-micron diameter have been integrated onto the flexible substrates to validate the theoretical predictions. In Chapter 5, FEA analysis proposed that a dot-in-wire

structure can be used for developing an optically invariant LED that external mechanical bending allowed mechanical tilting of the light sources. The nanowire (NW) LEDs with a 250 nm diameter were transferred onto plastic to experimentally demonstrate that the light emission wavelength was invariant while the brightness could be enhanced by a factor of two, verifying the FEA studies. Finally, Chapter 6 discusses the improvements that have been made in fabricating highly efficient micro-LEDs through the elimination of the major causes for non-radiative recombination; the LED sidewalls and the defective buffer region adjacent to the active layers of the LED. The latter is accomplished through the removal of the buffer layer after separation of the LED from the process wafer while the former is accomplished using a surround cathode gate electrode to deplete the sidewall of the LED, under forward bias, of free carriers. The thesis concludes with a summary of the total contribution that was made in the field of flexible light sources and proposals for future work.

Chapter 2

Direct-transfer of GaN micro-LED from sapphire substrate onto flexible TFT

2.1 Introduction

For driving micro-LED devices on flexible substrates, a low-cost and scalable technology in conjunction with mechanical durability is required. Thin-film transistors (TFTs) based on low-temperature poly-silicon (LTPS) technology have shown promising results for active matrix (AM) drivers for OLED displays [24], which is already commercialized in the smartphone market. However, LTPS technology has several downsides, such as poor TFT uniformity over large areas, complex fabrication requirements, and high cost [25, 26]. These disadvantages along with additional drawbacks from OLED integration have constrained this technology for being used in large-area and flexible display applications.

Hydrogenated amorphous silicon (a-Si:H) technology, which has been commonly used for AM liquid-crystal displays (LCDs), has an advantage over the LTPS technology in terms of its large-area uniformity, low-temperature fabrication capability, and lower cost. Even though the carrier mobility of a-Si:H TFTs is generally inferior, when combined with the higher performance micro-LED, the display can be operated at the same refresh rate as conventional AMLCDs with higher brightness capabilities. This motivation is used to develop an approach that enables high-resolution and high-efficiency large-area and flexible electronic systems as compared to OLED or AMLCD systems.

In this chapter, the successful driving feasibility of the GaN-based micro-LED integrated onto a flexible 2-TFT (2T) a-Si:H pixel circuit is demonstrated. High-quality a-Si:H TFTs were fabricated using low-temperature processes to allow direct integration onto flexible polyethylene naphthalate (PEN) substrates. After the fabrication of the TFT pixel, the micro-LED was flip-chip bonded (p-GaN down) onto the flexible TFT and transferred onto the flexible pixel circuit using a selective laser lift-off process. The goal was to demonstrated the electrical and optical characteristics of the pixel circuit show minimal or no degradation after the integration onto flexible substrate in order to demonstrate the efficacy of this approach for making high-brightness, energy-efficient, large-area flexible displays with a-Si:H TFT and GaN-based micro-LED.

2.2 Experimental Details

2.2.1 Integration process development

In order to release the micro-LEDs from sapphire using a laser-liftoff process, each device should first be integrated onto another substrate using a flip-chip bonding process (direct transfer technique). The process was initially developed by bonding micro-LED arrays onto a glass substrate using Au-Au thermocompression and Au-In eutectic methods. For Au-Au bonding, 200 nm Au was electron-beam coated on both silicon and micro-LEDs' surface with a 50 nm Cr adhesion layer. The fresh gold to gold surface was then bonded using a Tresky T-3000-FC3 die bonder at 150°C and 25 Kg/cm^2 force. Unfortunately, the available bonding tool was not able to apply a uniform force over the surface and the poor bonding quality meant that the micro-LEDs could not endure the laser shock (Figure 2.1a). Although the bonding tool was

able to provide a higher force, the sapphire substrate could not withstand forces higher than 25Kg/cm^2. This limitation was mitigated by employing thicker and softer metallic pads. For Au-In bonding, Au-In bilayer (150/2000 nm) was thermally coated on both micro-LEDs and the silicon substrate. Using the same bonding tool, the eutectic bonding was performed at 150°C and forces from 5-25 Kg/cm^2. Although the bonding result was better at the higher force, the melted indium also squeezed out from the micro-LED contact pad that created a short-circuit between neighboring devices (Figure 2.1b). While the process development was limited to this particular bonding tool and the micro-LED were aimed to be bonded onto plastic, the developed Au-In bonding process has been implemented on PEN substrates. An unexpected advantage for using plastic substrates in the bonding process was the plastic's ability to compensate the non-uniform force from the bonding head due to its softness, resulting in a more reliable and uniform bonding at a lower force (5 Kg/cm^2) (Figure 2.1c).

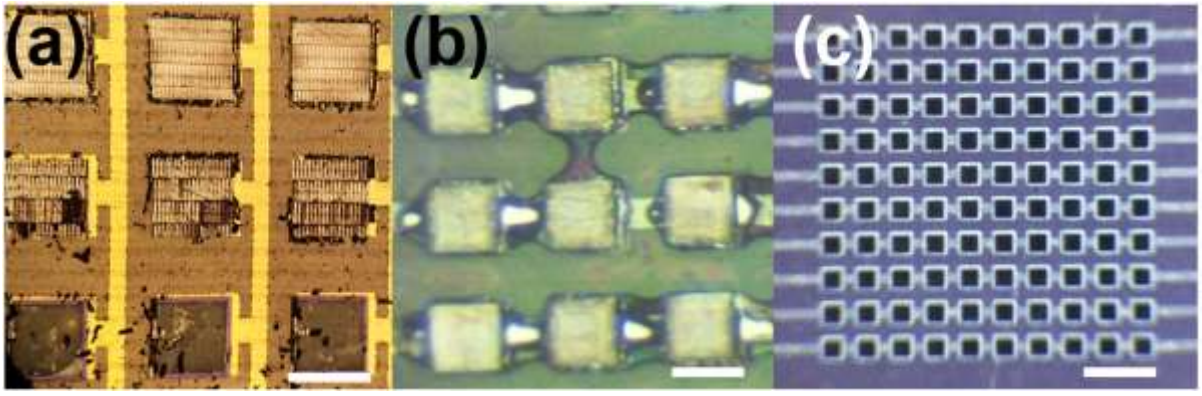

Figure 2.1 optical micrograph of the bonded micro-LEDs by (a) Au-Au (on silicon) (b) Au-In (on silicon) and (c) Au-In (on plastic) materials. The scale bars in (a), (b), and (c) are 90 µm, 90 µm, and 280 µm, respectively.

2.2.2 a-Si:H TFT fabrication on PEN substrates

The a-Si:H TFT fabrication was performed using a conventional back-channel etched (BCE) process with an inverted-staggered bottom gate TFT structure [27]. The maximum process temperature was 170°C. Before the start of the TFT fabrication process, a 500 nm amorphous silicon nitride (a-SiN_x:H) buffer layer was deposited on top of a 125 μm PEN substrate. This procedure minimizes the deformation of the substrate and improves the adhesion of the TFT layers to the PEN surface. A 70 nm thick Mo gate-metal layer was deposited at room temperature on top of the buffer a-SiN_x:H. The gate metal was then patterned followed by depositing a tri-layer structure of 350-nm a-SiN_x:H gate dielectric, 200-nm a-Si:H channel, and 40-nm n^+ a-Si:H source/drain (S/D) ohmic contact layers. The layers were sequentially deposited at 170°C using a 13.5 MHz plasma-enhanced chemical-vapor deposition (PECVD) system. After patterning the active area using dry etching, a 120 nm of Al/Cr (90 nm / 30 nm) bi-layer was deposited for the source/drain metal contacts and patterned. Then, the n^+ a-Si:H layer was dry-etched back to define the channel region followed by another passivation deposition of 500 nm a-SiN_x:H. After opening vias for the gate/source/drain metal contacts, the final one micron thick Al contact was deposited at room temperature and patterned (Figure 2.2a). The completed wafer was vacuum annealed at 150°C for two hours prior to electrical testing.

2.2.3 GaN micro-LED fabrication

Commercially available InGaN multiple-quantum-well (MQW) epitaxial structures (Prolux Advanced Semi-conductors) grown on 500 μm double-side polished sapphire by metal-organic

chemical-vapor deposition (MOCVD) were used to fabricate the micro-LEDs. The epitaxial layers consisted of 2.5 μm undoped GaN followed by 2.0 μm n-GaN, a 100 nm stress compensation n-AlGaN, a 2 μm n-GaN (8×10^{18} cm^{-3}), a low-temperature 200 nm n-GaN (1×10^{18} cm^{-3}), a 60 nm InGaN/GaN superlattice layer, 8 × 3 nm $In_{0.15}Ga_{0.85}N$ quantum wells separated by 10 nm thick GaN barrier layer, 55 nm p-AlGaN electron blocking layer, and finally a 60 nm p-GaN (4×10^{17} cm^{-3}) ohmic layer. First, organic contamination and metal ions on the wafers were removed using Piranha etch (H_2SO_4:H_2O_2 3:1) followed with HCl:deionized (DI) water (1:1) and rinsed with deionized water. A Ni/Au (15 nm / 15 nm) bi-layer was electron-beam evaporated on the p-GaN as an ohmic-contact and then patterned into square shapes to improve the current spreading. To enhance the contact properties, the samples were annealed at 550°C for 10 min in N_2:O_2 (4:1) ambient. After the deposition of a-SiN_x:H at 330°C as an etch mask (Figure 2.2d), the square-shaped micro-LEDs (100 μm × 100 μm) were patterned by inductively-coupled plasma (ICP) etching and the remaining a-SiN_x:H was defined by wet etching (Figure 2.2e). Next, a 300 nm a-SiN_x:H was deposited at 330°C as a sidewall passivation layer. The top contact via of the micro-LED was then opened followed by the deposition of Cr/Au (30 nm / 70 nm) bi-layer on the exposed p-GaN as preparation for bonding and transfer (Figure 2.2f). In addition, the reference micro-LEDs (100 μm × 100 μm) were also made by simply dry-etching of the p-GaN, forming a top p-GaN contact and a bottom n-GaN contact on the sapphire wafer (oriented with the p-GaN facing up), which was used for performance comparisons with the transferred devices (oriented with p-GaN facing down).

2.2.4 Micro-LED integration onto flexible TFTs

To integrate the micro-LEDs onto flexible TFTs, the LED contact via (120 μm × 120 μm) was first opened on top of the TFT source metal pad (Figure 2.2b). Then, a multi-layer Ti/Ni/Au (20/ 70/60 nm) was coated on the n-GaN contact on the micro-LED contact. Thermal evaporation was used to form a 2 μm thick indium layer on the source metal pad of the flexible TFT wafer (Figure 2.2c). The LEDs were bonded onto the indium pad of the TFT circuit using a flip-chip bonder (T-3002-PRO, Tresky) with a pressure of 0.5 N at 150°C. The LLO process selectively detached the micro-LEDs from the sapphire, enabling the transfer onto the TFTs through a 355 nm Nd:YAG laser (Callisto System, V-Technology) having a pulse-width and energy density of 5 ns and 0.9 J/cm^2, respectively (Figure 2.2g). The absorption of the laser at the GaN buffer layer interfaced with sapphire lead to the thermal decomposition of the GaN into nitrogen (N_2) gas and metallic gallium (Ga) when the high-pressure N_2 gas detached the sapphire substrate from GaN. The sample was then heated at 50°C to melt the gallium-rich decomposed GaN interface and remove the sapphire substrate (Figure 2.2h).

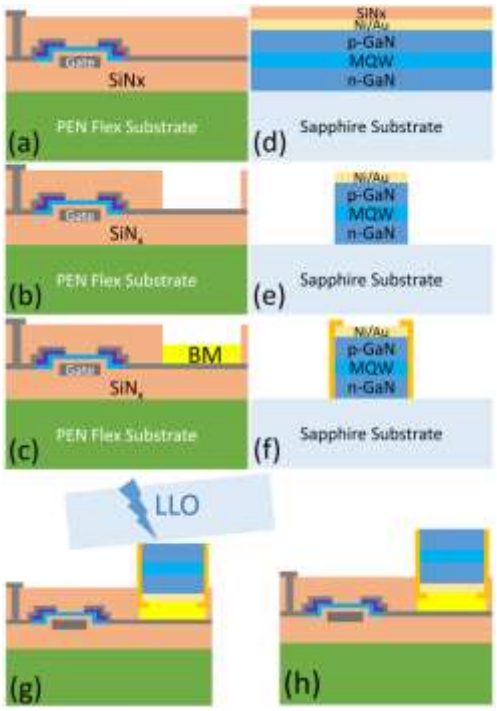

Figure 2.2 (a-h) Optical Figure: The process flow diagram of the integration of TFT and micro-LED on a flexible substrate (BM=Bonding Metal).

2.3 Optoelectrical Characteristics of the Flexible Pixel

The electrical properties of micro-LEDs were measured as isolated devices on the original sapphire substrate and compared with the micro-LEDs after transferring onto the flexible TFT wafer. In the former structure, the bare n-GaN and p-GaN were probed directly with 7 μm Tungsten probe tips. After the transfer process, because the p-GaN was bonded onto the source contact pad of the flexible TFT, the positive voltage contact was accessed through a metal pad pre-arranged on the TFT layout to supply the current to the micro-LED, while the exposed n-GaN was probed directly. The electroluminescence (EL) intensity of the micro-LEDs was measured by an optical fiber and a spectrometer (Ocean Optics, Flame system) after integrating the topside emission through two objective lenses.

The single-pixel measurements were carried out in two phases. First, the two voltage sources (Keithley 2400 and 6430) were applied to observe the EL intensity of the micro-LEDs under various gate biases (V_{data}) while the V_{DS} was kept constant at 20 V. Then, the 2T pixel circuit was fully engaged through an external driving scheme using a commercial micro-controller (Arduino-Mega) and level-shifting amplifiers. The row-select signal (V_1) and the data signal (V_{data}) were driven to accommodate a 60 Hz refresh rate to mimic the signal scheme of a conventional AMLCD display panel. In both test cases, the EL intensity and the output current of the micro-LEDs were measured and compared for the entire V_{data} range in order to characterize both the a-Si:H TFT and the driven micro-LED within the display pixels.

Figure 2.3a shows the fabricated 2T driving circuit on the PEN substrate before micro-LED integration. The overall size of the pixel was 0.25 mm^2 excluding probing pads, which translated to a resolution of 50 dots-per-inch (dpi). This resolution is suitable for large-screen television. For higher resolution displays having smaller micro-LED, the W/L of T_0 could be reduced. Figure 2.3b shows the completely transferred micro-LED on the flexible TFT pixel circuit with the micro-LED illuminated using two probes connected to both diode terminals.

Figure 2.3c shows the I-V of the micro-LED before and after transfer onto the flexible substrate. For both cases, the desired light-on voltage of 2.7 V and near-identical I-V behavior were observed. It has been reported that decreasing the ohmic contact area leads to increasing light-on voltage [28]. In this case, it should be noted that the low light-on voltage obtained was due to the optimized ohmic contact on the p-GaN that maximizes the contact area. In addition, near-identical leakage current in the negative bias-voltage range indicates the absence of any

measurable degradation of the quantum wells during the transfer process (shown in the inset of Figure 2.3c).

The comparison of EL intensity of both the reference sample on sapphire and the transferred micro-LED revealed an identical peak emission wavelength of 445 nm at 1 A/cm^2 current injection (Figure 2.3d). The micro-LED bonded onto the flexible substrate showed a 25% boost in EL intensity. This enhancement is due to the upward reflection of light by the Cr/Au bi-layer on the flipped p-GaN contact. These results indicate that the transfer process preserved the original electrical and optical properties of micro-LED after integration with a-Si:H TFTs on the flexible substrate.

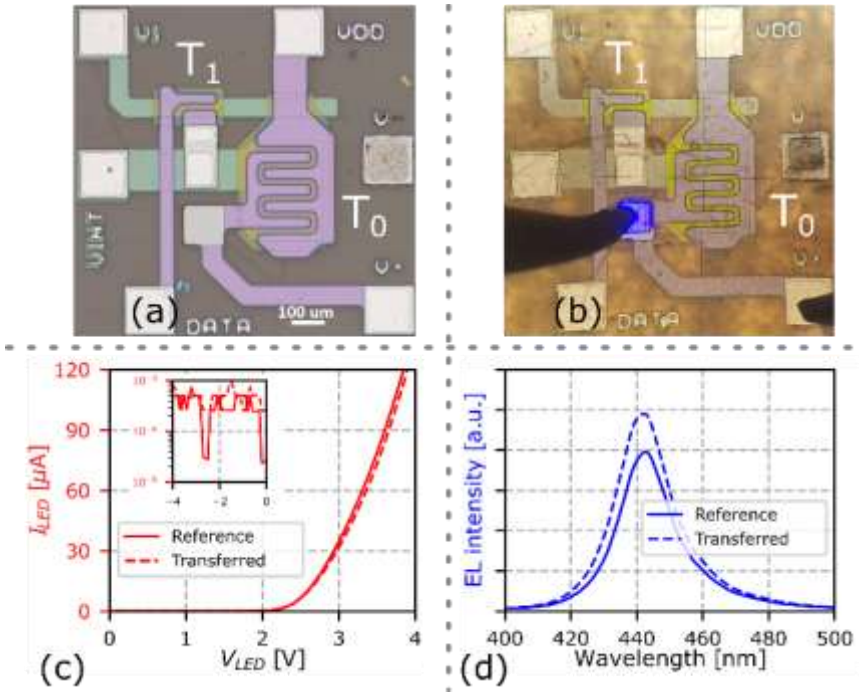

Figure 2.3 (a) The 2T pixel circuit before micro-LED transfer. (b) The 2T pixel circuit after transfer with micro-LED illuminating. (c) The I-V curves in positive voltage region (negative voltage region in the inset) and (d) the EL intensity of the micro-LED on the sapphire wafer with p-GaN facing up (Reference) and the transferred micro-LED on the flexible substrate with p-GaN facing down (Transferred).

When tested with T_0 only (Figure 2.4a), the supply current of the micro-LED ranged from 0.9 μA to 26 μA, as shown in Figure 2.4d. On the other hand, when tested with the 2T pixel circuit (Figure 2.4b), the operation was divided into two parts; the programming and emitting phases. As shown in Figure 2.4c, during the programming phase, V_1 was set high to 20 V, such that T_1 was switched on, and V_{data} could charge the V_{int} node to the desired voltage. At the start of the emitting phase, V_1 was turned low to 0 V, such that T_1 entered a high impedance mode, which cut off the V_{int} due to the interference of the toggling V_{data}. This high-to-low transition of V_1 causes a considerable charge-injection loss on the V_{int} node, which resulted in lower output current in the emitting phase ranging between 0.75 μA to only 17 μA (Figure 2.4d). This reduction of supply current is significant compared to the current supplied by only T_0. One constraint of designing pixel circuits on flexible platforms is the larger design rule constraints to alleviate the misalignment of multiple mask layers due to feature distortions on the flexible substrate as compared to a glass panel. Considerations such as higher thermal expansion coefficient mismatch and the thermal budget of the TFT process results in a higher misalignment between the TFT layers. Consequently, the gate-to-source electrode overlap area of T_1 is increased resulting in a larger gate-source-contact overlap capacitance ($C_{GS,1}$) and more charge-injection loss caused by the high-to-low transition of signal V_1.

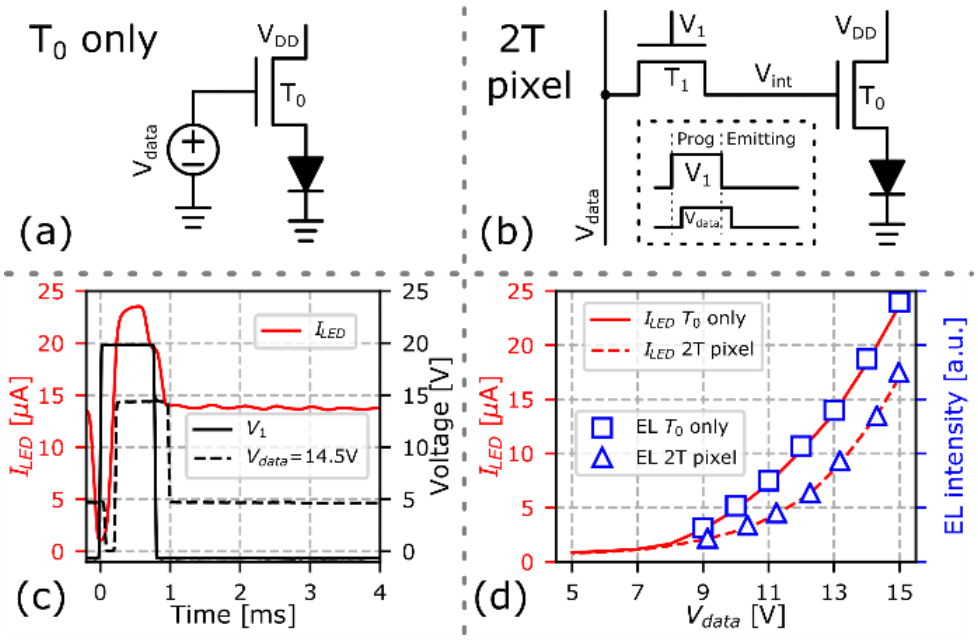

Figure 2.4 (a) The micro-LED driven by T_0 only. (b) The micro-LED driven by a 2T pixel circuit. (c) The first 4ms of transient voltage waveforms of the input signals V_1 and V_{ada}=14V and the corresponding output current I_{LED}. (d) The output current I_{LED} vs. V_{data} and the EL intensity of the micro-LED from V_{data} = 9V to 15V for both circuits shown in [(a) and (b)].

Figure 2.5a shows the EL intensity vs. wavelength of the micro-LED in the 2T pixel circuit under different V_{data} for short periods of time (on the order of several minutes). The results indicate that the heterogeneous integration process did not alter the peak emission wavelength under the entire V_{data} range. Also, the EL intensity matched the I_{LED} values so that the brightness of the micro-LED can be precisely determined by the current from T_0. Figure 2.5b shows optical micrographs of the brightness gradient of the micro-LED when operated with the 2T pixel circuit from V_{data} = 9 V to 15 V. At higher voltages, the brightness of the micro-LED showed excellent contrast with a contrast ratio of more than 10000:1 between the V_{data} operating voltages and is comparable to conventional back-lit LCD panels. Figure 2.5c shows the fully integrated pixel circuits on the flexible PEN substrate.

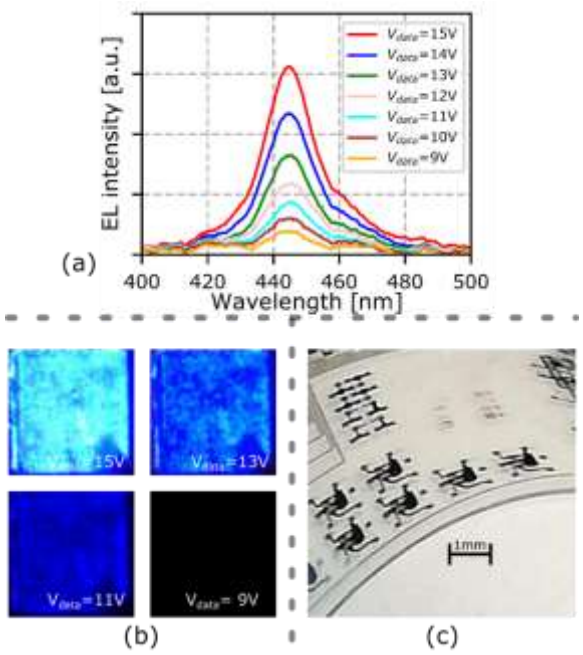

Figure 2.5 (a) The EL intensity vs. wavelength of the 2T pixel circuit at various V_{data} voltages. (b) The 2T pixel circuit light output gradient under different V_{data}. (c) The pixel circuits on the flexible substrate.

2.4 Summary

In summary, the successful integration of a-Si:H TFTs and micro-LED prototypes on flexible substrates was demonstrated. Conventional low-temperature TFT fabrication and a laser lift-off transfer process were implemented to create an addressable pixel circuit on PEN substrates. No degradation in the optoelectronic characteristics of the micro-LEDs was observed after the transfer from sapphire onto the flexible substrate. The integration of a low-cost backplane and a high-efficiency micro-LED provides new opportunities to enable the next-generation of flexible and large-area displays. These results demonstrate the efficacy of using conventional a-Si:H technology as an active driver for flexible micro-LED display technology.

Chapter 3

Demonstrating a low-power and high-brightness flexible micro-LED display with GaN micro-LED integration using a "double-transfer" approach

3.1 Introduction

It was shown, in the earlier chapter, that the high-performance GaN micro-LEDs can be driven by a-Si:H-based TFTs which benefit from high uniformity over a larger area and lower production cost. In addition, due to its amorphous nature, the a-Si:H TFTs can be made on flexible substrates with uniform electrical performance [29, 30]. However, the conventional pixel circuit introduced in the previous chapter is brought from the conventional OLED displays structures [31]. Normally, in the OLED manufacturing process, indium-tin-oxide (ITO) is used as the OLED anode contact and high-temperature annealing should be performed before the emissive layer deposition to achieve a low contact resistance. Due to this OLED process constraint, the OLED pixel circuits are structured with the diode anode-contact facing down on the source side of the drive transistor. Developing an inverted pixel circuit that can lead to lower power consumption and higher brightness motivates the studies in this chapter.

In this chapter, the "double-transfer" process is presented to enable the goal of integrating the cathode of the micro-LEDs onto the drain of the TFTs. Based on experimental measurements, the micro-LEDs driven by the proposed pixel circuit could be turned on with a 33% lower data voltage compared to the conventional pixel circuit, which leads to a higher dynamic range. In

the pixel circuit demonstrated in this chapter, a lower data voltage was required to program the storage capacitor resulting in lower power consumption on the external column data driver for the pixel. Applying the same data voltage to the micro-LED driven by the proposed pixel circuit was able to provide 2.4 times more than the conventional circuits (presented in Chapter 2).

Figure 3.1a shows the schematic of the conventional pixel circuit where the anode of the LED is connected to the source of the driving TFT (T_0). The proposed pixel circuit with the LED cathode connected to the T_0 drain electrode is presented in Figure 3.1b. As shown in the inset of Figure 3.1a, to switch T_0 into the linear mode, in the conventional circuit, the V_{data} voltage needs to be higher than the sum of T_0 threshold voltage (V_T) and the turn-on voltage of the LED (V_{ON}). After integrating the LED onto the drain electrode (shown in inset Figure 4.1b), the source electrode of T_0 is grounded and consequently, the lower bound of the V_{data} only needs to be the threshold voltage of T_0. The V_{data} upper bound remains the same for both the conventional and the proposed circuits (V_{dd}-V_T). By employing the proposed circuit, the dynamic range of V_{data} can be increased from V_{dd}-V_T-V_{ON} to V_{dd}-V_T. As a result, greater grayscales levels are feasible.

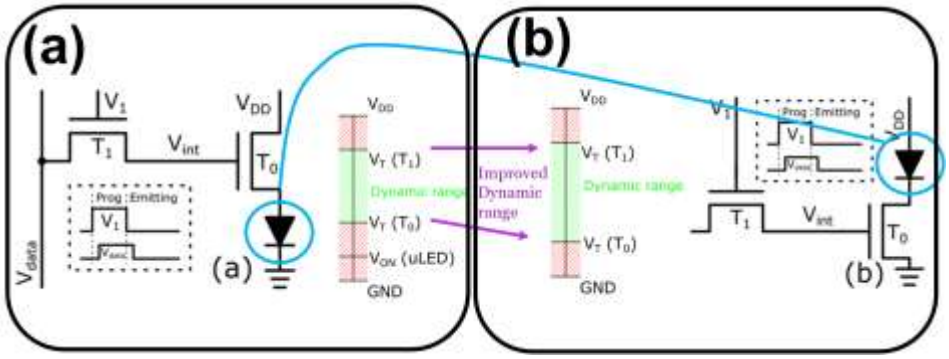

Figure 3.1 Schematic diagram of different configurations for micro-LED and TFT integration where (a) micro-LED's anode is connected to the ground side of the TFT and (b) micro-LED's cathode is connected to the source side. The dynamic ranges of the driving voltage of the micro-LED are shown inset of both figures.

3.1 Experimental details

In order to validate the advantages of the proposed pixel circuit and its compatibility with inorganic LEDs, an array of 2-TFT (2T) pixel circuit was initially fabricated on a plastic substrate and then an array of 90×90 μm^2 GaN micro-LEDs was transferred from rigid sapphire substrate onto the same flexible platform. Each pixel consists of 2 TFTs, one acting like a switch (T_1) and the other as a current driver (T_0) to deliver power to the micro-LEDs. To properly light-up a 90×90 μm^2micro-LED, T_0 is designed to have a W/L ratio of 50, so that the maximum current the pixel could supply approximately 50 µA. The pixel circuit design is 500 × 500 μm^2, resulting in a 50 dots-per-inch (dpi) resolution. The TFT driving circuit is then fabricated on a flexible polyethylene terephthalate (PET) substrate with an industry-standard 5-mask back-channel-etched (BCE) a-Si:H process. The maximum process temperature was set to 170°C to comply with the thermal limits of PET. Using a SiN_x layer as an etch mask, pixelated micro-LEDs (90×90 μm^2) were formed on a sapphire substrate when a Ni/Au (15/15 nm) bilayer was used a transparent ohmic contact to the p-GaN. The sidewall of the mesa was

then passivated using a thin (40 nm) Al_2O_3 dielectric layer. The "paste-and-cut" approach to transfer micro-LEDs onto the flexible platform is depicted schematically in Figure 3.2. By using a temporary wax layer, micro-LEDs were bonded onto a carrier substrate at 80°C using a hotplate (Figure 3.2a). The melted wax surrounded the micro-LEDs due to the capillary force between the wax and the Al_2O_3 passivation layer provided a strong bonding. To detach the micro-LEDs from the growth substrate, a 355 nm Nd: YAG laser beam was irradiated through the transparent sapphire substrate (Figure 3.2b). The wax around the micro-LEDs was etched selectively in a CF_4-based plasma process without degrading the Al_2O_3 passivation layer. As a result, an array of micro-LEDs was anchored from the topside onto a carrier substrate (Figure 3.2c). Afterward, a Cr/Au (30/150 nm) bilayer was e-beam evaporated on the micro-LEDs backside to serve as both n-contact and bonding metal (Figure 3.2d). In order to integrate the micro-LEDs onto flex, a tri-layer of Ti/Ni/Au (20/70/50 nm) and 2 µm indium (In) were evaporated on the drain electrode of the TFTs. A low-temperature (150°C) flip-chip bonding process was employed to bond the micro-LEDs onto the flexible driving circuit (Figure 3.2e). Because of the solubility of the wax in acetone, the carrier substrate was then released after the bonding process by immersing the structure in warm acetone for 1 min (Figure 3.2f). The scanning electron microscopy micrograph of the micro-LED bonded on the carrier after the LLO process and the release of the sapphire substrate is shown in Figure 3.2g. Noticeably, micro-LEDs are strongly bonded onto the carrier substrate without any disorder. Figure 3.2h presents the cross-sectional SEM micrograph of the micro-LEDs after dry etching of the excess wax layer. As shown in the inset, the wax layer and epitaxial layer thicknesses were 3 µm and

6.5 µm, respectively. Optical micrograph of the bent display structure with an 8 × 8 active matrix driver is provided in Figure 3.2i**;** where a thin polyethylene naphthalate (125 µm) serves as the substrate. The inset shows the optical micrograph of the successful integration of the micro-LEDs with active matrix driving TFTs on the flexible platform. Each pixel circuit consists of a 2T driving circuit and a micro-LED integrated using an indium bonding-pad.

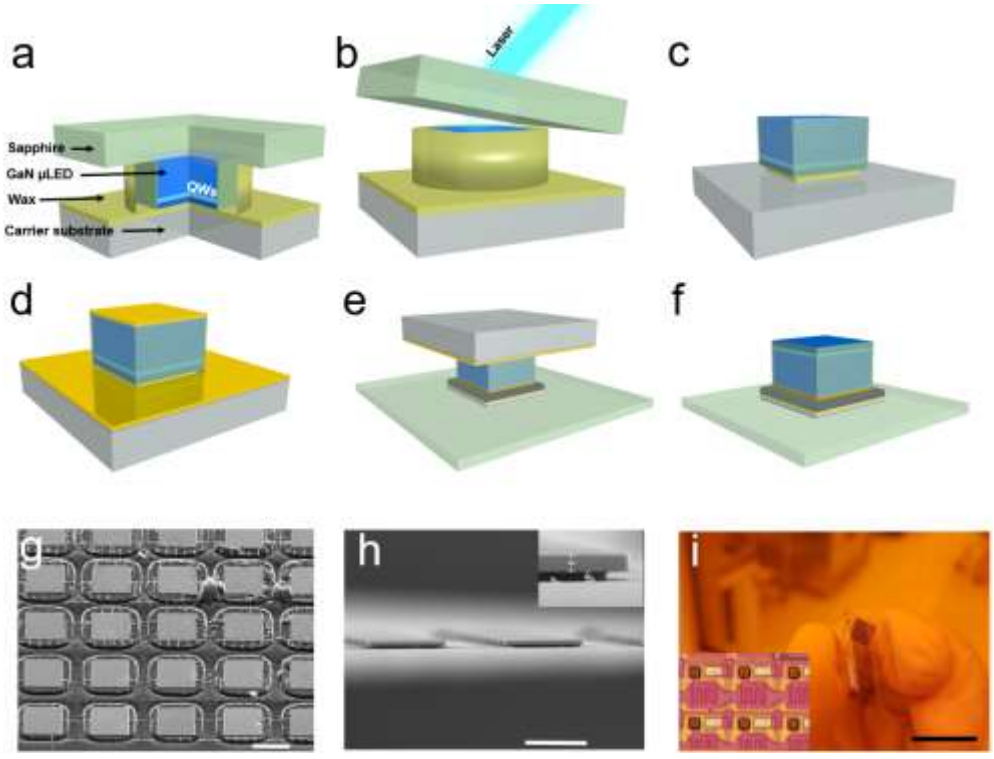

Figure 3.2 Schematic of the "paste-and-cut" process for transferring micro-LEDs from the rigid sapphire substrate onto the flexible platform. (a) Bonding micro-LEDs onto the temporary carrier substrate using a wax layer. (b) LLO process and removing the sapphire substrate. (c) µµDry etching of the excess wax around the micro-LEDs. (d) Coating a Cr/Au bilayer on the backside of the devices. (e) Flip-chip bonding of the micro-LEDs onto the indium pads on the flexible substrate. (f) Removing the carrier substrate after immersing the structure in warm acetone. (g) SEM micrograph of the micro-LEDs on the carrier substrate after removing the sapphire. (h) Cross-section SEM micrograph of the micro-LEDs after etching the excess wax layer. (i) Optical micrograph of the flexible display after successful bonding of the micro-LEDs onto the drain electrodes. The scale bar in (g), (h), and (i) are 90 µm, 70 µm, and 1 cm, respectively.

3.2 Results

The optoelectrical properties of the GaN micro-LEDs before and after transfer onto flex were characterized to investigate the effect of the transfer process on the devices' performance. Figure 3.3a shows the electrical characteristics of the micro-LEDs measured initially on the sapphire substrate and after transferring onto the PET substrate. Comparing the characteristics, no measurable electrical degradation was observed after the double-transfer process with an identical ON-voltage of 2.5 V. However, the series resistance of the micro-LED showed a 20 Ω increase after the transfer on flex. The schematic p- and n-GaN electrodes in both lateral and vertical structures are shown inset Figure 3.3a. The excess series resistance of the vertical micro-LED is due to the un-doped buffer GaN layer; while the highly doped n^+-GaN was directly probed for LED on the sapphire.

The electrical performance of the transferred micro-LEDs under mechanical strain is another important characteristic that enables the flexible display. This property was initially examined by measuring the I-V characteristics of the transferred micro-LEDs located at the array's four corners are shown in Figure 3.3b. The closely matched I-V characteristics in all micro-LEDs exhibit a good uniformity in the device fabrication process without defects generated during the LLO and transfer processes. Figure 3.3c shows the electrical characteristics of the flexible micro-LEDs at the flat state and under different mechanical bending conditions with curvature radius up to 32 mm. As shown in inset Figure 3.3c, the sample has been taped onto curved aluminum holders with concave up and down orientations to generate the compressive and tensile strain states in the devices. The measurement showed no degradation i.e. no shift in the

ON-voltage. A constant 1 nA leakage current and a 1 μA forward current was measured at -5 V and 2.5 V, respectively, for all bending situations. Such identical electrical behavior among all the micro-LEDs can be related to the strength of bonding onto the flexible substrate.

In order to determine the effect of the transfer process on the optical performance of the micro-LEDs, the electroluminescence (EL) spectra of the devices on sapphire and on PET substrate under flat conditions were also measured. Figure 3.3d shows a 15% enhancement in EL of the micro-LEDs after integration onto flex while the peak emission wavelength and FWHM remained fixed at 450 nm and 19 nm, respectively. The constant emission peak suggests that the separation of the micro-LEDs and subsequent integration onto the flexible substrate did not induce additional stress into the QWs region. The micro-LED structures on sapphire and PET are shown schematically inset Figure 3.3d. It is hypothesized that the reflective Cr/Au metallic layer coated on the backside of the micro-LEDs on PET reflects the downward emitted photons upward again which results in a topside emission enhancement. A 3-dimensional finite-difference-time-domain (3D-FDTD) model was used to simulate the optical power of micro-LEDs with and without a backside reflective layer. Figures 3.3e and 3.3f show the simulated optical power at the top side of the micro-LEDs where at the former device a Cr/Au bilayer is integrated at the backside. The simulation shows a 13% enhancement in optical power after the backside of the micro-LED was covered with the reflective metals, is consistent with the experimental results. In order to further increase the light-extraction efficiency, studies on using different reflective layers and optical length will be described in later chapters.

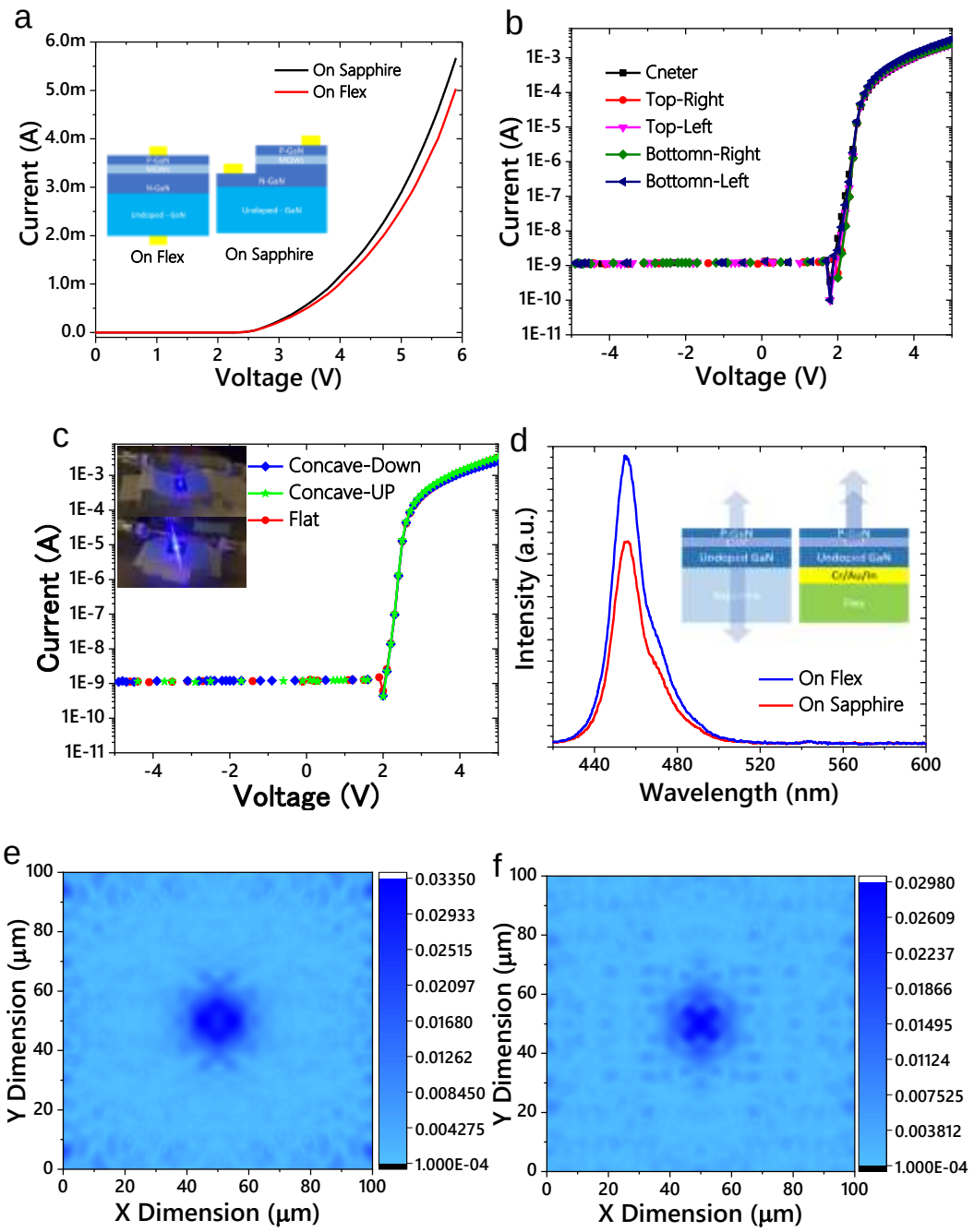

Figure 3.3 (a) I-V characteristics of the micro-LED on sapphire substrate and after transfer onto PEN substrates. (b) I-V characteristics of the different micro-LEDs on flex chosen from the center and four corners of the array. (c) Electrical characteristics of the micro-LED under flat state and under mechanical bending. (d) Measured EL intensity of the micro-LEDs before and after the transfer process. (e) and (f) 3D-FDTD simulated optical power of the micro-LEDs with and without backside reflective metal layer, respectively.

The optoelectrical performance of the fabricated flexible display pixel was characterized under flat conditions and applied tensile and compressive strains. The flexible micro-display was taped onto a curved sample holder and an Arduino Mega micro-controller was used to generate all the input signals (Figure 3.4a). An external digital-to-analog (DAC) and 20 V operational-amplifier ICs are connected to the output of the micro-controller and subsequent output signals of the ICs are sent to the micro-display. The proposed pixel circuit successfully provides a visible brightness under strong ambient illumination. The measured EL intensity of the proposed pixel circuit as a function of the V_{data} is presented in Figure 3.4b. The variation of the EL intensity at the tensile and compressive strains can be related to the change in the field-effect mobility of the TFTs or the change in the GaN piezoelectric fields under mechanical stress. As a result, further studies are necessary for compensating for these changes or minimizing the effect of bending on the device operation. Compared to the conventional driving circuit (presented in Chapter 2), the proposed pixel circuit provided 2.4 times stronger EL brightness under the same driving condition (Figure 3.4c). This enhancement can be explained by grounding the source electrode and accordingly eliminating a voltage drop equal to V_{ON} across the drive TFT after moving the micro-LED to the drain electrode of the T_0. In addition, the EL intensity was detectable by the spectrometer starting from $V_{data} \sim 6V$ while the detection did not occur until $V_{data} = 9$ V for the conventional pixel circuit. As a result, the proposed pixel circuit is generating the expected higher dynamic range.

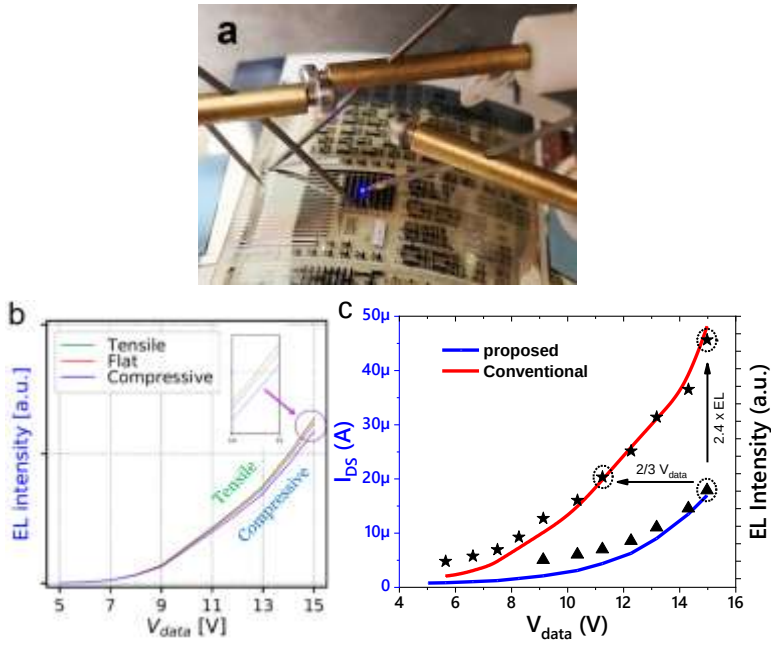

Figure 3.4 (a) The fabricated flexible display taped on a curved aluminum sample holder for measuring the optoelectrical performance. (b) Measured EL intensity of the proposed pixel circuit under different mechanical strain conditions. (c) Comparison between the optoelectrical performance of the proposed and conventional pixel circuit at different Vdata voltages.

3.3 Summary

In summary, a new micro-LED pixel circuit on a flexible platform was developed in order to overcome the deficiencies of the conventional driving circuits. Experimental results of the fabricated pixel circuits on flexible platforms showed micro-LED with 2.4 times higher brightness. Integrating the micro-LEDs onto the drain electrode enabled the pixel circuit to operate at a lower V_{data} voltage. Moreover, the operation of the flexible pixel circuits under mechanical bending showed a negligible variation in EL intensity only due to the a-Si:H TFT mobility variation under external strain. In conclusion, these findings demonstrated a novel insight for integrating and then driving micro-LEDs at lower power on flexible platforms that can be used for next-generation wearable and foldable displays.

Chapter 4

Thermal and Optical Properties of High-density GaN Micro-LED Arrays on Flexible Substrates

4.1 Introduction

The integration of high brightness micro-LEDs onto a flexible pixel circuit was demonstrated in the previous chapter. But the performance of a display on plastic is also affected by the poor thermal conductivity of the plastic substrate and the strain induced by mechanical bending [8, 14]. Flexible substrates, such as polyimide (PI), typically have poor thermal characteristics (thermal conductivity, $\kappa = 1.5\ Wm^{-1}K^{-1}$) resulting in a potential temperature increase during the micro-LED operation [15], [16]. The changes may result in reducing the reliability of the light output and the emission wavelength for display and medical applications, such as in-vivo optogenetic heart pacemakers [32]. In the latter applications, a compact array of micro-LED light sources on a flexible platform is introduced in-vivo for stimulating and monitoring heart activity. Although several technologies have been developed to transfer GaN-based micro-LEDs from their growth substrate onto flexible platforms [33-36], integration of high-resolution and high-performance LED arrays on thermally and electrically insulating plastic substrates still remains challenging. Motivated by finding solutions to these challenges, in this chapter, both the thermal and mechanical properties of the micro-LEDs on the flexible substrate will be investigated with the goal of determining the most efficient structure for wearable display applications. The design will then be fabricated and experimentally verified.

4.2 Mechanical bending simulation and analysis.

A finite element analysis (FEA) model was used to simulate the stress-induced strain in the micro-LEDs on flexible PI substrates with metallic bonding pads (PI/metal). In this study, a constant strain state was induced using a bending radius of 15 mm, with Cu employed as the bonding material. This radius was achieved in the model by using a bending moment of 0.208 N.m, calculated from the Stoney equation, $M = \frac{Ed^3w}{12R}$, applied at the ends of the flexible substrate. In the Stoney equation, E is the elastic moduli, d, w, and R are the flex platform thickness, width, and bending radius, respectively. The strain distribution in flexible micro-LEDs was modeled using this bending stress state for different LED diameters (from diameters, D, of 50 μm to 5 μm) under concave-down (CD) and concave-up (CU) orientations, shown in Figure 4.1a-f. In this simulation, tensile strain states were under CD orientations and compressive strain states were under CU conditions. The induced strain on the active quantum well (QW) region was found to be as high as 2.5×10^{-5} for devices with a 50 micron diameter. As the diameter decreases, the induced strain due to bending was found to decrease and is nearly zero within the QW region for micro-LEDs with D smaller than 20 μm which is in the range of the current wearable display resolution [37]. The results suggest the LED active region should experience very little or no induced piezoelectric field change due to this small mechanical strain and a constant electroluminescence wavelength peak should be observed under bending. To further develop and optimize the flexible LED design, the effect of thermal heating on an insulating flexible platform was studied using micro-LEDs with 20 μm diameters to determine the effect of the bonding configuration on the heat transfer.

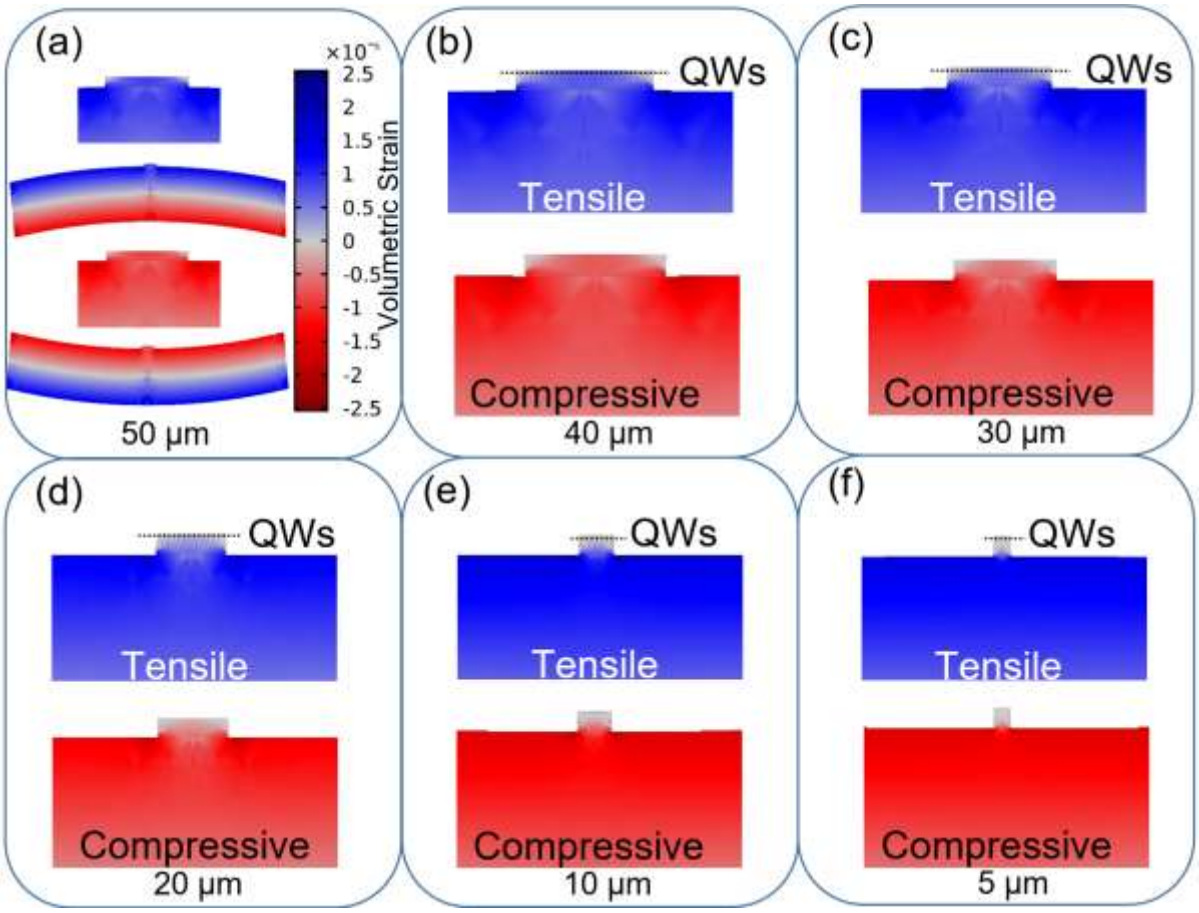

Figure 4.1 The simulated strain gradient for different sizes micro-LED on PI/Cu substrate with concave-down (Tensile stress) and concave-up (Compressive stress) bending radius of 15 mm; (a) 50 µm, (b) 40 µm, (c) 30 µm, (d) 20 µm, (e) 10 µm, and (f) 5 µm. The place of the quantum wells (QWs) is shown by a dashed line.

4.3 Thermal simulation and analysis.

The human eye can detect display color non-uniformities that are greater than 1 nm [38] that may result from a temperature rise due to self-heating of the LED during operation. A maximum allowable increase in temperature of 3°C is required in order to minimize color shifts in the display. In order to understand the impact of the substrate material on the thermal properties of micro-LEDs, three-dimensional steady-state modeling by a FEA method was

developed to simulate the heat flux and temperature distribution in 20 μm diameter micro-LEDs. Figure 4.2a-d shows the temperature distribution due to the generated heat in micro-LEDs using Cu as the bonding layer onto different substrates. Sapphire is also modeled as a reference point for the simulations. The maximum junction temperature of 58.5°C, 63.8°C, 34.8°C, and 26.1°C were achieved for the micro-LEDs on sapphire, PI/Cu/SU8 (150/3/1 μm), PI/Cu (150 μm/100 nm), and PI/Cu (150/1 μm), respectively. Unfortunately, this increase in the temperature, when operating in a room temperature environment, will cause a 9 nm red-shift in peak emission when the temperature of the LED is ~64°C due to the bandgap becoming smaller. The generated heat accumulates underneath the device on a sapphire substrate due to its poor thermal conductivity (Figure 4.2a). Recently, Li *et al.* demonstrated the transfer of the GaN LEDs onto a PI/Cu/SU8 flexible substrate [39]. This strategy was developed with the transfer of lateral (180×125 μm^2) LEDs on flex by using a 1 μm thick spin-coated SU8 polymeric adhesive layer to bond the devices onto flex. The thermal transport simulation of this structure (Figure 4.2b) shows that the polymeric adhesive layer prevented the effective heat-transfer from the micro-LEDs onto the metal-coated plastic where the junction temperature increased after transfer. In contrast, the heat decays more effectively when the micro-LEDs are in direct contact with metallic pads for both PI/Cu (150 μm/100 nm) and PI/Cu (150/1 μm) substrates (Figure 4.2c, d). As the metal thickness increases from 100 nm to 1 μm, the maximum temperature decreased from 34.8°C to 26.1°C. The thicker metal bonding layer in conjunction with the specific heat of Cu provides a larger heat sinking capacity that helps to lower the temperature of the LED active region. This Cu layer acts as a thermal buffer to store

the heat away from the LED while it dissipates through the insulating flexible substrate. While useful as an electrical contact and heat sink, the effect of this bond layer on the heat transfer characteristics was unexpected for such a small surface area. In comparison, the poor heat dissipation for the device on the sapphire accelerates the aging of the device and consequently causes more pronounced optical power reduction over time. Based on the simulation results, the increased heat exchange from the device to its surroundings caused by removing the sapphire substrate and integrating micro-LEDs onto PI/metal substrate can effectively alleviate the unfavorable heat build-up and consequently provides a more reliable platform for long-term operation of the flexible micro-LEDs.

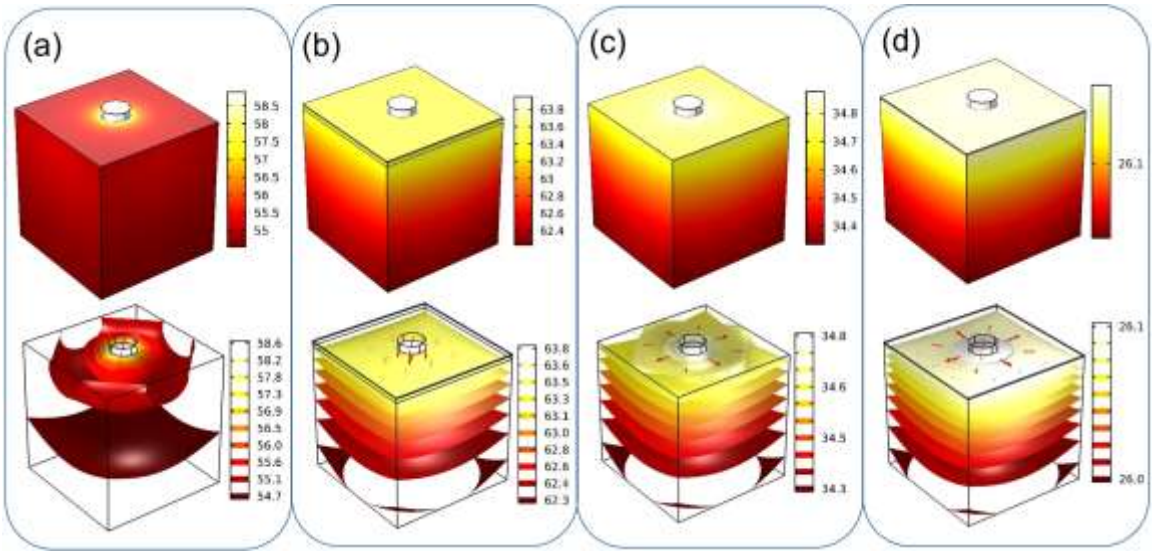

Figure 4.2 Temperature gradient and depth profile of the generated heat by a 20 µm LED on (a) sapphire, (b) PI/Cu/SU8 (150/3/1 µm), (c) PI/Cu (150 µm/100 nm), and (c) PI/Cu (150/1 µm), respectively.

In this chapter, blue light-emitting InGaN micro-LEDs, with diameters as small as 20 µm were transferred from sapphire substrates onto flexible platforms in order to investigate the effect of the adhesive layer and LED geometry on device performance. Simulations of the heat transfer

characteristics and modeling of the effect of externally applied mechanical stress within the LED/flexible substrate structure were investigated to optimize the diode performance. These models were examined experimentally with a demonstration of a robust array of 20 μm LEDs emitting at 450 nm had stable optical wavelength luminescence operating at 1 A/cm^2. The chosen 20 μm diameter can enable high-resolution displays [22] but at the expense of increasing the sidewall surface states. This design is ideal for scaling the LED for smaller pixels at the expense of increased surface states that may affect its brightness. The latter will be addressed in Chapter 6. Based on the modeling and experimental results, a flexible micro-LED array was demonstrated on the flexible PI/metal platforms that maximize the heat dissipation and optical output from the light emitters on plastic platforms.

4.4 Experiments Details

In order to validate the simulation results, the integration of a high density of LEDs onto the PI platform required an aggressive design to incorporate both small device geometry with selective metallic bonding. The major process steps involved in making a GaN micro-LED flexible display are schematically presented in Figure 4.3. In this approach, the key process is a "paste-and-cut" technique to release the micro-LEDs from a rigid sapphire substrate, transferring them onto flex. The micro-LEDs with a Ni/Au ohmic contact on the p-GaN were initially fabricated on sapphire using a chlorine-based dry etch. The devices were then passivated using Al_2O_3 thin film. After the LED structures were processed, the micro-LEDs were bonded onto a carrier substrate using a spin-coated temporary adhesive layer (Figure 4.3a). The removal of the sapphire substrate was performed by irradiating a 355 nm Nd:YaG

laser through the transparent sapphire to decompose the GaN layer at the interface with the sapphire (Figure 4.3b). Afterward, an O_2-based plasma dry etching process was carried out at room temperature to remove residual adhesive from the carrier surface. As illustrated in Figure 4.3c, the adhesive layer keeps the micro-LEDs mainly arranged on the carrier substrate while the oxygen plasma had no adverse effect on the passivation layer. The backside of the micro-LED was then coated by a tri-metal layer Cr/Cu/Au as a bottom contact, heat-sink, and bonding metal (Figure 4.3d). The passivated sidewalls prevent the short-circuit between p and n contact while the directional physical-vapor deposition (PVD) of the p- and n-metal layers have been used to minimize sidewall coverage. The micro-LEDs on the carrier substrate were then flipped over and bonded selectively onto the patterned Au/Sn contact pads on flex (Figure 4.3e). Figure 4.3f schematically shows the final selective-transfer of a column of micro-LEDs onto flex after the “paste-and-cut” process.

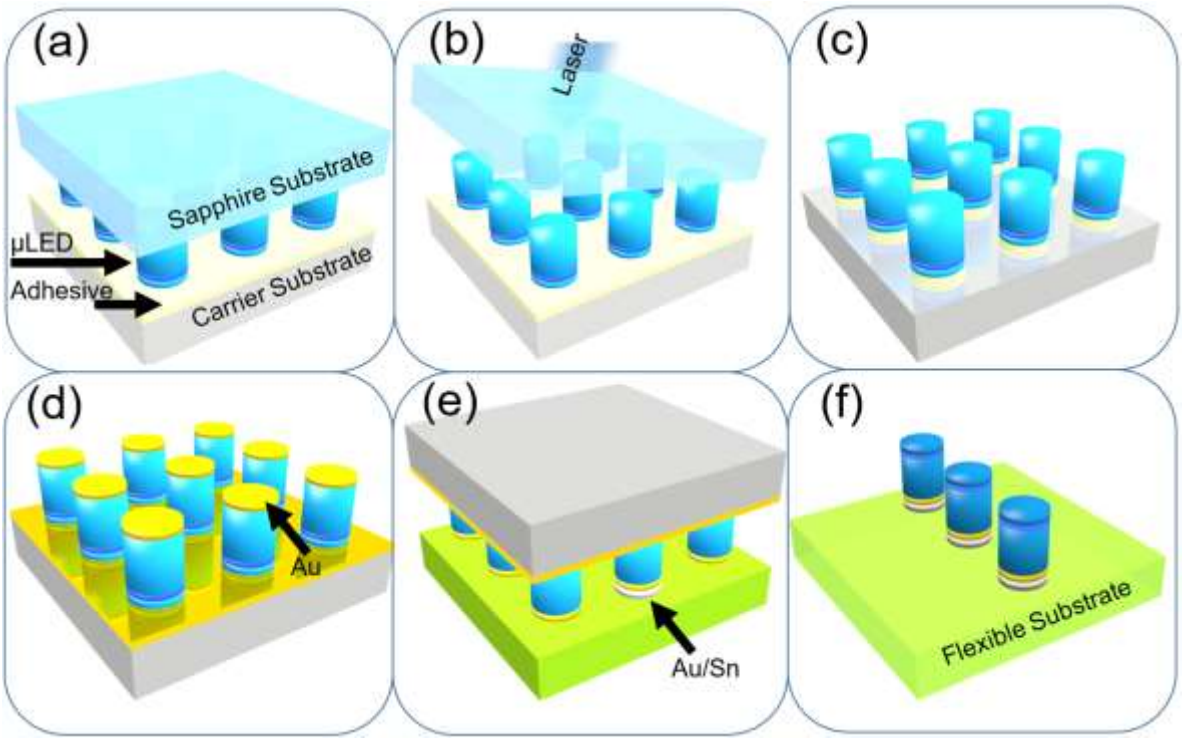

Figure 4.3 Schematic of the process flow for the selective mass-transfer of the GaN micro-LEDs from a sapphire substrate onto a flexible substrate; (a) bonding the micro-LEDs onto a carrier substrate through their p-side, (b) laser-liftoff and releasing the sapphire substrate, (c) dry-etching of the adhesive layer from the unwanted area in an oxygen plasma, (d) Coating of the micro-LEDs' backside with a Cr/Cu/Au (triple layer). The Au surface is shown by an arrow. (e) Flip-chip bonding of the micro-LEDs onto the desired places where Au/Sn pads are patterned, (f) releasing the carrier substrate.

4.5 Results

Figure 4.4a shows the plan-view scanning electron microscopy (SEM) micrograph of the 20 microns diameter micro-LED arrays with 40 μm pitch size after transfer on the carrier substrate when the sapphire substrate is removed by laser-liftoff. The strong uniform bonding of the micro-LEDs onto a carrier substrate resulted in a high yield for the first transfer. Figure 4.4b shows the SEM image of the micro-LEDs after integration onto the flex. The image shows no reasonable deformation of the flex and the structural integrity of the Au/Sn eutectic bonding indicates a strong interface between the micro-LEDs and the flex. In order to achieve a high

yield in the transfer process, the temporary bonding layer should be sufficiently selective to allow release the micro-LEDs after bonding on the flex and robust enough to keep the devices fixed during the LED processing. In contrast to conventional pick-and-place processes that use lateral anchors to keep devices fixed at their place during the release and transfer process, [40] this design bonds the micro-LEDs to the carrier substrate through the LED backside and enables higher resolution mass-transfer that is applicable for processing high-resolution displays. After surface planarization using bisbenzocyclobutene (BCB), a thin transparent conductive oxide layer was coated on the micro-LEDs to form a common anode contact.

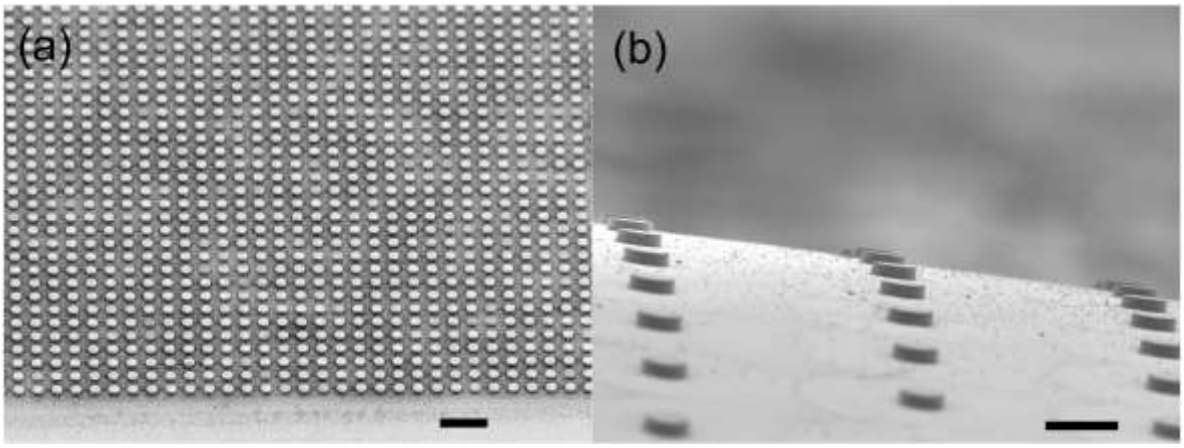

Figure 4.4 Plan view scanning electron microscopy of the (a) 20 μm micro-LED arrays transferred onto the carrier substrate after removing the sapphire substrate by laser-liftoff, (b) selective-mass-transferred micro-LEDs on the large-scale flex by using Au/Sn-based eutectic bonding. The scale bars at (a) and (b) are 100 μm and 20 μm, respectively.

Figure 4.5a shows the I-V characteristics of discrete 20 μm diameter micro-LEDs on sapphire substrates and after transfer onto the flex. The electrical performance of the micro-LED shows no measurable degradation after the "paste-and-cut" and both I-Vs are comparable. The measured diode leakage current density, in the order of 10^{-4} A/cm^2, indicates no emergence of defects in the active region due to the laser-liftoff process.

In order to investigate the variation of the electrical performance of the flexible micro-LEDs, 25 random devices were selected from the center and the four corners of the array and their electrical characteristics were measured under flat condition. Figure 4.5b shows the variation of the series resistance over the 25 devices. The maximum measured series resistance was 623 Ω and the minimum was 604 Ω, with a 2% variation in the series resistance over the whole array. The uniform series resistance at the center and four corners of the flexible device indicates that the contact degradation due to eutectic bonding is negligible. The variation in the threshold voltage of the micro-LEDs (the same means of Figure 4.5b) is presented in Figure 4.5c. The average threshold voltage was 2.5 V with 1.6% deviation that points out a 108% electrical contact efficiency, defined as V_p/V, where V is the operating voltage and V_p is the photon energy ($V_p = h\upsilon/q$; $h\upsilon$ is the photon energy and the *q* is the elemental charge unit). As has been reported earlier, [41] during low current density and low-temperature operation, V_p/V can exceed unity if the p-GaN ohmic contact is optimized.

Further characterization under mechanical strain was performed to evaluate the LED performance under bending. Mechanical test stability of the flexible micro-LEDs was performed by measuring the I-V characteristics with the devices having a bending radius of R = 15 mm concave-down. Figure 4.5d shows an identical I-V behavior of the micro-LEDs under both flat and bent (R = 15 mm) conditions, which demonstrate the mechanical stability of the flexible devices. Comparing the electroluminescence of the 20 μm LED on sapphire and after transfer on the flexible substrate shows an identical full-width half-maximum of 19 nm (Figure 4.5e). However, the EL of the device on the flex increased by 20% that can be explained by

the reflection of the downward-emitted photons from the backside metal electrode (Cr/Cu/Au). The C.I.E. 1931 color-space diagram of the fabricated micro-LEDs with x = 0.1527 and y = 0.0224 is shown as an inset in Figure 4.5e. To further investigate the effect of the bending on the emission properties of the flexible micro-LEDs, the EL spectra were measured at 1 A/cm^2 (to maintain low-injection conditions) [42] under flat, tensile, and compressive strain states, having a bending radius of 15 mm. Unlike previous reports with planar LEDs [43], the flexible micro-LED shows identical EL characteristics without an emission shift in the flat position and under all bending radii (Figure 4.5f). These larger flexible LEDs of 1×1 mm^2 showed a much greater emission shift of 3.8 nm due to the applied strain on the QW region. The experimental results are in agreement with the simulations, supporting the small bending stress inside of the QW region for the 20 μm diameter flexible micro-LEDs predicted by the model. This prediction and observation support the development of high-resolution flexible displays where the higher resolution provides both a visual as well as performance boost.

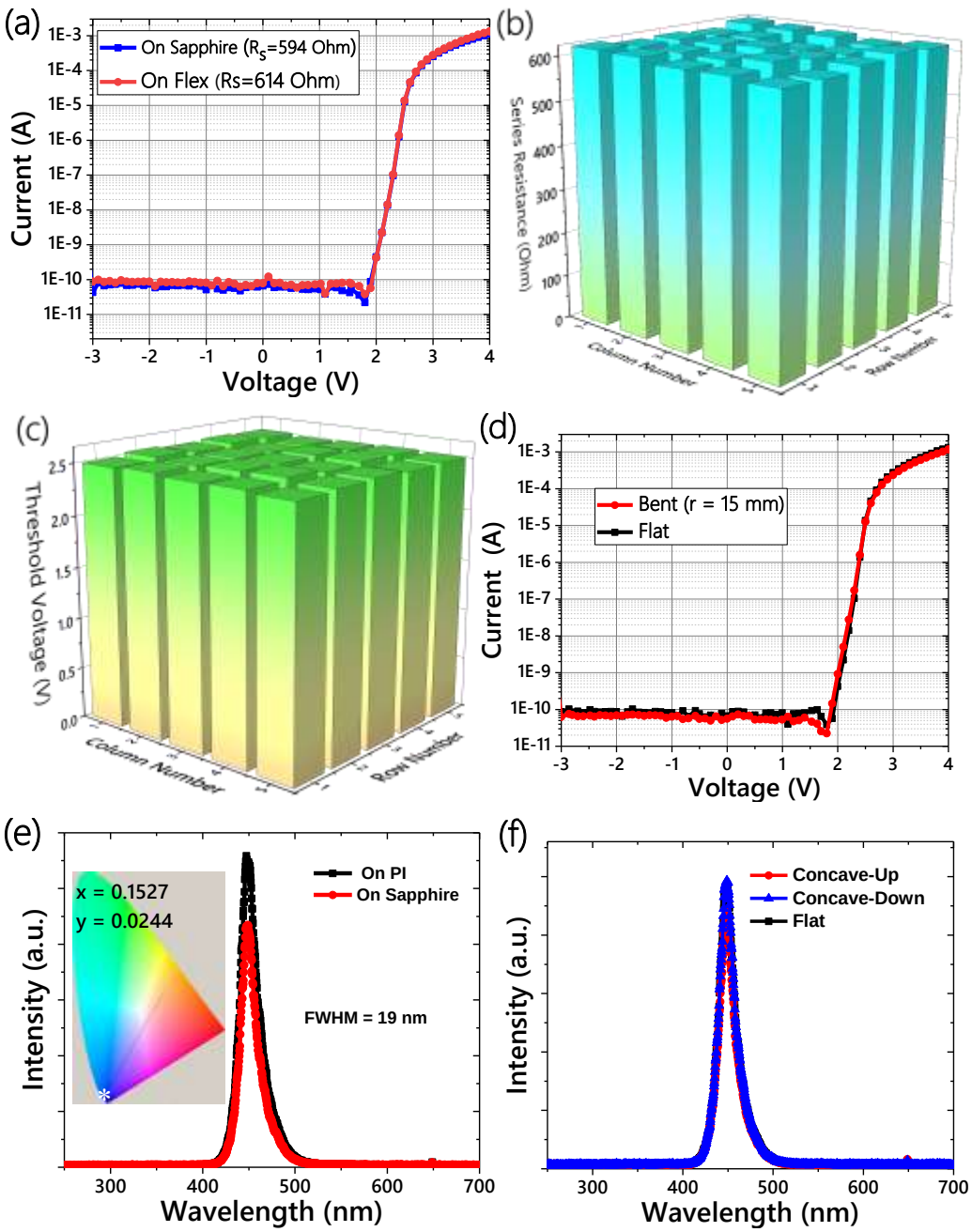

Figure 4.5 Electro-optical characterization of the 20 µm diameter micro-LEDs (a) The I-V characteristics of a micro-LED before transfer (on sapphire) and after transfer onto the flex. The series resistance (b) and threshold voltage (c) variation of the micro-LEDs after transfer onto the flex. The micro-LEDs are chosen from the center and four corners of the array. (d) I-V characteristics of the flexible micro-LED under flat and bending conditions. (e) EL before and after transfer. The inset presents the C.I.E 1931 color-space diagram of tested micro-LEDs (f) EL under different bending conditions.

In order to confirm the thermal simulations, the effect of the copper bonding on the thermo-electrical characteristics of the devices was investigated for several Cu thicknesses. The micro-LEDs released from sapphire were transferred onto a polyimide substrate with different Cu pad thicknesses of 100 nm, 300 nm, 600 nm, and 1 µm. Figure 4.6a depicts the EL characteristics of the un-encapsulated micro-LEDs on various copper pads driven continuously at 1 kA/cm^2. Compared to emission characteristics of micro-LEDs on 1 µm copper, the peak emission shift of 5, 3, 2 nm were measured for micro-LEDs on sapphire, and copper thicknesses of 100 nm, and 300 nm on PI, respectively. The EL characteristics of the devices on 1 µm and 600 nm copper were almost identical. The redshift in peak emission can be related to band-gap shrinkage due to the higher junction temperature in MQWs at the high current density. While the bandgap of the GaN is sensitive to the temperature, the emission peak shift or large temperature fluctuations [44]. These temperature changes may be determined by considering the measured emission shifts, the temperature of the devices was calculated using the following equations:

$$E_g(GaN) = 3.507 - \frac{0.909\times10^{-3}T^2}{T+830} \quad (1)$$

$$E_g(InN) = 1.994 - \frac{0.245\times10^{-3}T^2}{T+624} \quad (2)$$

$$E_g(In_xGa_{1-x}N) = (1-x)E_g(GaN) + xE_g(InN) - 3.8x(1-x) \quad (3)$$

where T is the device temperature and $E_g(GaN)$, $E_g(InN)$, and $E_g(In_xGa_{1-x}N)$ are the band gaps of GaN, InN and $In_xGa_{1-x}N$ materials, respectively. The calculated temperature and measured emission shift for micro-LEDs on sapphire and flex with different Cu thicknesses are presented in Figure 4.6b. Noticeably, the generated heat at high current density is dissipated effectively

even by having a copper layer thicker than ~ 600 nm on flex, corresponding well to the values predicted by the simulations.

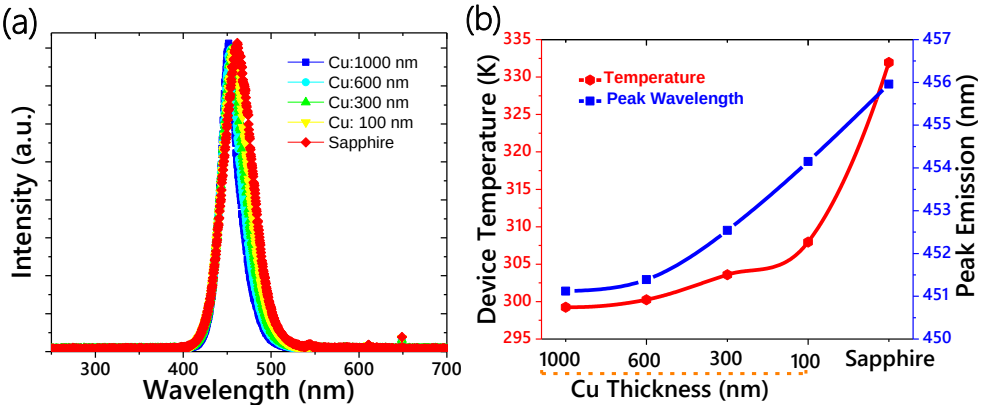

Figure 4.6 (a) Electroluminescence characteristics of micro-LEDs on sapphire and flex substrate with different copper thicknesses driven continuously at 1000 A/cm2. (b) Measured emission peak wavelength and calculated device temperature for devices on different substrates.

4.6 Summary

In conclusion, an array of 20 microns diameter GaN micro-LEDs were transferred from their sapphire process wafer onto flexible substrates. The theoretical modeling of the induced strain states for the LEDs under mechanical bending predicted very small or no induced strain under bending for LEDs having diameters below 20 microns. Experimental results for the micro-LEDs on flexible PI substrates confirmed this prediction and showed no measurable degradation of the optical and electrical properties under a mechanical strain up to bending curvatures of 15 mm. Both the thermal models and experimental results demonstrated plastic substrates coated with a copper pad thicker than 600 nm leads to an effective heat sink on thermally insulating platforms. As a result, these findings offer new insight for potential emitter-detector sensor array systems that would benefit from high-resolution micro-LEDs integrated onto compliant and flexible platforms.

Chapter 5

Optically invariant InGaN nanowire light-emitting diodes on flexible substrates under mechanical manipulation

5.1 Introduction

As it has been discussed in the previous chapter, shrinking the size of the micro-LED down to 20 microns is one solution to eliminate the strain-induced piezoelectric fields in quantum wells. GaN-based "dot-in-nanowire" light-emitting diodes, cylindrical devices that mimics a quantum dot within a nanowire (NW) structure, are also an emerging technology that allows the creation of nanowire LED arrays whose positions may be modulated by mechanically manipulating the flexible platform without introducing strain into the device active region [45, 46]. The emission from an array of LEDs, having a typical diameter of ~ 250 nm, is dependent on waveguide modes coupled through the geometry of the nanowire cylinder and the distance between neighboring devices. Geometric modifications through altering the LED diameter and spacing enables optimal light extraction within a network. Fundamental waveguide modes are established through a fixed periodic array of LEDs that creates a quasi-two-dimensional photonic crystal [47-49]. Earlier reports showed the integration of core/shell InGaN/GaN nanowire LEDs into a flexible polymeric substrate, by embedding the devices within an elastomeric layer [50]. While creating a flexible assembly, with an elastomeric encapsulation of the LEDs, the array of encapsulated LEDs would still experience mechanical strain within the active region of the device during substrate bending. To overcome this issue, the "dot-in-

nanowire" structure where the active region is located out of the plane stress is proposed for fabricating nanowire LEDs on flexible platforms. To confirm the feasibility, both the electroluminescence and the current-voltage (I-V) of the flexible nanowire under bending were characterized to understand the effect of the mechanical bending on the operation of the NW LED structures.

The goal of this chapter is to demonstrate the feasibility and develop an understanding for using vertical nanowire LED structures integrated on flexible substrates to separate the electrically active region of the LED from the bending platform. The work is motivated by minimizing the performance degradation encountered in flexible planar LED structures. This novel nanowire orientation avoids common problems observed in flexible LEDs such as peak emission wavelength shifts and decreased light output during applied mechanical stress [9, 11, 51]. This degradation is due mainly to a strain-induced piezoelectric response affecting the active region of the LED. As bending increases, piezoelectric fields produced in the quantum wells (QWs) create a measurable peak shift in the electroluminescence (EL) characteristics that affect spectral uniformity of the LEDs and degrades the performance of the light-emitters for applications such as solid-state lighting and next-generation displays. This effect is less significant for cylindrical LED structures that are oriented normal to the flexible platform. Under bending the LED devices are free to move since the plane of bending is outside of the active region of the nanowire device [52].

5.2 Mechanical bending simulation and analysis.

A finite-element analysis (FEA) method was used to predict the induced strain and motion of vertically-oriented NW structures on flexible platforms during substrate bending. The FEA model, based on actual structures grown by gas-source molecular-beam epitaxy (GSMBE), consisted of cylindrical nanostructures having diameters of 287 nm separated by a 350 nm pitch positioned on a 3 μm-thick GaN film in contact with a 1 micron thick metallic electrode bonded to a 175 microns thick flexible polyethylene terephthalate (PET) substrate. To simulate the bending stress on the PET substrate, a bending moment, M, applied along the ends of the substrate. The Stoney equation $M = \frac{Ed^3w}{12R}$ was used to calculate the bending moment of 0.02248 N·m for R = 38 mm, where d and w is the substrate thickness and width, respectively, and E is the elastic moduli. Figure 5.1 shows the stress distribution within the substrate and rod structures having a "concave-up" bending radius (bending in the direction of the light emission) of 38 mm. The FEA model shows a stress-induced strain gradient with a compressive strain of 4×10^{-4} at the surface, transitioning through the PET to a tensile strain of 6.5×10^{-4} at the backside of the substrate. The calculations show the stress within the LED structures to be nearly zero, suggesting the active region, near the tip of a cylinder, should not experience induced piezoelectric fields during bending of the substrate that may degrade the I-V characteristics and EL peak position of the light emitter.

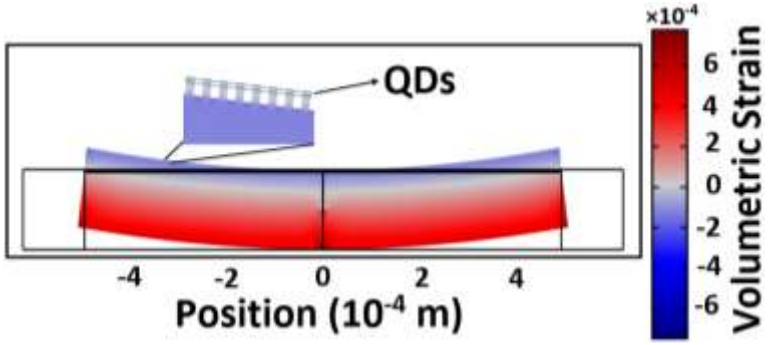

Figure 5.1 The simulated strain gradient for the NW devices on PET with R = 38 mm. The device active region, near the tips of the nanowires, was found to be strain-free. A calculated bending moment of 0.02248 N·m for R = 38 mm was used in the simulation.

5.3 Experiment

In order to experimentally validate the simulations and confirm the bending of the flexible substrate will not alter the optoelectronic properties of the LEDs, the integration of the cylindrical devices onto flexible platforms was achieved through a "paste-and-cut" process. The NW LEDs, grown by GSMBE, possessed a structure similar to the geometry used in the FEA model. After device fabrication, the GaN-based LEDs were bonded onto a temporary handle wafer to allow detaching the LEDs from their original sapphire process wafer [53, 54]. A laser liftoff (LLO) processes enabled the transfer of the GaN-based light emitters from their sapphire growth substrate onto the flexible PET film. This approach has been effective for planar thin-film structures, but the integration of three-dimensional cylindrically shaped optoelectronic devices on flexible substrates has not been demonstrated [55, 56].

Figures 5.2a-d schematically illustrate the process for the LED integration onto the PET. First, the NW LEDs are bonded with an epoxy adhesive onto a temporary receptor substrate (Figure 5.2a). A 266 nm pulsed laser light, with a 5 ns pulse width, was irradiated through the

transparent sapphire substrate. The laser pulse, absorbed by the GaN buffer layer, decomposes a thin region of the GaN at the GaN/sapphire interface. Following a low-temperature (40ºC) anneal to melt the decomposed interface (Figure 5.2b), the GaN LED structures are detached from the sapphire substrate.

The active region of the dot-in-wire LED is located near the tip of the cylinder structure and the transfer process positions this region at the receptor substrate surface, inverting the LED's original orientation and reducing the extracted light extracted. In order to return the device structure to its original orientation, a water-based silver adhesive is applied to the exposed LED back n-contact to bond the LED onto the flexible PET substrate (Figure 5.2c). Submerging the bonded structure in acetone selectively removes the epoxy bond, undercutting the LED structures and releasing the receptor substrate (Figure 5.2d). The silver adhesive now serves as both the bottom n-contact and as an optical reflector to enhance light emission from the LEDs. Figure 5.2e schematically shows the final fabricated dot-in-wire LEDs on the flexible substrate after the two-step "double-transfer" process. Structural characterization of the LEDs after separation from its growth substrate by field-emission (FE) scanning-electron microscopy (SEM), confirmed the efficacy of the transfer process to separate the devices from their original sapphire platform onto the flexible substrate (Figure 5.2f).

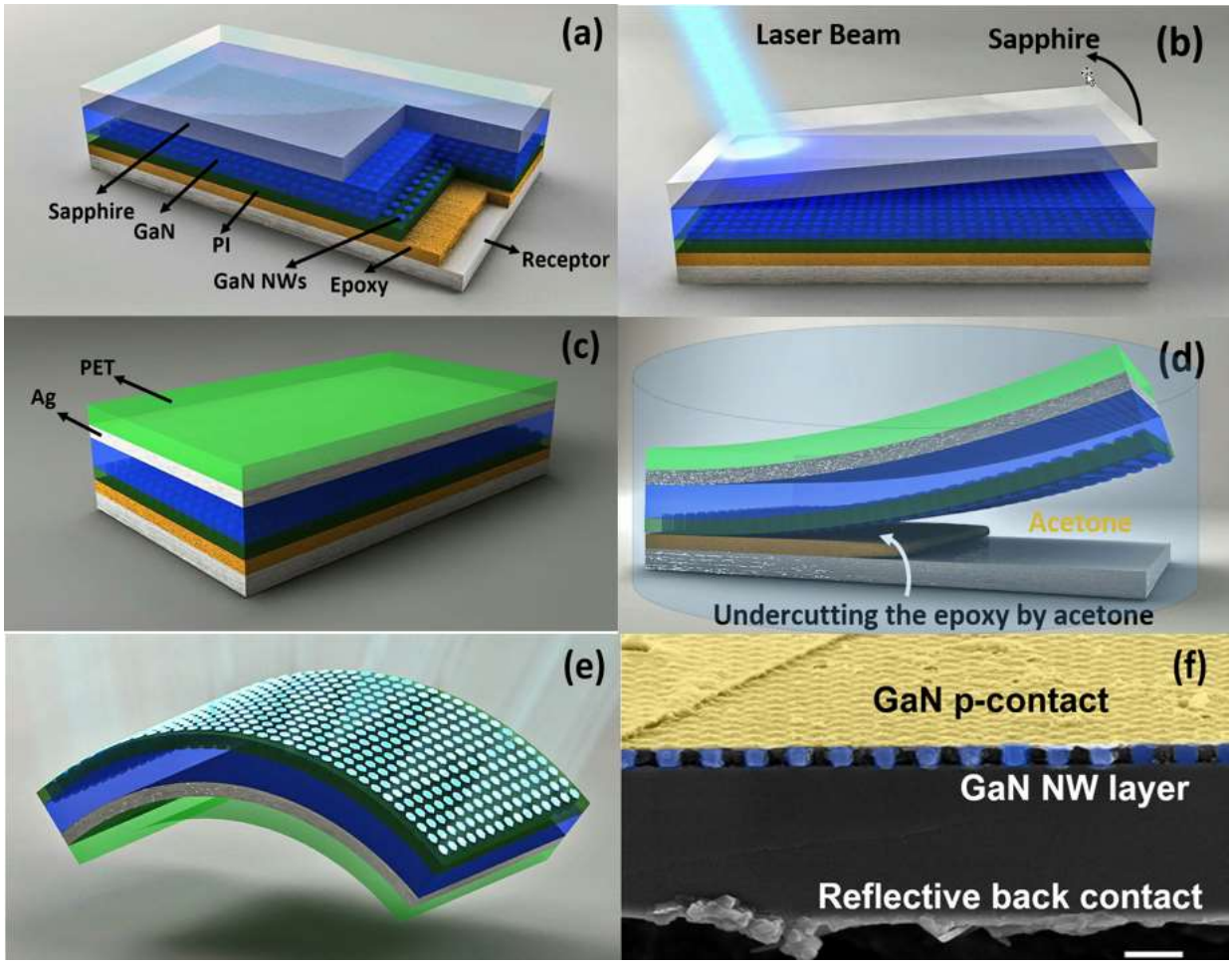

Figure 5.2 Process flow of the double-transfer process (a-d): (a) the NW LED device is bonded to a temporary receptor substrate, (b) the sapphire substrate is detached from the NW devices by illuminating a pulsed 266 nm Nd:YAG laser through the sapphire to decompose the GaN at the substrate interface, (c) a metallic Ag adhesive bonds the GaN NW devices/receptor substrate structure onto a 175 μm thick PET flexible substrate, and (d) the NW devices are transferred onto the PET by removing the epoxy bond using an acetone bath. (e) A schematic of the final transferred NW LED device on the PET substrate. (f) A cross-sectional FE-SEM image of an array of GaN NW LED devices transferred onto the flexible substrate. The golden and blue colors represent the ITO top contact and GaN NWs, respectively. Scale bar = 1 μm.

5.4 Results

The electrical characterization of the transferred NW LEDs supported the absence of the structural degradation observed in the FE-SEM and AFM analysis. Figure 5.3a shows the I-V

characteristics of the LEDs biased from -5 to 5 V before and after the integration process. A turn-on voltage of approximately 3 V was measured in both cases. The I-V characteristics of the LEDs on PET show a slight variation compared to the LEDs on sapphire; it is believed the Ag n-contact was responsible for the change. The Ag adhesive was not optimized for its electrical properties and was employed mainly for its use as a selective adhesive for complete integration onto the PET substrate. The electrical and electroluminescent measurements for the LEDs on flat and mechanically curved substrates were made using this contact; further studies are continuing to optimize the electrical contact of this bonding layer. The inset of Figure 5.3a shows the blue-light emission of the NW LEDs under forward bias (I_{drive} = 1 mA) operating on a curved sample holder having a 38 mm radius of curvature in a "concave down" orientation (bending is in the direction away from the light emission).

The effect of mechanically bending the PET substrate on the LED structures was predicted to have very little stress-induced strain on the active region of the light emitter since this area is out of the plane of bending. A constant 3 V turn-on voltage and an invariant forward current of 0.4 mA at 4 V were measured under different bending conditions demonstrates the measured electrical properties were independent of the applied bending. The I-V characteristics of the LEDs for a substrate with a "concave up" orientation (bending is in the direction towards the light emission) are shown in Figure 5.3b for bending radii of 38 mm, 32 mm, and 22 mm. Measured leakage current of 10 μA at -2 V reverse bias for the flat (unbent) LEDs did not change during bending for different orientations, providing additional evidence that mechanically flexing the PET substrate does not degrade the electrical properties of the 3-D

GaN LEDs structures. The motion of the nanowires was verified using scanning electron microscopy (SEM), with a JSM-7200F JEOL microscope, for an array of dot-in-wire structures on flexible substrates. Figures 5.3c-e show the changes in the spacing between the structures for different bending orientations at R = 32 mm. The tip separation of the structures was measured to be 68 nm in the flat orientation, 59 nm when concave up, and 76 nm apart when concave down, showing a ±8 to 9 nm range in tip separation depending on the bending direction, consistent with the finite element analysis.

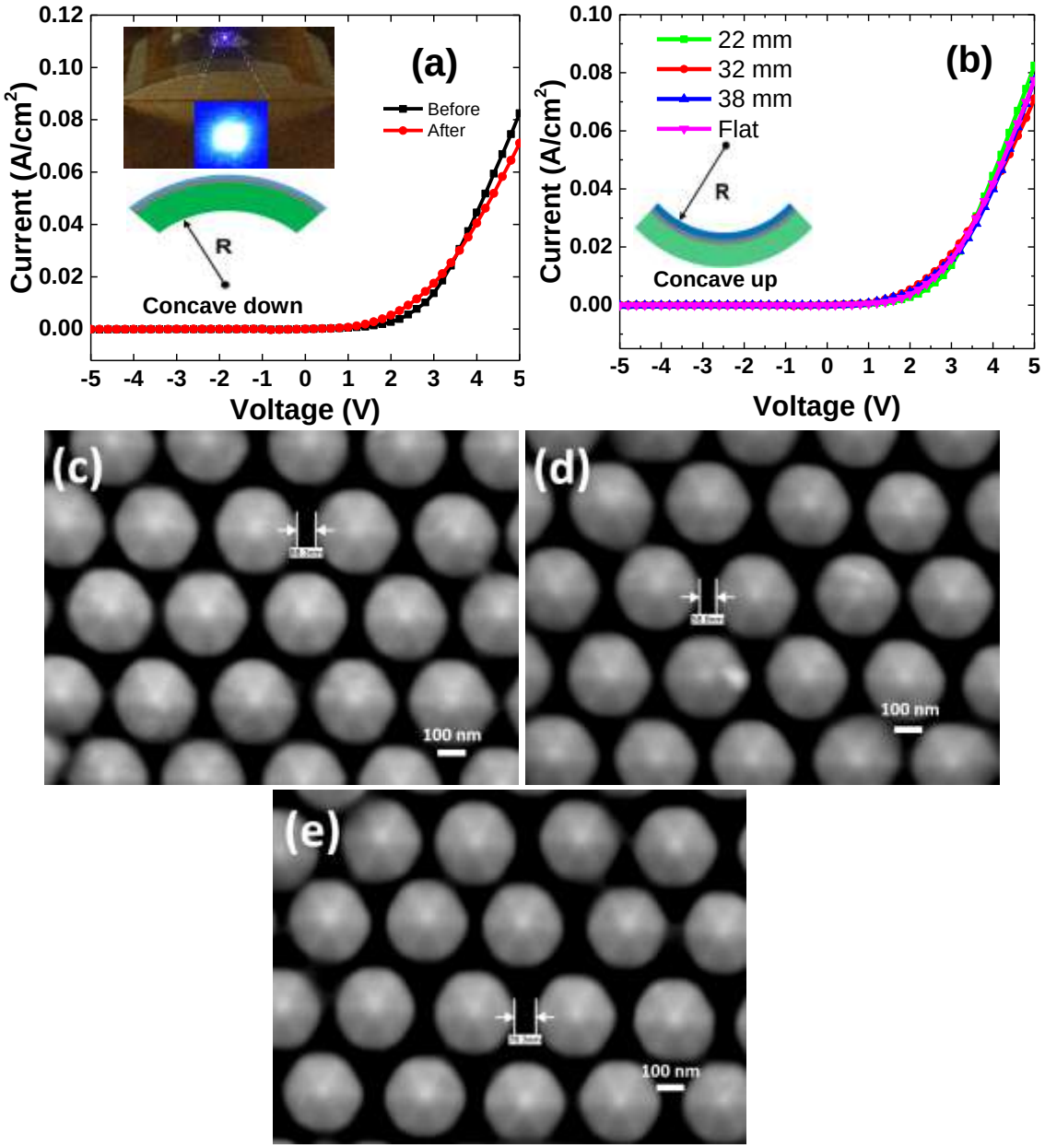

Figure 5.3 (a) I-V characteristics of the NW LEDs on the sapphire substrate before and after integration onto PET substrates; the slight variation in the forward current is due to the Ag contact used to bond the LEDs onto the PET. The inset shows the blue light emission of the GaN NW LEDs operating at a 1 mA forward current and the PET substrate flexed to a 38 mm radius of curvature. (b) The I-V characteristics of the LEDs on PET with different concave up bending conditions. The results show similar I-V characteristics at different radii of curvature between 22 to 38 mm. (c-e) Planview SEM images of GaN nanowire array sample mounted on flat, 32 mm concave-up, and 32 mm concave-down curved substrate holder at an electron-beam operation voltage of 5 kV.

The EL spectra of the light emitters before and after transfer onto PET (driven at 1 mA) is shown in Figure 5.4a. The 425 nm peak EL emission did not show a measurable shift after integration onto the PET, suggesting the release of the nanowires from the sapphire substrate did not induce additional intrinsic stress on the nanowire structures [14]. A measurable increase in intensity under flat conditions was observed after the PET integration and is attributed to enhanced reflectivity from the Ag n-contact bonding layer between the n-GaN and the PET. In this "flat" orientation, the cylinder structures act as a waveguide to direct light downward towards the metal contact that is back-reflected towards the surface. While the bending did not affect the electrical and peak emission wavelength, the intensity of the electroluminescence was observed to change during the mechanical bending of the substrate (Figure 5.4a) in the "concave up" configuration; surprisingly, the intensity was found to increase with decreasing substrate radii of curvature.

To further understand the effect of this behavior on the LED light emission, a finite-difference time-domain (FDTD) model was used to simulate the diode EL intensity changes as a function of the substrate bending. The FEA mechanical bending model, first used to predict the induced mechanical strain during bending (Figure 5.1), was also applied to determine the nanowire displacement, relative to each other, as a function of the radius of curvature (R) for the substrate. The simulated displacements calculated from Figure 5.4b were used to determine the tilt angles of the LEDs at R = 38 mm. The effect of different R values was calculated to determine the tilt of the NW structure during bending and the displacement of the NWs in the

x- and y-directions was calculated and referenced to the original position of the rods (inset Figure 5.4b).

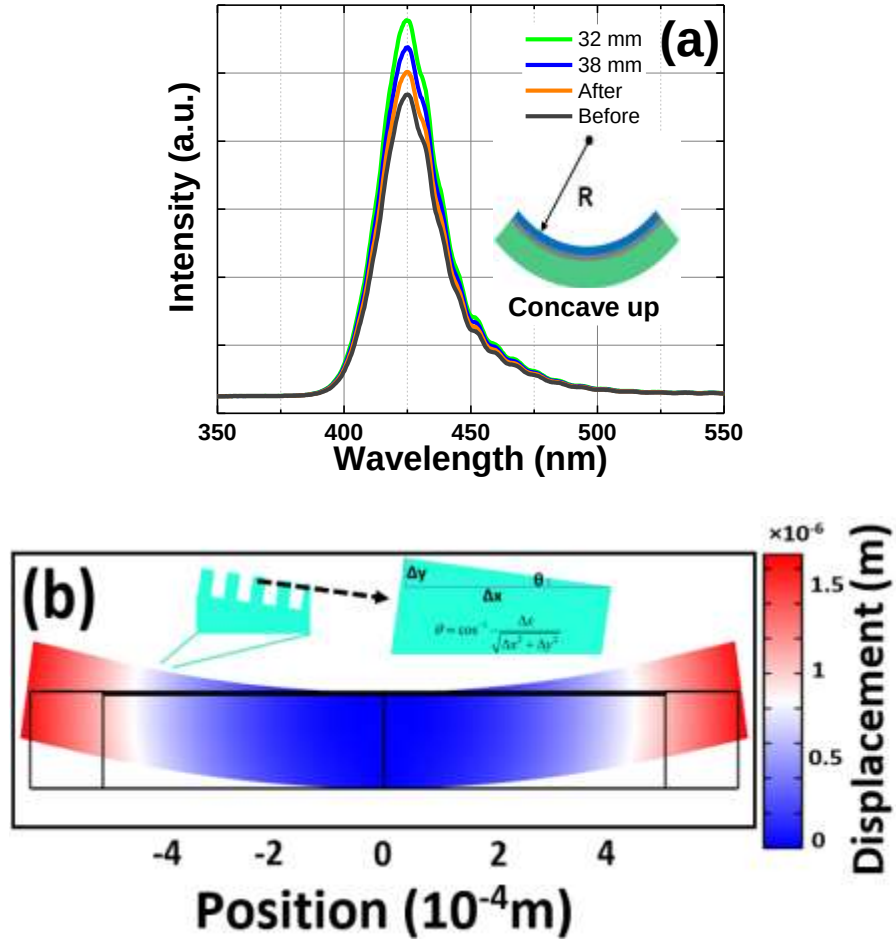

Figure 5.4 (a) The measured EL spectra of the blue NW LEDs on PET before and after the double-transfer process. The transferred devices show no emission shift with different concave up bending conditions while the EL intensity increases with decreasing radii of curvature. (b) The displacement of the flexible devices with 38 mm concave-up radius. The tilt angles of NWs were calculated based on displacement results using $\theta = \cos^{-1}\frac{\Delta x}{\sqrt{\Delta x^2 + \Delta y^2}}$, where θ is the angle between the nanowire structure during bending after shifting in the x and y-direction.

Using the calculated tilt angles, a network of 121 NW LEDs (within an 11×11 nanowire array) on a GaN buffer layer having an n-contact Ag adhesive layer, at a wavelength range between 420-430 nm, was simulated. Figure 5.5a shows the calculated near-field light intensity change of the LEDs, before and after transfer onto the PET and as a function of bending for different radii of curvature. The simulation and the experimental data show a similar trend of enhanced light-extraction due to the substrate bending. The predicted and observed improvement in light output for smaller bending radii represents an interesting and unexpected light-output enhancement regime for flexible photonic device operation. To understand this phenomenon further, the light intensity profile, collected from the top side of the NW LEDs, was investigated for: (a) LED structures before the transfer, (b) LEDs integrated with the silver adhesive onto PET, and c) structure (b) with the PET having a bending radius of 38 mm (Figure 5.5b, c, and d, respectively). Initially, the increased light output after integration onto the PET (Figure 5.5c) is due mainly to the increased reflectivity from the silver bonding layer used to attach the nanowire structures onto the PET. The measured light output also showed a similar but slightly lower increase in the EL; the difference is due in part to the non-ideal optical reflection of the adhesive and the non-optimized electrical contact of the Ag junction. The FDTD results suggest light collection from the curved substrate is related to reducing the distance between the tips of adjacent LEDs, creating increased light integration over a smaller area away from the substrate surface. The highest light intensity was predicted to be from the NW devices on a substrate with a concave-up

orientation (Figure 5.5c). This geometry provides a higher effective density of light-emitting quantum dots as the tips move closer to each other during bending along with increased electromagnetic coupling between the light emitters (supplementary information). The higher light-emission intensity is a result of the constructive phase interference between emitted and downward reflected light for an array of cylindrical LED structures. The broader emission peaks of the experimental EL spectrum shown in Figure 5.4a compared to the simulations may be due to a slight non-uniformity in the diameter of the fabricated LED devices. Combining the results from the FEA and FDTD analysis provides persuasive support for implementing nanowire LEDs for optimizing photonic devices using flexible platforms. This approach may be used for a broad range of applications, from flexible displays to conformal solid-state lighting, which requires high brightness without additional energy consumption while maintaining uniform emission wavelengths.

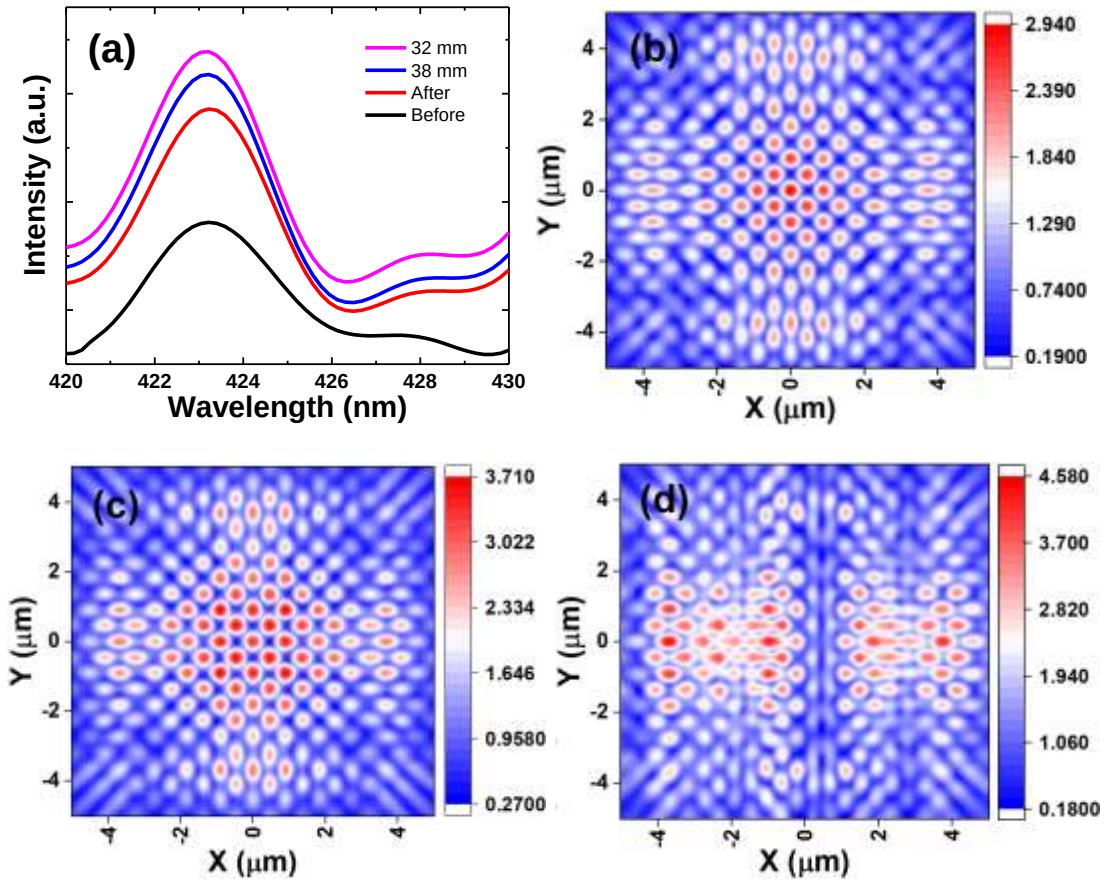

Figure 5.5 (a) 3D-FDTD simulated light-extraction efficiency for NW LEDs on different curved surfaces. The light intensity emitted from the topside of a (b) free-standing NW LED device and (c) after bonding to the PET substrate using the reflective Ag adhesive. (d) The light intensity for NW LEDs on a flexible PET substrate having a 38 mm radius of curvature.

5.5 Summary

The simulated and experimental findings show that substrate bending provides a means to mechanically manipulate NW LED structures that enhances their light output compared to planar device counterparts. Peak emission wavelengths remain constant during the applied mechanical bending of the substrate due to the predicted small in-plane strain within the rod structure. The mechanical bending of the flexible substrate in the concave-up direction

increases the light-extraction efficiency as a function of the substrate radius of curvature without introducing a shift in the peak emission wavelength. These findings add new insight to the implementation of flexible photonic structures to achieve higher light output through mechanical manipulation, providing a novel approach for realizing flexible GaN-based NW LED devices that have increased functionality and improved performance.

Chapter 6

Demonstration of highly efficient surface-emitting vertical GaN LED by optimizing the epitaxial layer thickness, and self-aligned sidewall gating

6.1 Introduction

As a final consideration, the micro-LED performance itself should be improved to reduce the power consumption of portable flexible displays. This chapter is motivated by developing novel approaches to enhance the light output of the LED by minimizing the non-radiative recombination events within the diode. The "paste-and-cut" process developed in this research provides a novel approach to examine and understand the parameters that affect the micro-LED performance and allows further optimization of the LED brightness. Recently, a vertical micro-LED structure with a reflective metal coated on the backside has proved to be one of the best candidates for FPDs because of its merit over lateral structures [36, 57]. The refractive index of GaN is about 2.5 and most of the generated photons are trapped inside the micro-LED bulk due to its small critical angle (θ_c = 25°) for the light escape cone [58] [15, 21, 59]. In addition, the trapped light can be easily absorbed by intrinsic crystal defects in the GaN layers [15]. Therefore, optimized control of the epitaxial layer thickness and an efficient carrier transport between cathode and anode regions of the device is essential to maintain a high electroluminescence and light extraction efficiency [60, 61].

These optical and electrical properties are also highly dependent on the crystal quality of the device materials and the intrinsic defects developed during the device processing [62, 63]. The resulting defects deteriorate device performance which may result in poor color uniformity over an array of light-emitters in the display [37]. Several approaches are used to minimize the defect density including surface passivation and chemical treatment to reduce trap states at surfaces and interfaces [64, 65]. Nevertheless, conventional sidewall passivation still results in an interfacial layer that acts as a region for charge recombination during device operation.[66]

In this chapter, a combination of electrical and optical modeling was used to optimize the micro-LED epilayer thickness in order to achieve the goal of increasing the LED brightness. The design was implemented using a modified paste-and-cut process to enhance the device performance by removing the defective undoped layer from the device backside and employing a cathode-connected surrounded gate to enhance the light coupling efficiency of the LED topside emission.

6.2 Theoretical Simulation

To determine the theoretical improvement that may be achieved through modifying the cathode region thickness and minimizing sidewall recombination in the micro-LED structure, a finite-difference time-domain (FDTD) technique was used to predict the light-extraction efficiency of vertical blue GaN micro-LEDs with different epitaxial layer thicknesses. Figure 6.1a shows the light extraction efficiency of the vertical micro-LED emitting from 440 nm to 460 nm at different device thicknesses when a reflective aluminum layer covered the backside. The

FDTD simulation shows a significant improvement (~180%) in light-extraction efficiency (LEE) after thinning the micro-LED epitaxial layer thickness from 6.5 μm to 1.5 μm. The improvement in LEE is related to the constructive interference of the top-side emitted photons and reflected photons from the aluminum mirror backside. The intensity of the topside extracted photons ($I^2(\omega)$) with frequency ω can be formulated as:

$$I^2(\omega) = I_0^2(\omega)\left|1 \pm re^{2i\phi(w)}\right|^2 = I_0^2(\omega)(1 + r^2 \pm 2r\cos 2\phi(\omega)) \qquad (1)$$

where $I_0(\omega)$ is the intensity of the generated light at the quantum wells, r is the reflectivity of the backside mirror, and $\phi(\omega)$ is the phase shift of the reflected photons from the backside mirror. While the phase shift due to the nature of the reflective electrode is negligible, the optical phase shift of the backside reflected photons can be explained as:

$$2\varphi = 2kt\cos\theta \qquad (2)$$

where k is the wave vector, t is the optical cavity length (thickness of the micro-LED), and θ is the incident angle of the photons towards backside and vice-versa. Due to the small critical angle of GaN material (±23°), according to Eq.2, the cavity length (t) dominates the phase-shift. Consequently, constructive interference is expected when $2kt = 2m\pi$ (where m is an integer). Figure 6.1b presents the time-averaged photon flow radiated from the micro-LED thinned to 1.5 μm with an aluminum thin-film layer used as a reflective backside. Noticeably, part of the generated photons in the quantum well (QW) are extracted through the sidewalls and are found to not contribute to top emission.

In order to improve the micro-LED directional emission, a new structure with a reflective aluminum layer, on both the backside and the mesa sidewalls, is proposed. Figure 6.1c shows the FDTD calculated light-extraction efficiency of the new structure. Compared to the previous design, using the Al sidewall reflection, a 40% improvement for the top light-extraction is achieved. As shown in Figure 6.1d, the micro-LED sidewall emission is blocked; photons only emit from the micro-LED topside. According to simulation results, the expected light-extraction efficiency may improve by as much as 220% after optimizing the epitaxial layer thickness and sidewall coverage with reflective metals. This design cannot be obtained easily through conventional epitaxial growth processes given the inherent difficulty of growing GaN directly onto a reflective metal and having a thin cathode layer due to the lattice mismatch between the sapphire substrate and the GaN film. Since, the epitaxial layer thickness optimization is designed to be through the micro-LED backside, any conventional transparent ohmic contact on the p-GaN can be employed in practice.

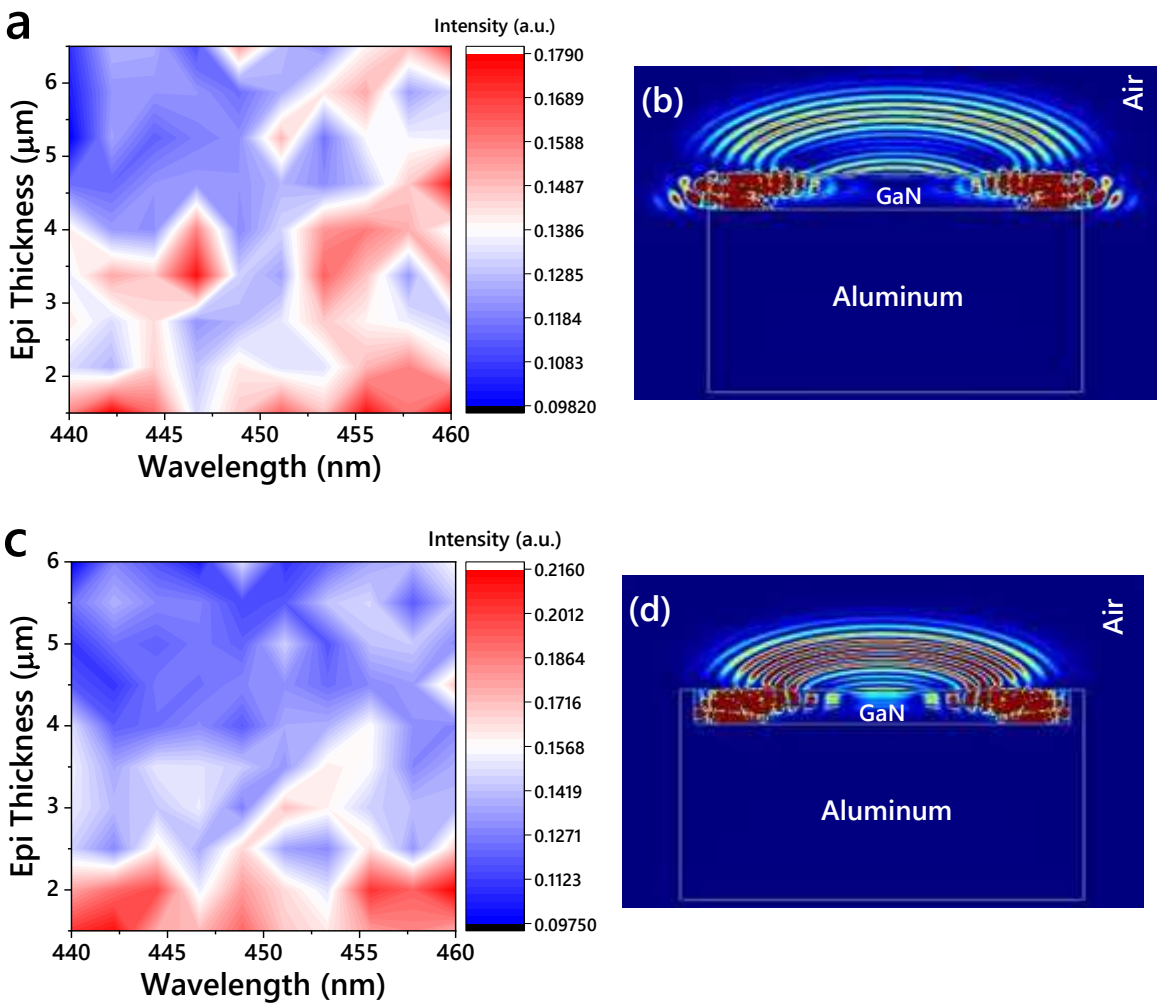

Figure 6.1 Light extraction efficiency of the blue GaN micro-LED in the range of 440-460 nm as a function of the epitaxial layer thickness when (a) only the device backside is covered with a reflective metal layer. (b) Time-averaged photon flow radiated from a TE mode dipole source mimicking the QWs. (c) The light extraction efficiency of the blue micro-LED structure as a function of the epitaxial layer thickness when both backside and sidewalls are covered with reflective aluminum. (d) Time-averaged photon emission of the device with both sidewalls and backside reflective layers.

6.3 Experiments

In order to validate the proposed design, a 10 ×10 array of (90 × 90 μm^2) micro-LEDs was fabricated on sapphire substrates using an inductively coupled plasma (ICP) etching process and a SiN_x etch mask. A Ni/Au (10/10 nm) bilayer was used as a transparent ohmic-contact to

the p-GaN and the mesa sidewalls were passivated by using a 100 nm plasma-enhanced chemical vapor deposited SiO_2. The process flow for transferring micro-LEDs from the sapphire substrate onto silicon is presented schematically in Figure 6.2. First, the micro-LED array was bonded onto a glass temporary substrate by using a thin adhesive layer (Figure 6.2a). The sapphire substrate is then removed by using a laser-liftoff process (Figure 6.2b). The epitaxial layer thickness of the micro-LEDs was then modified by ICP-etching of the exposed GaN n-layer at room temperature for different etch times between 5 to 20 minutes (Figure 6.2c). The process was followed by RF sputtering of a 500 nm reflective aluminum layer on the backside and sidewalls of the micro-LEDs (Figure 6.2d). After thermally evaporating a Cr/Au bilayer on the micro-LEDs' backside, the diodes were flip-chip bonded onto gold pads using a 1 μm thick indium bonding metal (Figure 6.2e). Figure 6.2f shows the scanning electron microscopy (SEM) micrograph of a micro-LED pixel bonded onto a glass substrate after releasing the sapphire substrate. The plan view SEM micrograph of a micro-LED after thinning the backside is presented in Figure 6.2g. Noticeably, the SiO_2 at the sidewall has a lower etch-rate than GaN and a well-like structure is created where the GaN is recessed from the SiO_2 sidewall. This structure can help the micro-LEDs penetrate into the soft indium pads, providing a secure mechanical bond at lower temperatures. Figure 6.2h shows the SEM micrograph of micro-LED arrays after transfer onto the silicon substrate.

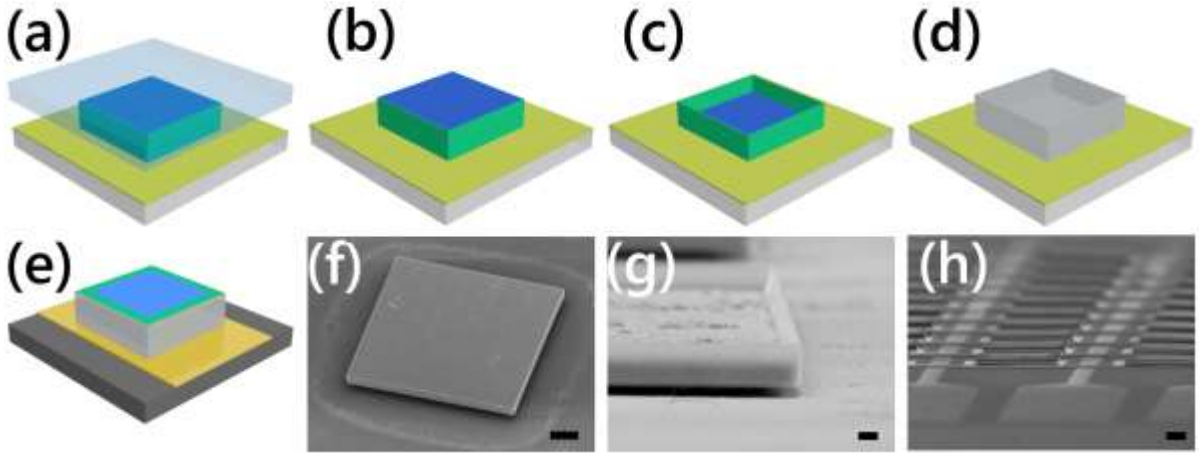

Figure 6.2 Process flow for micro-LED epitaxial layer thickness engineering process: (a) Adhesive bonding the micro-LED onto a glass substrate, (b) Releasing the sapphire substrate after the LLO process, (c) Thinning the micro-LED backside by an ICP etching process, (d) Sidewalls and backside coating with a highly reflective aluminum layer (e) Flip-chip bonding of the micro-LEDs from the carrier substrate onto the final silicon substrate and releasing the carrier. (f) The SEM micrograph of a micro-LED pixel after bonding onto glass and releasing the sapphire substrate. (g) The SEM micrograph of the same micro-LED after backside thinning for 15 min and coating the sidewalls and backside with a 500 nm reflective aluminum layer. (h) The SEM micrograph of the 90 × 90 μm^2 micro-LED arrays after final transfer onto the silicon substrate.

6.4 Results and Characterization

Figure 6.3a shows the measured electroluminescence (EL) intensity from the top side of the micro-LEDs with different epitaxial layer thickness. The emitted photons have been collected through an objective lens with a numerical aperture (NA) of 0.4 providing a collection angle of ~60°. This NA was chosen to selectively capture only the light emitting from the topside of the LED since photon emission outside this region would effectively be lost through angular color mismatch with the adjacent pixel in a full color display or absorbed by the surrounding black matrix sidewall. A reference micro-LED (REF) was also used without thinning and sidewall coverage in comparison to the thinned micro-LEDs having the surround cathode contact. For easier comparison, the quantified EL improvement at 450 nm and etch depth

(measured from the backside) for each micro-LED are depicted together in Figure 6.3b. In order to investigate the etch profile in micro-LEDs, the epitaxial structure is shown schematically at the image right side. At epitaxial thickness = 5.3 μm, a 21% enhancement in the EL was measured; the trapped photons are still absorbed by internal defects in the GaN bulk. After thinning the optical epitaxial layer to 4.1 μm (10 min each time), a 196% enhancement in the EL was achieved. However, the measured EL intensity was observed to decline (the enhancement dropped to 80%) at an epitaxial layer thickness of 2.9 μm. This observation of the light extraction decrease is due to the destructive interference of the reflected light within the LED structure (Eq. 2). Further thinning of the sample resulted in an EL intensity enhancement of 440% for an epitaxial layer thickness of 1.7 μm. Part of this EL improvement (40%) may be originating from the micro-LED metallic sidewall coverage that helps directional emission through the top of the device, which was collected through the objective lens. The optical micrograph of the REF micro-LED and the 5.3 μm epitaxial thick micro-LED with sidewall coverage driven at 10 A/cm^2 is shown in Figure 6.3c, 6.3d. As shown in Figure 6.3d, the edges of the LED sidewall are well defined compared to the reference device, demonstrating the efficacy of the Al-surround contact in confining the light within the diode region. Figure 6.3e shows the far-field pattern of the REF micro-LED and the 5.3 μm epitaxial thick device with reflective metal sidewall coverage. The points are the normalized measured values fitted with a solid line. In the REF micro-LED, a higher EL intensity was measured between 40° to 60°, though, the emission pattern of the micro-LED with reflective sidewall coverage follows a Lambertian pattern, which can be related to the sidewall coverage.

As a potential application, this method can be used to reduce the angular color shift in micro-LED displays originating due to different refractive indexes of the other device materials used to generate red and green in full-color displays [21]. Unexpectedly, the simulated light extraction efficiency underestimated the experimental data (a 220% theoretical maximum compared to a measured 440% enhancement).

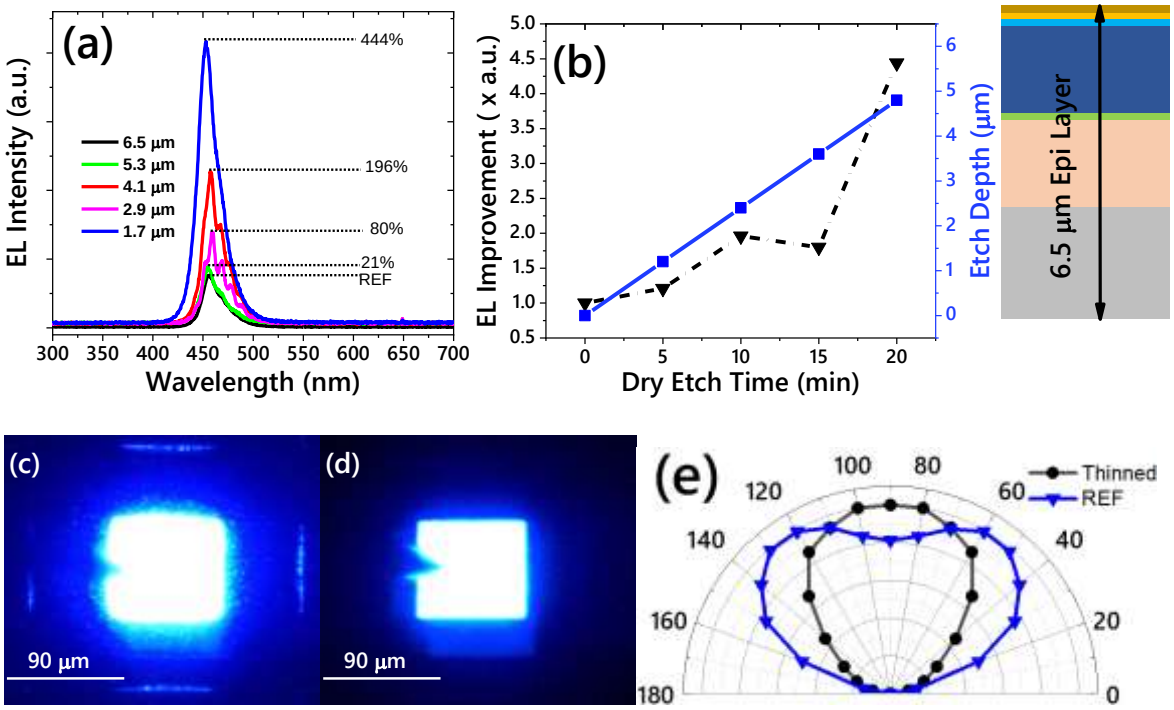

Figure 6.3 (a) EL spectra of the REF GaN micro-LEDs and micro-LEDs with different epitaxial layer thicknesses. (b) The etch depth from the backside and the EL improvement versus the dry etch time. The sidewall of REF micro-LED is not covered with reflective metal. The schematic of the device structure with a total thickness of 6.5 µm is shown on the right side of the spectra. Optical micrographs of (c) REF micro-LED and (d) bonded onto a silicon substrate driven with continuous 10 A/cm^2. (e) The measured far-field radiation pattern of REF micro-LED and 5 min.

One possibility for this disparity is that the surface roughness of the etched devices was not considered in the model. The roughness of the micro-LED backside was measured by atomic force microscopy (AFM) after releasing the sapphire and after 20 min backside thinning. The maximum roughness after the sapphire removal and thinning process were 107 nm and 450 nm, respectively. Initially, a flat interface was considered in the simulations and incorporating the measured backside roughness in the calculations led to ~ 40% more light extraction (Figure 6.4a). However, the model suggests when the micro-LED is very thin (~ 1.5 μm) the light-extraction efficiency is not strongly dependent on the backside roughness. The light paths inside a thin micro-LED and thick micro-LED are schematically shown in Figure 6.4b. When the incident angle of a photon emitted from a quantum well (QW) is less than the critical angle (θ_c), according to Snell's law, the light coupling-out of the surface is high. However, when the micro-LED epitaxial layer is thicker, the light path is longer and there is a higher chance of light absorption in the QWs, intrinsic defects, and the bulk. Since the calculated light extraction efficiency (262%) is still far from the experimental results (440%), the electrical effect of the Al-surround contact was considered.

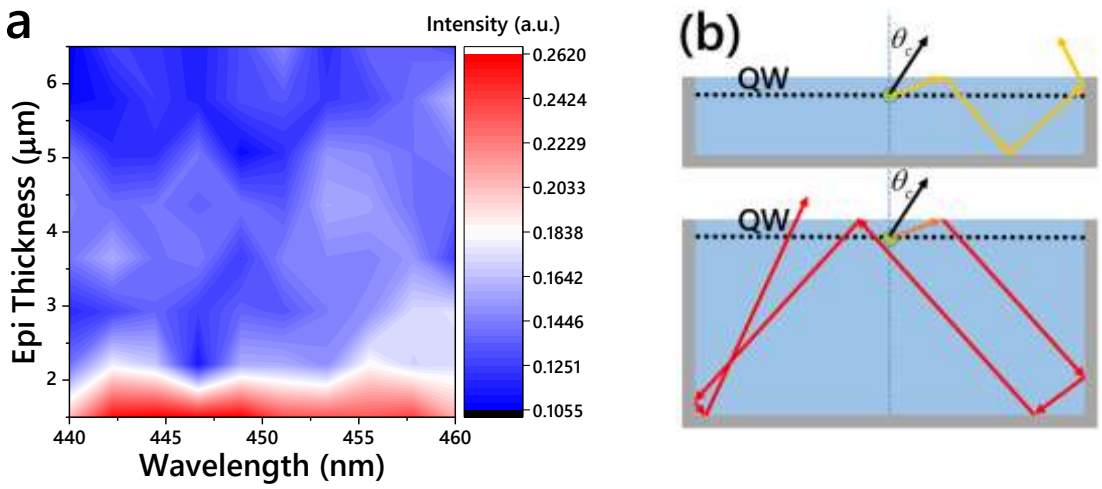

Figure 6.4 (a) Light-extraction efficiency calculated for 20 min thinned blue micro-LED. (b) Schematic of the light path in a thinned micro-LED and thick micro-LED. The QW is shown by a dashed line and the photon source is mimicked by a green point.

Figure 6.5a shows the semi-logarithmic I-V characteristics of the micro-LEDs measured at room temperature and under dark conditions. The boxed numbers inside the figure shows three main regions of the curve. In **Region 1**, the REF LED showed 2×10^{-8} A of leakage current at -4 V where a leakage current of 5×10^{-9} A was measured at -4 V for all thinned micro-LEDs. While all the micro-LEDs are made on the same epitaxial wafer, a uniform defect density is expected for all devices across the wafer. Since the same 100 nm SiO_2 passivates all the micro-LEDs' sidewall, it can be hypothesized that a gating effect at the sidewall creates a depletion layer along the sidewalls, minimizing defect-assisted recombination. This gating mechanism is schematically shown inset in Figure 6.5a where the metal on the dielectric layer is connected to the cathode electrode and consequently depletes carriers from the edge towards the middle of the diode. As a result, surface recombination at the sidewall is expected to be reduced. For an applied voltage below the on- voltage (V_{ON}) (**Region 2** in Figure 6.5a), the I-V curve of the

REF micro-LED was substantially different from the thinned devices. The observed higher current in the REF device at low voltages, maybe due to surface recombination along the sidewalls. This possibility is supported by a higher extracted ideality factor of (n=4) for the REF devices, as shown in Figure 6.5b. The calculated ideality factors for all thinned LED with Al-surround sidewall gate is substantially smaller at n=1.4. In earlier reports[44, 67, 68], the high ideality factor in InGaN/GaN-based LEDs was attributed to several factors such as tunneling current at QWs, rectifying characteristics of the heterojunctions, and the shape of the barrier layers. However, these results may be also attributed to sidewall recombination centers [69] and the lowering of the measured ideality factor was obtained after applying passivation along with the cathode-connected self-aligned gating surrounded the sidewalls.

In order to further understand the effect of the sidewall gating on the device operation, a typical micro-LED with 4 QWs was simulated using a commercial technology computer-aided design (TCAD) software. Figure 6.5c shows the TCAD simulated electric field distribution at the sidewall with and without gating under 2.4 V forward bias. A uniform electric field within the quantum wells was obtained when a reflective gate electrode is connected to the cathode electrode. As a result, a lower electron density at the sidewall of the surround-contact micro-LED is expected to have reduced defect-assisted recombination. Figure 6.5d shows the Shockley-Read-Hall (SRH) recombination distribution inside the quantum wells. Noticeably, a lower SRH recombination at the sidewall was observed due to the unbalanced distribution of electrons and holes close to the sidewalls. The simulation results support the hypothesis that sidewall gating is responsible for the smaller ideality factor compared to the REF structure.

When the applied voltage is sufficiently high enough (high-injection condition), the I-V characteristics deviate from the Shockley equation by a series resistance (**Region 3** in Figure 6.5a). The experimental linear I-V characteristics of the REF micro-LED and thinned devices with various epitaxial layer thicknesses are depicted in Figure 6.5e. The extracted series resistance versus the backside thinning process time is also presented in Figure 6.5f. Since the p-GaN contact resistance and heterojunctions resistance are identical in all devices, the difference in series resistance can be attributed to the n-GaN contact resistance and the bulk resistance. Titanium with the same thickness throughout the samples was used as an ohmic-resistance to n-GaN in all devices so the n-GaN contact resistance may be assumed to be the same. As shown schematically in Figure 6.5f, the micro-LED bulk series resistance consists of the undoped GaN resistance (R_1), lightly doped GaN (R_2), and highly doped (8×10^{18} cm^{-3}) GaN (R_3). The measured REF micro-LED series resistance ($R_1 + R_2 + R_3$) was 0.12 Ω and decreased to 0.08 Ω for an optical length of 5.3 μm. Etching away the undoped region to the lightly doped GaN resulted in a measured series resistance ($R_2 + R_3$) of 13 $\times10^{-3}$ Ω. Finally, the lowest series resistance (R_3) of 5.6×10^{-4} Ω was achieved when the LED structure was 1.7 μm thick. The very low series resistance also contributes to the enhanced micro-LED performance due to the smaller voltage drop across the device structure and more efficient carrier injection into the active region.

Further TCAD simulations of micro-LED operation provided additional insight into the sidewall gating effect at the higher voltages. Figure 6.5g shows the electron density inside the QWs for both the REF micro-LED with conventional dielectric passivation and the micro-LED

with the Al-surround gate sidewalls at 6 V. The electron density is distributed uniformly inside the quantum wells when the sidewalls are passivated with only the SiO_2 layer. After introducing the reflective surrounding cathode, the micro-LED sidewall became almost depleted from electrons due to the gating effect. The simulated current density close to the sidewall for the same structures are shown in Figure 6.5h. Due to the lower electron density, the current density in the vicinity of the sidewall at the gated structure (1.5×10^3 A.cm^{-2}) is almost an order of magnitude less than the conventional LED (4×10^4 A.cm^{-2}). As a result, the sidewall is depleted of negatively charged electrons and consequently, unbalanced carrier concentrations decrease the defect-assisted non-radiative recombination and higher quantum efficiency is expected. Therefore, part of the EL improvement in thinned micro-LEDs can be attributed to electrical performance enhancement by both an efficient carrier injection into the active region due to the thinner LED structure and less non-radiative recombination at the sidewalls of the device due to the sidewall gating effect.

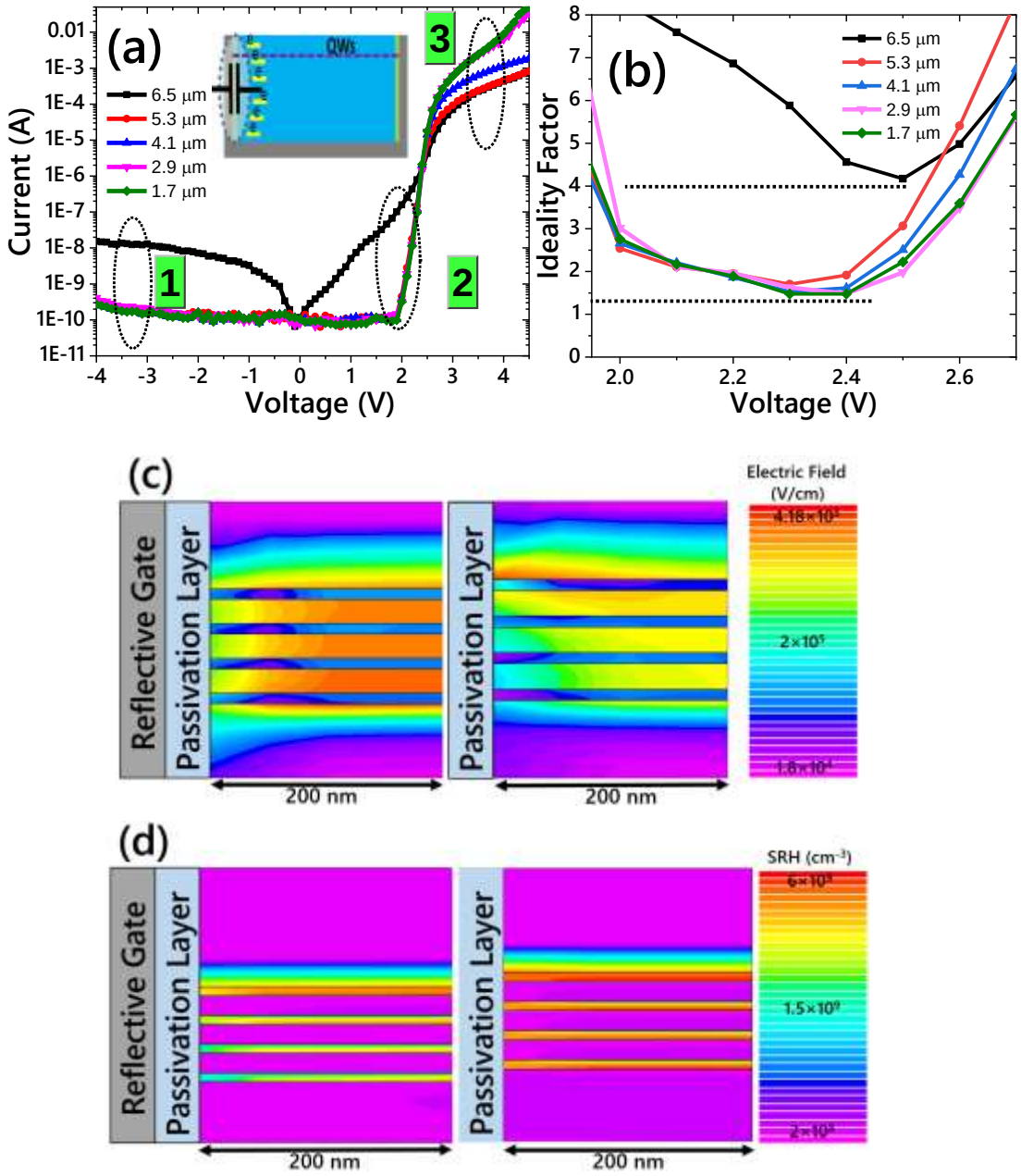
(a)
6.5 μm
5.3 μm
4.1 μm
2.9 μm
1.7 μm
QWs
1
2
3
Current (A)
Voltage (V)
(b)
Ideality Factor
Voltage (V)
(c)
Reflective Gate
Passivation Layer
Passivation Layer
200 nm
200 nm
Electric Field (V/cm)
(d)
Reflective Gate
Passivation Layer
Passivation Layer
200 nm
200 nm
SRH (cm⁻³)

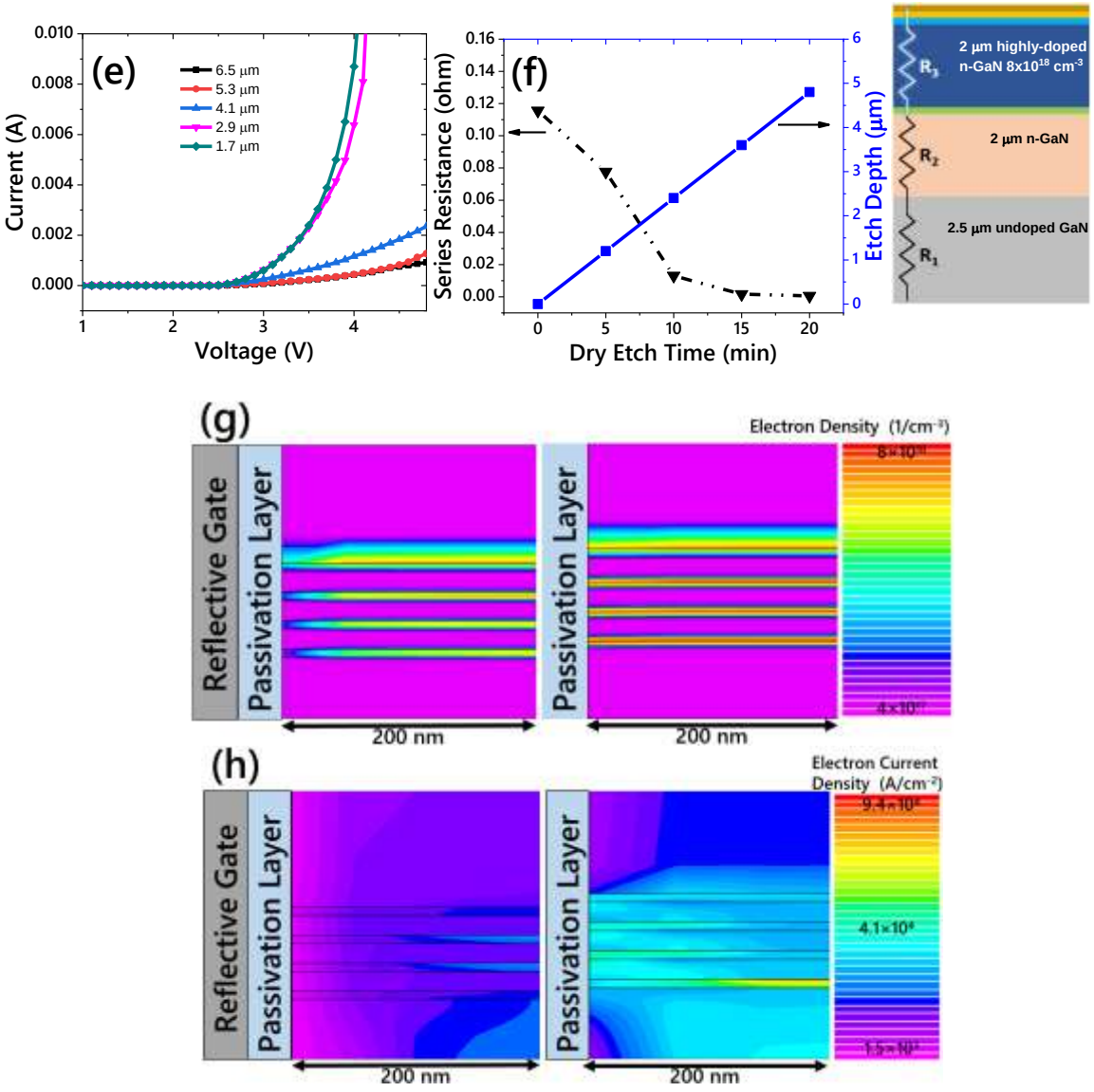

Figure 6.5 (a) Semi-logarithmic scale I-V characteristics of the REF micro-LED and micro-LEDs with different epitaxial layer thicknesses. The numbers in the picture show three main regions of the I-V characteristic. (b) The ideality factor of different devices extracted from I-V characteristics at region 2. (c) Simulated electric field distribution within the active region of REF-micro-LED and device with the gated sidewall. (d) Simulated SRH recombination profile in the QWs at the vicinity of the conventionally sidewall passivated and sidewall gated structure. (e) Linear scale I-V characteristics of the REF micro-LED and thinned devices. (f) Extracted series resistance versus dry etch time for thinning the backside. The etch depth in the epitaxial structure is schematically presented at the right side. (g) A numerically simulated electron density at the quantum wells in the vicinity of the passivation layer. (h) Simulated electron current densities at the QWs interfaced with the dielectric. The structure with gated sidewall passes 10 times lower current density at the sidewall.

6.5 Summary

The topside directional electroluminescence was improved by 440% after thinning the epitaxial layer thickness from 6.5 μm to 1.7 μm and applying a self-aligned sidewall gated reflective electrode. According to simulations, 220% of the EL enhancement can be attributed to a higher light extraction efficiency due to the constructive photon interference. Moreover, the reflective sidewall coverage produced a Lambertian emission pattern that can be used to resolve the angular color-shift in micro-LED displays. Further, the 40% improvement in EL is related to the micro-LED backside textures made during the thinning process. The remaining remained 180% is credited to the enhanced electrical performance. The proposed process decreased the series resistance from 0.12 Ω to 5.6×10^{-4} Ω by removing the defective bulk layer. According to simulations, the self-aligned sidewall gating decreased the current density from 4×10^{4} Acm^{-2} to 1.5×10^{3} Acm^{-2} at 6 V forward bias. The unbalanced electron and hole density caused fewer defect-assisted non-radiative recombination at the sidewall dangling bonds. While both self-aligned gate electrode and cathode are connected, without the requirement to an additional electrode and complex driving circuit, this technique can be used in high-resolution micro-LED displays. In addition, the achieved zero crosstalk between neighbor pixels due to the sidewall coverage facilitates the micro-LEDs and sensors integration on the same backplane without interference. As a result, further functionality without additional cost can be realized.

Chapter 7

Conclusion and Future Works

7.1 Conclusion

This thesis describes the process and techniques for transferring micro-LEDs from a sapphire growth substrate onto a flexible substrate as a building block for flexible displays. The developed processes presented in the individual chapters are primarily ordered according to down-scaling the size of the micro-LEDs from 100×100 μm^2 to NW LEDs. In addition, higher light-extraction efficiency from vertical micro-LEDs was achieved by tuning the micro-LED epitaxial layer thickness. As a new concept, the self-aligned sidewall gating around the micro-LED mesa structure was used to deplete the sidewalls from one carrier and reduce the defect-assisted non-radiative recombination. The following is the list of the novel contribution of this Ph.D. research on the field of flexible displays:

1- Direct transfer and integration of the vertical GaN micro-LEDs onto a-Si:H –based TFTs on a plastic substrate.

2- Demonstration of a low-power pixel circuit for flexible displays by integrating GaN-micro-LED cathode onto the drain of the TFT (n-side down); realized by a double-transfer process.

3- Theoretical investigation of the behavior of the micro-LEDs on various dissimilar substrates and proposing an effective bonding structure for dissipating the generated heat during the operation of the diode.

4- Theoretical simulation of the micro-LEDs with different geometries on a flexible substrate and experimental verification from fabricate micro-LEDs on flexible substrates.
5- Optoelectrical enhancement of GaN NW LEDs by mechanical bending on plastic substrates.
6- Enhanced light extraction of surface-emitting vertical GaN light-emitting diodes by self-aligned sidewall gated cathode electrode and epitaxial layer thickness modulation.

GaN micro-LEDs fabricated on a sapphire substrate were flip-chip integrated onto the TFT driving circuit using a low-temperature bonding process. The micro-LEDs were then released by using laser-liftoff process. No degradation in micro-LEDs optoelectrical characteristics was observed after the transfer from sapphire onto the flexible substrate. The integration of a low-cost backplane and a high-efficiency micro-LED was the first step for realizing the next-generation flexible and large-area displays.

In order to overcome the deficiencies of the conventional driving circuits, a new micro-LED pixel circuit on a flexible platform was developed by employing a double-transfer process. Micro-LEDs were transferred onto a carrier substrate followed by final integration onto the flexible backplane. Experimental results of the fabricated pixel circuits on flexible platforms confirmed the predictions and showed micro-LED pixels having 2.4 times higher brightness. Integrating the micro-LEDs onto the drain electrode also enabled the pixel circuit to operate at a lower V_{data} voltage.

The theoretical modeling of the micro-LEDs with various sizes demonstrated an invariant piezoelectric field in micro-LEDs with a diameter smaller than 20 μm under mechanical bending. The experimental process was developed to validate the theory. Experimental results for the micro-LEDs on flexible PI substrates confirmed this prediction and showed no measurable degradation of the optical and electrical properties under a mechanical strain up to bending curvatures of 15 mm. In addition, the theoretical modeling predicted that bonding micro-LEDs on Cu pads can effectively remove the generated heat in device operating under forward bias. Both the thermal models and experimental results demonstrated plastic substrates coated with a copper pad thicker than 600 nm leads to an effective heat sink on thermally insulating platforms.

A unique approach was introduced to eliminate the micro-LED degradation under mechanical bending by employing dot-in-wire structures, using cylindrical light-emitting heterostructures that protrude above the flexible platform, separating the active light-emitting region from the bending substrate. The mechanical bending of the flexible substrate in the concave-up direction increases the light-extraction efficiency as a function of the substrate radius of curvature without introducing a shift in the peak emission wavelength. The I–V characteristics of the nanowire LEDs showed negligible change after integration onto the plastic substrate. A significant advantage for the nanowire devices on plastic was demonstrated by tilting the LEDs through substrate bending that increased the electroluminescence (EL) intensity, while the I–V characteristics and the EL peak position remained constant.

The topside directional electroluminescence of InGaN blue micro-LEDs was improved by 440% by tuning the epitaxial layer thickness, removing the defective backside GaN and employing a novel self-aligned sidewall gating. According to simulations, 220% of the EL enhancement was attributed to a higher light extraction efficiency due to the optimized constructive photon interference. The diode series resistance decreased from 0.12 Ω to 5.6×10^{-4} Ω through the removal of the defective interfacial GaN layer. The self-aligned gating surrounded the sidewall of the micro-LEDs was also used to enhance the device performance by decreasing defect-assisted non-radiative recombination.

7.2 Future work

Based on the results and analysis that have been shown in this dissertation, the below-mentioned areas are recommended for further study:

1- Developing a flexible transparent common electrode for displays based on vertical micro-LEDs. Although ITO has both low resistance and transparency, it might be brittle under mechanical bending. As a result, a new flexible transparent electrode based on Ag NWs or other materials should be developed. However, the externally applied strain can be eliminated by putting the transparent electrode in the neutral plane of the mechanical bending. This requires further mechanical simulations.

2- Developing a flip-chip bonding process with a lower bonding temperature. In this Ph.D. research, most of the bonding processes were based on the liquid transient phase of Au-In and Au-Sn materials. The bonding temperatures in both cases have been decreased to be lower than 200°C to make them compatible with the flexible

substrates. However, a new class of materials such as Ag-In can be developed with a bonding temperature as low as 170°C which is lower than the glass transition temperature of PET and PEN substrates.

3- Improving the efficiency of the ultraviolet (UV) LEDs by using the introduced thinning process. In the UV region, the dominant factor of the low external quantum efficiency is the poor light extraction efficiency. The AlGaN-based LEDs dominantly emit transverse magnetic (TM) polarized photons due to the valence band structure of the material in the high Al content. As a result, most of the photons travel perpendicular to the c-axis (growth direction) of the LED and consequently may be absorbed by the GaN or AlGaN underlayers. Thinning the backside of the LED can be helpful for enhancing the light extraction and consequently quantum efficiency.

7.3 Published articles and conference papers

Journal papers:

1- **Mohsen Asad**, Renjie Wang, Yong-Ho Ra, Pranav Gavirneni, Zetian Mi, William Wong, Optically invariant InGaN nanowire light-emitting diodes on flexible substrates under mechanical manipulation, npj Flexible Electronics, 2019 3.16,1-6.
2- **Mohsen Asad**, Qing Li, Czang-Ho Lee, Manoj Sachdev, William S Wong, Integration of GaN light-emitting diodes with a-Si: H thin-film transistors for flexible displays, Nanotechnology, 2019, 30(32), 324003.
3- **Mohsen Asad**, Qing Li, Manoj Sachdev, William S Wong, Size-dependent optoelectrical properties of 365 nm ultraviolet light-emitting diodes, Nanotechnology, 2019, 30(50), 504001.

4- **Mohsen Asad**, Qing Li, Manoj Sachdev, and William S. Wong, Thermal and optical properties of high-density GaN micro-LED arrays on flexible substrates, Nano Energy, accepted.
5- **Mohsen Asad**, Qing Li, Manoj Sachdev, and William S. Wong, Demonstrating highly efficient surface-emitting vertical GaN light-emitting diodes by self-aligned sidewall gating and epitaxial layer thickness modulation, under formal peer review, Nature Communications NCOMMS-20-13038-T.
6- **Mohsen Asad**, Qing Li, Czang-Ho Lee, Manoj Sachdev, William S. Wong, Design and demonstration of high-brightness low-power flexible micro-LED pixel circuits, under review, Nano Energy NANOEN-D-20-01360.
7- Qing Li, Czang-Ho Lee, **Mohsen Asad**, William S Wong, Manoj Sachdev, CMOS-Like Logic Circuits With Unipolar Thin-Film Transistors on Flexible Substrate, IEEE Transactions on Electron Devices, Vol 67, No. 2, 512-517, 2020.
8- Qing Li, Czang-Ho Lee, **Mohsen Asad**, William S Wong, Manoj Sachdev, A 6-TFT charge-transfer self-compensating pixel circuit for flexible displays, IEEE Journal of the Electron Devices Society, Vol 7, 792-800, 2019.
9- **Mohsen Asad**, William S. Wong, Green GaN micro-LEDs incorporated with gold surface plasmons, under preparation.

Conferences and proceedings:

1- **Mohsen Asad**, Renjie Wang, Yong-Ho Ra, Zetian Mi, William S. Wong, Electrical and optical properties of flexible nanowire blue light-emitting diodes under mechanical bending, SPIE Photonic West. San Francisco, 2017.
2- **Mohsen Asad**, Qing Li, Czang-Ho Lee, Manoj Sachdev, William S. Wong, Flexible InGaN micro-LED arrays integrated with amorphous-silicon thin-film transistors, SPIE Photonic West, San Fransisco, 2018.

3- **Mohsen Asad**, Renjie Wang, Yong-Ho Ra, Zetian Mi, William S Wong, Light extraction efficiency enhancement of InGaN nanowire light-emitting diodes on flexible substrates, ISSLED 2017, Banff, Canada.

4- **Mohsen Asad**, Qing Li, Czang-Ho Lee, Manoj Sachdev, William S. Wong, Heterogeneous Integration of InGaN Micro-LEDs with a:Si TFT Arrays on Flexible Substrates, IEEE IFETC 2019, Vancouver, Canada.

5- **Mohsen Asad**, Qing Li, Manoj Sachdev, William S. Wong, Integration of GaN micro-LED arrays onto plastic substrates for flexible display applications, IMID 2019, Gyeongjo, Korea.

Bibliography

[1] J. Day, J. Li, D. Y. C. Lie, C. Bradford, J. Y. Lin, and H. X. Jiang, "III-Nitride full-scale high-resolution microdisplays," *Applied Physics Letters,* vol. 99, no. 3, Jul 18, 2011.

[2] J. G. Um, D. Y. Jeong, Y. Jung, J. K. Moon, Y. H. Jung, S. Kim, S. H. Kim, J. S. Lee, and J. Jang, "Active-Matrix GaN μ-LED Display Using Oxide Thin-Film Transistor Backplane and Flip Chip LED Bonding," *Advanced Electronic Materials,* vol. 5, no. 3, 2019.

[3] Z. J. Liu, W. C. Chong, K. M. Wong, and K. M. Lau, "GaN-based LED micro-displays for wearable applications," *Microelectronic Engineering,* vol. 148, pp. 98-103, Dec 1, 2015.

[4] C.-C. Lee, Y.-S. Shih, C.-S. Wu, C.-H. Tsai, S.-T. Yeh, Y.-H. Peng, and K.-J. Chen, "Development of robust flexible OLED encapsulations using simulated estimations and experimental validations," *Journal of Physics D: Applied Physics,* vol. 45, no. 27, 2012.

[5] M. H. Park, J. Y. Kim, T. H. Han, T. S. Kim, H. Kim, and T. W. Lee, "Flexible Lamination Encapsulation," *Adv Mater,* vol. 27, no. 29, pp. 4308-14, Aug 5, 2015.

[6] Y. Kajiyama, K. Kajiyama, and H. Aziz, "Maskless RGB color patterning of vacuum-deposited small molecule OLED displays by diffusion of luminescent dopant molecules," *Opt Express,* vol. 23, no. 13, pp. 16650-61, Jun 29, 2015.

[7] Y.-C. Jeong, J.-H. Yu, K.-Y. Shin, S. Lee, C.-R. Yoon, and S.-H. Lee, "Microstructure-based analysis of fine metal mask cleaning in organic light emitting diode display manufacturing," *Micro and Nano Systems Letters,* vol. 7, no. 1, 2019.

[8] J. Chun, Y. Hwang, Y. S. Choi, J. J. Kim, T. Jeong, J. H. Baek, H. C. Ko, and S. J. Park, "Laser lift-off transfer printing of patterned GaN light-emitting diodes from sapphire to flexible substrates using a Cr/Au laser blocking layer," *Scripta Materialia,* vol. 77, pp. 13-16, Apr 15, 2014.

[9] S. Shervin, S. H. Kim, M. Asadirad, S. Y. Karpov, D. Zimina, and J. H. Ryou, "Bendable III-N Visible Light-Emitting Diodes beyond Mechanical Flexibility: Theoretical Study on Quantum Efficiency Improvement and Color Tunability by External Strain," *Acs Photonics,* vol. 3, no. 3, pp. 486-493, Mar, 2016.

[10] C.-H. Cheng, T.-W. Huang, C.-L. Wu, M. K. Chen, C. H. Chu, Y.-R. Wu, M.-H. Shih, C.-K. Lee, H.-C. Kuo, D. P. Tsai, and G.-R. Lin, "Transferring the bendable substrateless GaN LED grown on a thin C-rich SiC buffer layer to flexible dielectric and metallic plates," *Journal of Materials Chemistry C,* vol. 5, no. 3, pp. 607-617, 2017.

[11] R. H. Horng, C. H. Tien, S. H. Chuang, K. C. Liu, and D. S. Wuu, "External stress effects on the optical and electrical properties of flexible InGaN-based green light-emitting diodes," *Opt Express,* vol. 23, no. 24, pp. 31334-41, Nov 30, 2015.

[12] B. Hwang, S. Lim, M. Park, and S. M. Han, "Neutral plane control by using polymer/graphene flake composites for flexible displays," *Rsc Advances,* vol. 7, no. 14, pp. 8186-8191, 2017.
[13] H. E. Lee, J. H. Shin, J. H. Park, S. K. Hong, S. H. Park, S. H. Lee, J. H. Lee, I. S. Kang, and K. J. Lee, "Micro Light-Emitting Diodes for Display and Flexible Biomedical Applications," *Advanced Functional Materials,* vol. 29, no. 24, Jun, 2019.
[14] C. Jaeyi, H. Youngkyu, C. Yong-Seok, J. Tak, B. Jong Hyeob, K. Heung Cho, and P. Seong-Ju, "Transfer of GaN LEDs From Sapphire to Flexible Substrates by Laser Lift-Off and Contact Printing," *IEEE Photonics Technology Letters,* vol. 24, no. 23, pp. 2115-2118, 2012.
[15] M. Kneissl, T. Y. Seong, J. Han, and H. Amano, "The emergence and prospects of deep-ultraviolet light-emitting diode technologies," *Nature Photonics,* vol. 13, no. 4, pp. 233-244, Apr, 2019.
[16] J. Ruschel, J. Glaab, B. Beidoun, N. L. Ploch, J. Rass, T. Kolbe, A. Knauer, M. Weyers, S. Einfeldt, and M. Kneissl, "Current-induced degradation and lifetime prediction of 310 nm ultraviolet light-emitting diodes," *Photonics Research,* vol. 7, no. 7, 2019.
[17] G. Yang, Y. Jung, C. V. Cuervo, F. Ren, S. J. Pearton, and J. Kim, "GaN-based light-emitting diodes on graphene-coated flexible substrates," *Opt Express,* vol. 22 Suppl 3, pp. A812-7, May 5, 2014.
[18] L. M. Zhou, B. C. Ren, Z. W. Zheng, L. Y. Ying, H. Long, and B. P. Zhang, "Fabrication and Characterization of GaN-Based Resonant-Cavity Light-Emitting Diodes with Dielectric and Metal Mirrors," *Ecs Journal of Solid State Science and Technology,* vol. 7, no. 3, pp. R34-R37, 2018.
[19] R. H. Horng, B. R. Wu, C. H. Tien, S. L. Ou, M. H. Yang, H. C. Kuo, and D. S. Wuu, "Performance of GaN-based light-emitting diodes fabricated using GaN epilayers grown on silicon substrates," *Opt Express,* vol. 22 Suppl 1, pp. A179-87, Jan 13, 2014.
[20] K. H. Lee, M. Asadirad, S. Shervin, S. K. Oh, J. T. Oh, J.-O. Song, Y.-T. Moon, and J.-H. Ryou, "Thin-Film-Flip-Chip LEDs Grown on Si Substrate Using Wafer-Level Chip-Scale Package," *IEEE Photonics Technology Letters,* vol. 28, no. 18, pp. 1956-1959, 2016.
[21] F. Gou, E. L. Hsiang, G. Tan, P. T. Chou, Y. L. Li, Y. F. Lan, and S. T. Wu, "Angular color shift of micro-LED displays," *Opt Express,* vol. 27, no. 12, pp. A746-A757, Jun 10, 2019.
[22] T. Z. Wu, C. W. Sher, Y. Lin, C. F. Lee, S. J. Liang, Y. J. Lu, S. W. H. Chen, W. J. Guo, H. C. Kuo, and Z. Chen, "Mini-LED and Micro-LED: Promising Candidates for the Next Generation Display Technology," *Applied Sciences-Basel,* vol. 8, no. 9, Sep, 2018.
[23] G. Chen, A. M. Hoang, S. Bogdanov, A. Haddadi, S. R. Darvish, and M. Razeghi, "Effect of sidewall surface recombination on the quantum efficiency in a Y2O3

passivated gated type-II InAs/GaSb long-infrared photodetector array," *Applied Physics Letters*, vol. 103, no. 22, Nov 25, 2013.
[24] X. Gao, L. Lin, Y. Liu, and X. Huang, "LTPS TFT Process on Polyimide Substrate for Flexible AMOLED," *Journal of Display Technology*, vol. 11, no. 8, pp. 666-669, 2015.
[25] W. Liu, G. Yao, C. Jiang, Q. Cui, and X. Guo, "A New Voltage Driving Scheme to Suppress Non-Idealities of Polycrystalline Thin-Film Transistors for AMOLED Displays," *Journal of Display Technology*, vol. 10, no. 12, pp. 991-994, 2014.
[26] C.-Y. Chen, J.-W. Lee, S.-D. Wang, M.-S. Shieh, P.-H. Lee, W.-C. Chen, H.-Y. Lin, K.-L. Yeh, and T.-F. Lei, "Negative Bias Temperature Instability in Low-Temperature Polycrystalline Silicon Thin-Film Transistors," *IEEE Transactions on Electron Devices*, vol. 53, no. 12, pp. 2993-3000, 2006.
[27] C.-H. Lee, N. P. Papadopoulos, M. Sachdev, and W. S. Wong, "Effect of Mechanical Strain on Hydrogenated Amorphous Silicon Thin-Film Transistors and Compensation Circuits on Flexible Substrates," *IEEE Transactions on Electron Devices*, vol. 64, no. 5, pp. 2016-2021, 2017.
[28] Z. Tian, Y. Li, X. Su, L. Feng, S. Wang, W. Ding, Q. Li, Y. Zhang, M. Guo, F. Yun, and S. W. R. Lee, "Super flexible GaN light emitting diodes using microscale pyramid arrays through laser lift-off and dual transfer," *Opt Express*, vol. 26, no. 2, pp. 1817-1824, Jan 22, 2018.
[29] G. F. Chen, H. C. Chen, T. C. Chang, S. P. Huang, H. M. Chen, P. Y. Liao, J. J. Chen, C. W. Kuo, W. C. Lai, A. K. Chu, S. C. Lin, C. Y. Yeh, C. S. Chang, C. M. Tsai, M. C. Yu, and S. D. Zhang, "An Energy-Band Model for Dual-Gate-Voltage Sweeping in Hydrogenated Amorphous Silicon Thin-Film Transistors," *IEEE Transactions on Electron Devices*, vol. 66, no. 6, pp. 2614-2619, Jun, 2019.
[30] Q. Li, C.-H. Lee, M. Asad, W. S. Wong, and M. Sachdev, "CMOS-Like Logic Circuits With Unipolar Thin-Film Transistors on Flexible Substrate," *IEEE Transactions on Electron Devices*, pp. 1-6, 2019.
[31] R. Chaji, and A. Nathan, "13.2:Invited Paper: LTPS vs Oxide Backplanes for AMOLED Displays: System Design Considerations and Compensation Techniques," *SID Symposium Digest of Technical Papers*, vol. 45, no. 1, pp. 153-156, 2014.
[32] P. Gutruf, R. T. Yin, K. B. Lee, J. Ausra, J. A. Brennan, Y. Qiao, Z. Xie, R. Peralta, O. Talarico, A. Murillo, S. W. Chen, J. P. Leshock, C. R. Haney, E. A. Waters, C. Zhang, H. Luan, Y. Huang, G. Trachiotis, I. R. Efimov, and J. A. Rogers, "Wireless, battery-free, fully implantable multimodal and multisite pacemakers for applications in small animal models," *Nat Commun*, vol. 10, no. 1, pp. 5742, Dec 17, 2019.
[33] C. Linghu, S. Zhang, C. Wang, and J. Song, "Transfer printing techniques for flexible and stretchable inorganic electronics," *npj Flexible Electronics*, vol. 2, no. 1, 2018.
[34] W. Zheng, and H. O. Jacobs, "Self-Assembly Process to Integrate and Connect Semiconductor Dies on Surfaces with Single-Angular Orientation and Contact-Pad Registration," *Advanced Materials*, vol. 18, no. 11, pp. 1387-1392, 2006.

[35] S. Biswas, M. Mozafari, T. Stauden, and H. O. Jacobs, "Surface Tension Directed Fluidic Self-Assembly of Semiconductor Chips across Length Scales and Material Boundaries," *Micromachines (Basel),* vol. 7, no. 4, Mar 28, 2016.
[36] M. Asad, Q. Li, C. H. Lee, M. Sachdev, and W. S. Wong, "Integration of GaN light-emitting diodes with a-Si:H thin-film transistors for flexible displays," *Nanotechnology,* vol. 30, no. 32, pp. 324003, Aug 9, 2019.
[37] K. Ding, V. Avrutin, N. Izyumskaya, U. Ozgur, and H. Morkoc, "Micro-LEDs, a Manufacturability Perspective," *Applied Sciences-Basel,* vol. 9, no. 6, Mar 22, 2019.
[38] B. S. Gundlach, M. Frising, A. Shahsafi, G. Vershbow, C. Wan, J. Salman, B. Rokers, L. Lessard, and M. A. Kats, "Design considerations for the enhancement of human color vision by breaking binocular redundancy," *Sci Rep,* vol. 8, no. 1, pp. 11971, Aug 10, 2018.
[39] L. Z. Li, C. B. Liu, Y. Z. Su, J. C. Bai, J. Q. Wu, Y. J. Han, Y. B. Hou, S. X. Qi, Y. Zhao, H. Ding, Y. F. Yan, L. Yin, P. Wang, Y. Luo, and X. Sheng, "Heterogeneous Integration of Microscale GaN Light-Emitting Diodes and Their Electrical, Optical, and Thermal Characteristics on Flexible Substrates," *Advanced Materials Technologies,* vol. 3, no. 1, Jan, 2018.
[40] S. I. Park, Y. Xiong, R. H. Kim, P. Elvikis, M. Meitl, D. H. Kim, J. Wu, J. Yoon, C. J. Yu, Z. Liu, Y. Huang, K. C. Hwang, P. Ferreira, X. Li, K. Choquette, and J. A. Rogers, "Printed assemblies of inorganic light-emitting diodes for deformable and semitransparent displays," *Science,* vol. 325, no. 5943, pp. 977-81, Aug 21, 2009.
[41] L. Y. Kuritzky, C. Weisbuch, and J. S. Speck, "Prospects for 100% wall-plug efficient III-nitride LEDs," *Opt Express,* vol. 26, no. 13, pp. 16600-16608, Jun 25, 2018.
[42] L. Wang, C. Lu, J. Lu, L. Liu, N. Liu, Y. Chen, Y. Zhang, E. Gu, and X. Hu, "Influence of carrier screening and band filling effects on efficiency droop of InGaN light emitting diodes," *Opt Express,* vol. 19, no. 15, pp. 14182-7, Jul 18, 2011.
[43] P. Tian, J. J. McKendry, E. Gu, Z. Chen, Y. Sun, G. Zhang, M. D. Dawson, and R. Liu, "Fabrication, characterization and applications of flexible vertical InGaN micro-light emitting diode arrays," *Opt Express,* vol. 24, no. 1, pp. 699-707, Jan 11, 2016.
[44] M. Asad, Q. Li, M. Sachdev, and W. S. Wong, "Size-dependent optoelectrical properties of 365 nm ultraviolet light-emitting diodes," *Nanotechnology,* vol. 30, no. 50, pp. 504001, Dec 13, 2019.
[45] H. P. Nguyen, S. Zhang, A. T. Connie, M. G. Kibria, Q. Wang, I. Shih, and Z. Mi, "Breaking the carrier injection bottleneck of phosphor-free nanowire white light-emitting diodes," *Nano Lett,* vol. 13, no. 11, pp. 5437-42, 2013.
[46] K. H. Li, X. Liu, Q. Wang, S. Zhao, and Z. Mi, "Ultralow-threshold electrically injected AlGaN nanowire ultraviolet lasers on Si operating at low temperature," *Nat Nanotechnol,* vol. 10, no. 2, pp. 140-4, Feb, 2015.
[47] S. L. Diedenhofen, O. T. Janssen, M. Hocevar, A. Pierret, E. P. Bakkers, H. P. Urbach, and J. G. Rivas, "Controlling the directional emission of light by periodic

arrays of heterostructured semiconductor nanowires," *ACS Nano,* vol. 5, no. 7, pp. 5830-7, Jul 26, 2011.
[48] G. Grzela, R. Paniagua-Dominguez, T. Barten, Y. Fontana, J. A. Sanchez-Gil, and J. Gomez Rivas, "Nanowire antenna emission," *Nano Lett,* vol. 12, no. 11, pp. 5481-6, Nov 14, 2012.
[49] D. van Dam, D. R. Abujetas, R. Paniagua-Dominguez, J. A. Sanchez-Gil, E. P. Bakkers, J. E. Haverkort, and J. Gomez Rivas, "Directional and Polarized Emission from Nanowire Arrays," *Nano Lett,* vol. 15, no. 7, pp. 4557-63, Jul 8, 2015.
[50] X. Dai, A. Messanvi, H. Zhang, C. Durand, J. Eymery, C. Bougerol, F. H. Julien, and M. Tchernycheva, "Flexible Light-Emitting Diodes Based on Vertical Nitride Nanowires," *Nano Lett,* vol. 15, no. 10, pp. 6958-64, Oct 14, 2015.
[51] G. Tabares, S. Mhedhbi, M. Lesecq, B. Damilano, J. Brault, S. Chenot, A. Ebongue, P. Altuntas, N. Defrance, V. Hoel, and Y. Cordier, "Impact of the Bending on the Electroluminescence of Flexible InGaN/GaN Light-Emitting Diodes," *IEEE Photonics Technology Letters,* vol. 28, no. 15, pp. 1661-1664, 2016.
[52] M. K. Pathirane, and W. S. Wong, "Optical and Electrical Characteristics of Hybrid ZnO Nanowire/a-Si:H Solar Cells on Flexible Substrates under Mechanical Bending," *Small,* vol. 12, no. 19, pp. 2554-8, May, 2016.
[53] W. S. Wong, T. Sands, N. W. Cheung, M. Kneissl, D. P. Bour, P. Mei, L. T. Romano, and N. M. Johnson, "Fabrication of thin-film InGaN light-emitting diode membranes by laser lift-off," *Applied Physics Letters,* vol. 75, no. 10, pp. 1360-1362, Sep 6, 1999.
[54] W. S. Wong, T. Sands, and N. W. Cheung, "Damage-free separation of GaN thin films from sapphire substrates," *Applied Physics Letters,* vol. 72, no. 5, pp. 599-601, Feb 2, 1998.
[55] M. Kneissl, W. S. Wong, D. W. Treat, M. Teepe, N. Miyashita, and N. M. Johnson, "Continuous-wave operation of InGaN multiple-quantum-well laser diodes on copper substrates obtained by laser liftoff," *IEEE Journal of Selected Topics in Quantum Electronics,* vol. 7, no. 2, pp. 188-191, 2001.
[56] T. I. Kim, Y. H. Jung, J. Song, D. Kim, Y. Li, H. S. Kim, I. S. Song, J. J. Wierer, H. A. Pao, Y. Huang, and J. A. Rogers, "High-efficiency, microscale GaN light-emitting diodes and their thermal properties on unusual substrates," *Small,* vol. 8, no. 11, pp. 1643-9, Jun 11, 2012.
[57] H. E. Lee, J. Choi, S. H. Lee, M. Jeong, J. H. Shin, D. J. Joe, D. Kim, C. W. Kim, J. H. Park, J. H. Lee, D. Kim, C. S. Shin, and K. J. Lee, "Monolithic Flexible Vertical GaN Light-Emitting Diodes for a Transparent Wireless Brain Optical Stimulator," *Adv Mater,* vol. 30, no. 28, pp. e1800649, Jul, 2018.
[58] J. Q. Xi, H. Luo, A. J. Pasquale, J. K. Kim, and E. F. Schubert, "Enhanced light extraction in GaInN light-emitting diode with pyramid reflector," *IEEE Photonics Technology Letters,* vol. 18, no. 21-24, pp. 2347-2349, Nov-Dec, 2006.

[59] P. Zhao, and H. Zhao, "Analysis of light extraction efficiency enhancement for thin-film-flip-chip InGaN quantum wells light-emitting diodes with GaN micro-domes," *Opt Express,* vol. 20 Suppl 5, pp. A765-76, Sep 10, 2012.
[60] P. Tian, P. R. Edwards, M. J. Wallace, R. W. Martin, J. J. D. McKendry, E. Gu, M. D. Dawson, Z.-J. Qiu, C. Jia, Z. Chen, G. Zhang, L. Zheng, and R. Liu, "Characteristics of GaN-based light emitting diodes with different thicknesses of buffer layer grown by HVPE and MOCVD," *Journal of Physics D: Applied Physics,* vol. 50, no. 7, 2017.
[61] V. K. Malyutenko, S. S. Bolgov, and A. N. Tykhonov, "Research on Electrical Efficiency Degradation Influenced by Current Crowding in Vertical Blue InGaN-on-SiC Light-Emitting Diodes," *Ieee Photonics Technology Letters,* vol. 24, no. 13, pp. 1124-1126, Jul 1, 2012.
[62] J. Kou, C. C. Shen, H. Shao, J. Che, X. Hou, C. Chu, K. Tian, Y. Zhang, Z. H. Zhang, and H. C. Kuo, "Impact of the surface recombination on InGaN/GaN-based blue micro-light emitting diodes," *Opt Express,* vol. 27, no. 12, pp. A643-A653, Jun 10, 2019.
[63] M. S. Wong, S. Nakamura, and S. P. DenBaars, "Review-Progress in High Performance III-Nitride Micro-Light-Emitting Diodes," *Ecs Journal of Solid State Science and Technology,* vol. 9, no. 1, Nov 7, 2019.
[64] M. S. Wong, C. Lee, D. J. Myers, D. Hwang, J. A. Kearns, T. Li, J. S. Speck, S. Nakamura, and S. P. DenBaars, "Size-independent peak efficiency of III-nitride micro-light-emitting-diodes using chemical treatment and sidewall passivation," *Applied Physics Express,* vol. 12, no. 9, Sep 1, 2019.
[65] M. S. Wong, D. Hwang, A. I. Alhassan, C. Lee, R. Ley, S. Nakamura, and S. P. DenBaars, "High efficiency of III-nitride micro-light-emitting diodes by sidewall passivation using atomic layer deposition," *Opt Express,* vol. 26, no. 16, pp. 21324-21331, Aug 6, 2018.
[66] G. Chen, B. M. Nguyen, A. M. Hoang, E. K. Huang, S. R. Darvish, and M. Razeghi, "Elimination of surface leakage in gate controlled type-II InAs/GaSb mid-infrared photodetectors," *Applied Physics Letters,* vol. 99, no. 18, Oct 31, 2011.
[67] J. M. Shah, Y. L. Li, T. Gessmann, and E. F. Schubert, "Experimental analysis and theoretical model for anomalously high ideality factors (n≫2.0) in AlGaN/GaNp-njunction diodes," *Journal of Applied Physics,* vol. 94, no. 4, pp. 2627-2630, 2003.
[68] H. Masui, "Diode ideality factor in modern light-emitting diodes," *Semiconductor Science and Technology,* vol. 26, no. 7, Jul 7, 2011.
[69] H. P. T. Nguyen, M. Djavid, and Z. Mi, "Nonradiative Recombination Mechanism in Phosphor-Free GaN-Based Nanowire White Light Emitting Diodes and the Effect of Ammonium Sulfide Surface Passivation," *Wide-Bandgap Semiconductor Materials and Devices 14,* vol. 53, no. 2, pp. 93-100, 2013.

Appendix A

Details of materials and methods from Chapter 3

Flexible a-Si:H TFT fabrication process. A conventional back-channel-etching (BCE) process has been employed to fabricated TFTs on a PEN substrate. Starting the fabrication process, a 500 nm SiN_x buffer layer was coated on the flex using plasma-enhanced chemical vapor deposition (PECVD) at 170°C. Next, the gate metal was formed by wet etching of a 70 nm RF sputtered molybdenum. In a single step, a 350 nm SiN_x was deposited as the gate dielectric followed by the deposition of 200 nm a-Si:H and 40 nm n^+ a-Si:H without breaking the vacuum in a cluster-tool PECVD system. The TFT active area was then defined by reactive ion etching (RIE) process. For source and drain (S/D) metal contact, a bilayer of Al/Cr (90 nm / 30 nm) was RF supported and then patterned. The n^+ a-Si:H was then etched back using S/D contact mask in the RIE chamber. Next, a 1 μm SiN_x passivation layer was deposited followed by a via-open pattern with wet etching. As an external contact metal, a 1 μm Al was RF sputtered and patterned. Next, a negative tone photoresist was patterned (110 × 110 μm^2) on the drain pad for the lift-off process. Then, a Ti/Ni/Au (20/70/50 nm) layer was coated with electron beam evaporation on the TFT drain electrode followed with thermal evaporation of 2 μm indium. The lift-off process was finished by overnight immersing the samples in an NMP-based stripper.

GaN micro-LED fabrication. Commercially available blue LED epitaxial structures (Prolux Advanced Semiconductors) grown on 500 nm double-side polished sapphire was used to fabricate the micro-LEDs. The epitaxial layers consisted of 2.5 μm undoped GaN followed by 2.0 μm n-GaN, a 100 nm stress compensation n-AlGaN, a 2 μm n-GaN (8×10^{18} cm^{-3}), a low-

temperature 200 nm n-GaN (1×10^{18} cm^{-3}), a 60 nm InGaN/GaN superlattice layer, 8 × 3 nm $In_{0.15}Ga_{0.85}N$ quantum wells separated by 10 nm thick GaN barrier layer, 55 nm p-AlGaN electron blocking layer, and finally a 60 nm p-GaN (4×10^{17} cm^{-3}) ohmic layer. The process starts with immersing the wafers into a Piranha solution (H_2SO_4:H_2O_2 3:1) followed with rinsing in HCl: deionized (DI) water (1:1) to remove organic residues and metallic ions. After drying the sample with an N_2 stream, a Ni/Au (15 nm /15 nm) was electron beam evaporated as the p-GaN ohmic contact. The square-shape patterns were formed by optical lithography and wet etching. To improve the contact resistance, the sample was annealed at 550°C in air for 10 min. As the GaN dry etch mask, a 1400 nm SiNx was coated on the sample by using a PECVD system (System 100, Oxford Instruments) at 330°C and patterned by a photoresist mask and SF6-bases dry etching process (ICP 380, Oxford Instrument). Then a chlorine-based dry-etching (Cl_2:Ar 20:4) process (ICP 380, Oxford Instrument) was employed to define the lateral dimension (100 × 100 μm^2) of micro-LEDs. The residual SiN_x was then removed by immersing the sample into a BOE solution for 2 min. Finally, a 40 nm Al_2O_3 was deposited at 330°C as the sidewall passivation layer and the anode contact was exposed by optical lithography (AZ4620 AZ Electronic Materials; 10 μm thick) and wet etching.

TFT-micro-LED integration on flex. For integrating the GaN micro-LEDs onto a flexible substrate, initially, they should be transferred onto a carrier substrate after releasing the sapphire substrate. As preparation for wafer bonding, a thin layer (3 μm) of wax was spin-coated on a glass substrate at 3000 rpm and baked at 80°C for 5 min to evaporate the solvent. The bonding of micro-LEDs (on sapphire) occurred by mounting the sample flipped onto the

glass substrate on the hot-plate. Due to the capillary force, the melted wax surrounds the micro-LEDs and made a strong bond. For the LLO process, a 355 nm single-pulse Nd: YAG laser with 0.98 J/cm^2 energy density and 5 ns pulse-width directed through the sapphire surface. Due to the absorption of high-energy photons at the GaN-sapphire interface, GaN was decomposed into Ga metal drops and nitrogen (N_2) gas. After heating the sample to 40°C, the sapphire was then removed easily. To remove the residual Ga droplets from the micro-LEDs' backside, the sample was dipped in HCl:DI Water (1:1) for 1 min. The excess wax layer was removed from the micro-LEDs' sidewalls by an RIE process (CF_4:O_2 15:85) at room temperature. The wax layer underneath of micro-LEDs was not removed and remained to serve as tethers to hold the devices fixed on the carrier substrate. Next, a double-layer of Cr/Au (30 nm / 150 nm) was electron-beam evaporated on the micro-LEDs' backside as an ohmic contact and bonding electrode. Then, by using a die bonder (T-3000 FC3, Tresky), the micro-LEDs were positioned above the TFTs' drain pad (with 2 μm indium) followed by eutectic flip-chip bonding at 150°C and 5 N force for 10 min. Afterward, the carrier substrate was removed by immersing the structure into warm acetone for 1 min. Coating with photo-definable PI (HD4100, 10 μm) followed by optical lithography, the micro-display was passivated and planarized. After fully curing the PI at 300°C at N_2 ambient, 600 nm aluminum-doped zinc oxide was RF sputtered over the sample. Finally, using a positive photoresist mask the AZO was patterned with a wet etch process (HCl:H_2O 1:10).

TFT electrical characterization. The characterization of a-Si:H TFTs was performed by two Keithley source meters at room temperature. The first one, model 2400 was used to supply

pulsed gate voltages. The second one, model 6430, was used to supply a fixed DC voltage of 1 V as the drain bias of the TFT while measuring the drain-source current. Each pulsed gate voltage lasted for 40 ms required for the drain-source current to be properly measured. The delay between pulses was set to 1 sec to minimize the impact from the previous pulse. In order to characterize the flexible TFTs, the plastic substrate was taped onto a curved aluminum sample holder.

micro-LED optoelectrical characterization. In order or characterize the micro-LEDs, a Keithley 2400 parameter analyzer and Micromanipulator 7000 probe station was used. The Electroluminescent measurement of the micro-LEDs on both flat and curved structures was performed by taping the sample onto a curved aluminum holder. The devices were then probed directly and the EL spectrum was then measured by an optical fiber and spectrometer (Flame system, Ocean Optics with 1 nm resolution) after integrating the topside emitted photons using 2 objective lenses.

3-dimensional finite-difference time-domain simulation. The top-side light-extraction efficiency of the micro-LEDs without and with a reflective backside metal electrode was calculated using 3-dimensional finite-difference time-domain (3D-FDTD) simulations. The micro-LED width, length, and height were considered 5, 5, 6.5 μm, respectively. A perfectly matched layer (PML) boundary condition was considered around the micro-LED to prevent reflection from the medium. The attenuation factor (σ) and auxiliary attenuation coefficient (κ) set to 0.25 and 2, respectively. A stability factor of 0.076 fs and a minimum mesh size of and 40 nm were chosen to improve the simulation accuracy. The quantum well was modeled as a

transverse electric (TE) mode dipole with the center wavelength of 450 nm and span wavelength of 20 nm.

Appendix B

Details of materials and methods from Chapter 4

Modeling and Simulation. The bending-induced strain in GaN micro-LEDs on PI/Cu flexible platform was simulated using a commercially available tool, COMSOL Multiphysics. To mimic the applied bending stress on the PI substrate, a bending moment of M applied along with the ending of the PI while the center was kept fixed. M was calculated using the Stoney equation $M = \frac{Ed^3w}{12R}$ for a 15 mm radius of curvature where E, d, and w are elastic moduli, substrate's thickness and width, respectively. All mechanical properties of the materials were considered linearly elastic and temperature independent.

To simulate the temperature gradient of the prototypes, a 3-D model has been developed. This analysis was conducted using COMSOL finite element analysis (FEA) tool on the three prototypes. A cylindrical GaN micro-LED with a 6 μm height was modeled on various substrates while a 7×10^4 W/m^2 heat source was placed 50 nm below the surface to mimic the heat from quantum wells. The temperature distribution of the micro-LED in x, y, and z directions was calculated using the following equation:

$$\frac{\partial}{\partial x}(k_x \frac{\partial T}{\partial x}) + \frac{\partial}{\partial y}(k_y \frac{\partial T}{\partial y}) + \frac{\partial}{\partial x}(k_z \frac{\partial T}{\partial z}) + H = \rho c \frac{\partial T}{\partial t}$$

where k_x, k_y, and k_z are the heat conductivity coefficients of the material is x, y, z directions, H is the overall heat generation density, ρ is the materials density, and c is the specific heat capacity of the material. All thermal properties are assumed to be homogenous, isotropic and temperature independent. The thermal conductivity of air, sapphire, GaN, copper, and

polyimide were considered 0.024, 23.1, 130, 400, and 0.12 W/m.K, respectively. In addition, the heat flux at the boundaries was modeled by the following equation:

$$k_x \frac{\partial T}{\partial x} n_x + k_y \frac{\partial T}{\partial y} n_y + k_z \frac{\partial T}{\partial z} n_z = -\varphi$$

where n_x, n_y, and n_z are the normal direction outside of the boundaries and the φ is the heat flow from the heat source to the atmosphere by the natural convection.

Fabrication of the GaN micro-LEDs. For making blue GaN micro-LEDs, commercially available epitaxial structures (Prolux Advanced Semiconductors) were used. The epitaxial layers include 8 × 3 nm $In_{0.15}Ga_{0.85}N$ quantum wells (QWs) separated by 10 nm thick GaN barrier layer from the top 55 nm p-AlGaN electron blocking layer, and finally a 60 nm p-GaN (4×10^{17} cm^{-3}) ohmic layer. The epitaxial layer at the bottom of the QWs consisted of 2.5 μm undoped GaN followed by 2.0 μm n-GaN, a 100 nm stress compensation n-AlGaN, a 2 μm n-GaN (8×10^{18} cm^{-3}), a low-temperature 200 nm n-GaN (1×10^{18} cm^{-3}), a 60 nm InGaN/GaN superlattice layer, all grown on a 500 μm double-side polished sapphire. The fabrication process starts with removing the organic residues on the wafers by immersing the samples into Piranha (H_2SO_4:H_2O_2 3:1) for 15 min and then rinsing in deionized (DI) water. The metallic ions and native oxides can be removed from the p-GaN surface by immersing the wafers in HCl:DI water (1:1) for 5 min followed by rinsing in DI water for 2 min. The epitaxial wafers then immediately were loaded into the electron-beam evaporation system (Intlvac, Nanochrome II) to coat a Ni/Au (15/15 nm) ohmic contact to the p-GaN. The Ni/Au bilayer was then patterned by optical lithography (Microposit S1811; 1.1 μm thick) and standard wet etching (nickel etchant TFG, gold etchant TFA; Transene Inc.). In order to improve the contact

property and current spreading of the Ni/Au bilayer, the samples were annealed in N_2/O_2 (4:1) ambient at 550°C for 5 min. The process to define the vertical micro-LEDs first involve 330°C plasma-enhanced chemical vapor deposition (PECVD) coating of a 1.4 μm SiN_x layer and then patterned by using an SF_6-based reactive ion etching (RIE). The lateral geometry of the GaN micro-LEDs was defined by a chlorine-based (Cl_2:Ar 20:4) inductively coupled plasma reactive ion etching through the SiN_x etch mask. After removing the residual SiN_x by immersing the sample in a buffered oxide-etchant (BOE), a 40 nm atomically layer deposited (ALD) Al_2O_3 was used to passivate the micro-LEDs' sidewall.

Selective-mass-transfer of the micro-LEDs onto the flex. Fig. **4.3** schematically illustrates the process for the mass-transfer of the GaN micro-LEDs onto a flexible substrate. First, a thin uniform adhesive layer (10 μm) was spin-coated at 3000 rpm for 30 sec on a silicon substrate followed with baking for 30 min at 80°C to evaporate its solvent. The micro-LEDs were flip-chip bonded onto a silicon carrier substrate with a temporary adhesive layer by using a Tresky T-3000-FC3 Die Bonder at 150°C. The strong bonding prevents cracking the micro-LEDs during the laser-liftoff process. Then a 355 nm Nd:YAG laser with 5 nm pulse width and 0.98 J/cm^2 energy density was irradiated through the sapphire substrate to be absorbed in the GaN interface with sapphire. The thermal decomposition of GaN resulted in Ga metal droplets and nitrogen (N_2) gas. Due to this decomposition, the sapphire was released easily from the micro-LEDs at a temperature of 30°C (melting point of Ga). By using an oxygen-based reactive ion etching (RIE), the adhesive layer was etched from everywhere except underneath the micro-LEDs. A triple thin-film layer of Cr/Cu/Au (50/500/100 nm) was then electron-beam

evaporated on the backside of the micro-LEDs to serve as n-GaN ohmic contact (Cr), heat-sink (Cu), and bonding metal (Au), respectively. The flexible substrate (Kapton® Type HPP-TS, Dupont) was then coated with a bilayer of Cr/Cu (20/1000 nm) as an electrical backside contact. To transfer the micro-LEDs selectively on a place of interest, Au/Sn (150/100 nm) pads were then patterned on the flex by using a lift-off process (Microchemicals n-LOF 2035; 3.5 µm thick). Flip-chip bonding at a temperature and pressure of 250°C and 1 N, respectively, was used to fix the micro-LEDs onto the flex followed by peeling them away from the carrier substrate. Finally, the residue of the adhesive layer was etched away in a CF_4-based plasma at room temperature for 2 min. The carrier substrate is then ready for the next transfer step.

Surface planarization and the anode contact. Coating the flex substrate with a benzocyclobutene (BCB) thin film (CYCLOTENE™ 4026 Advanced Electronics Resin) at 1000 rpm for 30 sec, curing at 190°C for 1 hour and then a back dry etching for 1 min in oxygen, prepared the device for coating the common anode electrode. RF sputtered 600 nm aluminum-doped zinc oxide (AZO) at 150°C was employed as a transparent conductive oxide (TCO) anode pad. The AZO was then patterned by using optical lithography (AZ Electronic Materials, AZ3312; 1.5 µm thick) and a 15 sec HCl:DI water (1:10) wet etching.

Electro-optical characterization. The I-V characteristics of LEDs were measured by a Keithley 2400 source meter with voltage sweep mode. To characterize the devices at different bending conditions, the LEDs were taped on aluminum structures with predefined curvature. The electroluminescence (EL) of LEDs on different substrates were measured from the topside of devices using an optical fiber connected to a spectrometer (Ocean Optics, Flame System)

after integrating the photons using 2 objective lenses. All the measurements were performed at room departure.

Appendix C

Details of materials and methods from Chapter 5

Modeling and simulation: The LED structures were modeled using the commercially available FEA simulation tool, COMSOL Multiphysics. To mimic an applied bending stress on the PET substrate, a bending moment, M, applied along the ends of the substrate was determined using the Stoney equation ($M = \frac{Ed^3w}{12R}$) for various radii of curvature, R; where d and w is the substrate thickness and width, respectively, and E is the elastic moduli. All materials properties were assumed to be linearly elastic and temperature-independent with an initial zero bending stress. Relative tolerance of 0.001 was used for solving stationary equations with higher accuracy.

The 3D FDTD calculations were performed using the commercial software tool, Lumerical. Perfectly Matched Layer (PML) boundary conditions were employed to calculate the light extraction efficiency based on integrating the Poynting vector over time along the NW surface. To increase the accuracy of the calculations, the PML attenuation factor (σ) and auxiliary attenuation factor (κ) were set to 0.25 and 2, respectively. To have meaningful results, the electromagnetic field should not change significantly from one mesh grid to another one. Accordingly, a minimum mesh step of 0.25 nm and a time step of 0.0326 fs were used in all simulations. The light emission properties were modeled as dipole sources having a wavelength range between 420-430 nm. The region of the nanowire below the active region was also considered as a photonic waveguide, providing two-dimensional light confinement

along the transverse direction in the longitudinal z-direction along the length of the nanowire, assuming matched layer-boundary conditions along the sidewalls of the nanowire. A network of 121 NW LEDs (within an 11×11 array) on a GaN buffer layer was integrated with the n-contact silver bonding layer.

Laser Liftoff Process: GaN NW LEDs were bonded onto a Silicon wafer using Crystallbond 509-3 mounting adhesive. Following the bonding process, a 266 nm Nd:YAG laser with a power density of 900 mJ/cm^2 was raster scanned at 4 Hz through the transparent sapphire to decompose the GaN at the GaN/sapphire interface. The spot size of the laser beam was 140 μm × 25 μm and was rastered across a sample area of 1 cm × 1 cm. The samples were annealed on a hotplate at 40°C for 1 minute to melt the decomposed GaN and detach the sapphire substrate. A thin layer of High-Performance TED PELLA silver paste, dispersed in an inorganic silicate aqueous solution, was used to attach the exposed n-side of the GaN devices onto the flexible PET substrate. This structure was immersed into a hot acetone bath to selectively dissolve the Crystallbond adhesive layer and release the silicon carrier substrate. The samples were then sequentially immersed in fresh acetone and alcohol baths for 5 minutes each to wash out any adhesive residue from the top side of the NW LEDs and metal contacts. The "double-transfer" process was completed by drying the samples with nitrogen gas.

Device Characterization: The NW LED I-V characteristics were measured before and after integration onto the PET substrates using a Micromanipulator 7000 probe station and a Keithley 6430 parameter analyzer. The EL measurements of the devices on a curved PET substrate was accomplished using the same instrumentation with the samples attached to

curved substrate holders made from machined aluminum. The samples were taped onto the holders using adhesive Kapton® tape. The devices were then probed directly in a curved orientation of different radii of curvature.

The EL measurements were accomplished using an Ocean Optics SB2000+UV-VIS spectrophotometer with a Sony ILX511B 2048 element linear silicon CCD array with an optical resolution of 1.5 nm (full-width at half maximum). The devices were attached to the substrate holders and were then probed directly in flat and curved orientations of different radii of curvature.

Structural Characterization: The SEM images were taken using a JSM-7200F JEOL microscope system. The experiments were performed with 0°, 90º, and 45° angle sample holders to observe the device cross-section. An accelerating voltage of 10 kV was used for imaging.

Appendix D

Details of materials and methods from Chapter 6

FDTD Simulation. The light-extraction efficiency of the micro-LEDs with different backside etch depth from 0 to 5 μm was calculated using 3-dimensional finite-difference time-domain (FDTD) simulations. While the FDTD calculation requires a considerable amount of memory and computation time, in our simulations, the same structure height as real micro-LEDs (6.5 μm) was used and the device geometry was reduced to 5×5 μm^2 (instead of 90×90 μm^2). To prevent any reflection from the medium, a perfectly matched layer (PML) condition was set around the simulation area with attenuation factor (σ) and auxiliary attenuation coefficient (κ) set to 0.25 and 2, respectively. A minimum mesh size of 40 nm and a stability factor (*dt*) of 0.076 fs were considered to improve the calculation accuracy. In order to mimic the quantum well emission, a single Gaussian Transverse electric (TE) mode dipole with the center wavelength of 450 nm and span wavelength of 20 nm was positioned at 200 nm below the structure's topside.

TCAD Simulation. The numerical calculations consist of Poisson's equations, Schrodinger's equations, current continuity equations were performed using commercial Silvaco TCAD device simulator at room temperature. Since TCAD simulation consumes a huge amount of time and computation resources and we only want to check the phenomena in the devices' sidewall, the device length and height were considered 1 μm and 5 μm respectively. A uniform doping concentration for the p-GaN, p-AlGaN, and n-GaN were considered 4×10^{17} cm^{-3}, 1×10^{17} cm^{-3}, 1×10^{19} cm^{-3}, respectively. To consider the positive and negative charges at the

heterostructures' interface due to the lattice mismatch and strain, polarization with a polar-scale of 0.15 was introduced in calculation. To maintain the consistency in solving carrier continuity equations at the sidewalls, the emission and capture of the electrons by both donors-like and acceptor-like traps (D_α and A_β) need to take into account in modeling. As a result, the below modified SRH recombination equations are used;

$$R = \sum_{\alpha=1}^{l} R_{D_\alpha} + \sum_{\beta=1}^{m} R_{A_\beta}$$

where l is the number of donor-like traps and m is the number of acceptor-like traps. The recombination for donor-like traps can be formulated as:

$$R_{D_\alpha} = \frac{pn - n_i^2}{\tau_n \left[p + g n_i \exp\left(\frac{E_i - E_t}{K_B T_L} \right) \right] + \tau_p \left[n + \frac{1}{g} n_i \exp\left(\frac{E_t - E_i}{K_B T_L} \right) \right]}$$

and for acceptor-like traps the recombination equation is:

$$R_{A_\beta} = \frac{pn - n_i^2}{\tau_n \left[p + \frac{1}{g} n_i \exp\left(\frac{E_i - E_t}{K_B T_L} \right) \right] + \tau_p \left[n + g n_i \exp\left(\frac{E_t - E_i}{K_B T_L} \right) \right]}$$

where p , n , n_i are the hole, electron, and intrinsic carrier concentrations, g is the degeneracy factor, E_i and E_t are the intrinsic Fermi level and trap energies, K_B and T_L are the Boltzmann constant and lattice temperature, τ_n and τ_p are the electron and hole carrier lifetimes. Both τ_n and τ_p are directly related to the capture cross-section of traps which is dominated by the crystal defects at the micro-LED's sidewalls. In order to consider the variation in the band structure and effective mass of carriers at the quantum wells, K.P model was used to analyze

the expression of the band dispersion. The simulated LED was biased from 0 V to 6 V in 0.1 V step size

GaN LED fabrication and thinning process. A commercial epitaxial structure grown on 500 μm sapphire substrate using metal-organic chemical vapor deposition was used to fabricate the GaN-based micro-LEDs. The epitaxial structure consists of the following layers: a 2.5 μm undoped GaN, a 2.0 μm n-GaN, a 100 nm stress compensation n-AlGaN, a 2 μm highly doped n-GaN (8×10^{18} cm^{-3}), a low-temperature 200 nm n-GaN (1×10^{18} cm^{-3}), a 60 nm InGaN/GaN superlattice layer, 8 × 3 nm $In_{0.15}Ga_{0.85}N$ quantum wells separated by 10 nm thick GaN barrier layer, 55 nm p-AlGaN electron blocking layer, and finally a 50 nm Mg-doped p-GaN (4×10^{17} cm^{-3}) ohmic layer. After removing the organic contaminations using a 20 min cleaning in the H_2SO_4:H_2O_2 (3:1) solution, the wafer has been immersed in HCl:H_2O (1:1) for 5 min to remove the native oxide from p-GaN. Then, a Ni/Au (10/10 nm) layer was deposited onto the p-GaN as a transparent ohmic contact and a current spreading layer. In order to improve the ohmic contact properties with the p-GaN, the wafer was annealed at 550°C in N_2:O_2 (4:1) for 5 min. The micro-LED mesa structure (90×90 μm^2) was etched using an inductively-coupled plasma (ICP) etching (Cl_2:Ar 20:40) down to the sapphire substrate with a 1.5 μm plasma-enhanced chemical vapor deposited (PECVD) SiN_x etch mask layer. After wet etching, the etch mask residues by immersing the wafer in buffered oxide etchant (BOE) for 3 min, a 500 nm SiO_2 layer was deposited by PECVD to passivate the device's sidewalls. Using conventional optical lithography and wet etching, the SiO_2 film was patterned to access the anode contact.

Then a liquid wax was spin-coated onto a glass substrate followed by baking at 80°C for 5 min to get a 3 µm thick adhesive layer on the carrier substrate. The micro-LEDs were then bonded onto the carrier substrate in a vacuum at 110°c for 10 min. A laser-liftoff process by using a Nd:YAG laser with a 5 ns pulse-width and energy density of 0.9 Jcm^{-2} removed the sapphire substrate from the GaN devices. While the devices were flipped on the carrier substrate, an ICP etching process was used for thinning the micro-LEDs' backside in various etch time. The measured GaN etch rate was 240 nm/min in Cl_2:Ar (20:4) chemistry, RF power of 50 watts, and ICP power set to 500 watts. After thinning the devices, a Ti/Al (5/500 nm) reflective metal bilayer was RF sputtered on micro-LEDs' sidewall and backside. In order to prepare the devices for flip-chip bonding onto a silicon substrate, a Cr/Au (50/200 nm) double-layer was e-beam evaporated only on the devices' backside. To transfer micro-LEDs onto the final silicon substrate, a flip-chip bonder was used to bond LEDs onto Cr/Au/In (50/250/1000 nm) pads with a pressure of 5 N at 250°C. After releasing the temporary carrier substrate, the wax residue was washed out using acetone and IPA.

Optical Measurements. The electroluminescence was measured while driving micro-LEDs under 10 A/cm^2 continuous current at room temperature. The topside emitted photons were collected using an objective lens with a numerical aperture (NA) = 0.4 at a working distance of 22 mm coupled to an optical fiber. With this NA, a collection angle of ~60° was used to collect light emitting mainly from the LED topside. A spectrometer (Ocean Optics, Flame system) with 1 nm resolution was used to quantify the emission intensity and wavelength.

Surface topography measurements. JEOL JSM-7200F scanning electron microscope was used to analyze the 3-dimensional structure of the micro-LEDs on carrier substrate before and after the backside thinning process. Atomic force microscopy (VEECO dimension 3000 AFM) in contact mode was used to measure the micro-LEDs' backside roughness after LLO and after 20 min backside thinning processes.

Electrical Measurements. After integrating onto the silicon substrate, the electrical properties of the micro-LEDs were measured at room temperature using a Keithley 2400 system at voltage sweep mode. One probe tip (25-μm diameter Tungsten) was mounted on the pad connected to the cathode while the other probe tip (7-μm diameter Tungsten) was directly on the anode contact. The device without backside thinning and sidewall coating is called REF and the other devices are called based on their epitaxial layer thickness.